Dissertation

submitted to the

Combined Faculties for the Natural Sciences and for Mathematics

of the Ruperto-Carola University of Heidelberg, Germany

for the degree of

Doctor of Natural Sciences

presented by

Mohamed Abouelmaaty Abdelgawad, MSc

born in Al Jahra, Kuwait

Oral-examination: 14th of June 2018

Reprogramming of Basic Cellular Metabolism by Vitamin D in Tumor Cells

Referees:

Prof. Dr. Stefan Wölfl (IPMB, Heidelberg University)

Prof. Dr. Steven Dooley (Medical Faculty Mannheim, Heidelberg University)

Table of contents

I. Acknowledgements

I am sincerely grateful to my supervisor, Prof. Dr. Stefan Wölfl, for encouraging me to pursue my scientific passion by allowing me to choose a research direction for my PhD, and for fostering an environment of intellectual freedom in his lab. Thank you very much for your responsible and wise guidance, and most importantly, for showing me an example of being a successful scientist and a great guy. For that, I will be forever indebted.

Prof. Dr. Steven Dooley, my second supervisor and member of my thesis advisory committee (TAC), for the support I could always count on in scholarship extensions, and for the constructive criticism during TAC meetings. Dr. Vytaute Starkuviene-Erfle, for agreeing to be a member of my TAC, and for all the useful comments and discussions in meetings.

The German Academic Exchange Service (DAAD), for awarding me a long-term scholarship that enabled me to pursue my dream of doing a doctorate. I would especially like to thank all staff members at their regional office in Cairo, for their professionalism, transparency, and above all, patience. I would also like to thank the different contact persons based in the DAAD headquarters in Bonn, who facilitated my move to Germany, and addressed all the issues and concerns I faced as an international student.

My great colleagues at the Wölfl lab, thank you very much for welcoming me when I first joined the group and for your support over the years. Always keep up the friendly atmosphere in the lab, and stay very passionate about your diverse projects. I would especially like to thank certain members of the group who undoubtedly left their mark on me, both personally and professionally. Firstly, my closest best friend in the world, Yasmin Dabiri. Thank you for being an endless source of inspiration and motivation in my life, and for all the support you offered me during my PhD. Ali Ghanem, also known as “Lulu”, for our great, extended (and occasionally time-wasting) conversations about science, culture, and world politics. I’ll definitely miss your sophisticated, overarching, cultural “grand models”! Jannick Theobald, for not only introducing me to the field of “lab-on-a-chip”, but also to the upcoming genre of “German rap”! I truly enjoyed the time we spent working together. Fadi Almouhanna, my colleague and neighbor, for the great “metabolism” discussions we had on our walks to and from the lab.

I would also like to thank former members of the group, especially Nadine Pfaller, Chiara Kraemer, and Thomas Kolenda, the very talented technicians who offered me tremendous help in doing experiments. I am truly grateful for that. Dr. Hamed Alborzinia, for showing me the ropes when I first started in the lab. Dr. Pavlo Holenya, for introducing me to ELISA microarrays. Dr. Jingjing Zhang, for setting an example of humility and scientific excellence, and for being a great friend and travel companion. I would also like to thank all the exceptional students I had the honor of supervising over the years, especially Shehryar "Shay" Khan and Wendy Strassburger.

I am also grateful for the fruitful collaboration I had with Dr. Michael Büttner from the Metabolomics Core Facility at Heidelberg University, who performed GC/MS-based metabolite quantification, which was very instrumental to my project.

I am very thankful to Prof. Dr. Mohamed Z. Gad (Dean of the Faculty of Pharmacy and Biotechnology, German University in Cairo), my former supervisor, for believing in me, and for the continued support, and essentially, for being the first person to introduce me to the fascinating world of vitamin D signaling.

In the end, I would like to thank my parents, Dr. Moshira Omar and Mr. Abdulla Abouelmaaty, for being the main driving force behind all my achievements, for encouraging me to recognize the value of education over many things, and for all the sacrifices they made to provide me the best opportunities in life. Their love and support are with me every day. I dedicate this work to them.

Mohamed A. Abouelmaaty

II. Summary

Recent years have witnessed a resurgence in tumor metabolism research. Cancer cells are known to exhibit multiple distinct aberrations in energy-utilization that help them sustain rapid growth and proliferation, as well as cope with harsh microenvironment conditions, such as limited nutrient availability and oxygenation. Amplified growth factor and oncogenic signaling have been implicated in the observed metabolic reprogramming in cancers, and thus, drugs that target these signaling aberrations have also been shown to impact metabolism. Furthermore, several drugs have been developed or repurposed to interfere with metabolic processes in transformed cells. In this thesis, the results of my investigations into the ability of 1,25-dihydroxyvitamin D_3 [$1,25(OH)_2D_3$] (also referred to as calcitriol)—the hormonally active form of vitamin D_3—to influence metabolic pathways in different cancer models are presented. Using prostate cancer cell lines with different androgen sensitivities, as well as breast cancer cell lines representing different molecular subtypes, it is shown that $1,25(OH)_2D_3$ is a major regulator of energy-utilization and glucose-sensing networks in these cancer cells. Detailed investigation of cellular metabolism using biosensor technology, GC/MS-based metabolomics, RT-qPCR gene expression analyses, enzymatic activity assays, FACS analyses, and immunoblotting, illustrates that $1,25(OH)_2D_3$ induces global rewiring of glucose-metabolizing pathways, as well as modulates energy-related signaling molecules including AMP-activated protein kinase and thioredoxin-interacting protein (TXNIP). My results also show, that in contrast to the long-standing association between TXNIP and calcitriol, the former is not universally regulated by the latter in cancer cell lines of various tissue origins, and that the canonical regulation is subject to glucose-availability. In conclusion, I like to propose that regulation of onco-metabolism is a mechanism through which calcitriol induces its anti-cancer effects, and argue that continued investigations into this theme would elucidate ways to improve the molecule's therapeutic potential.

III. Zusammenfassung

Im letzten Jahrzehnt ist ein wiederauflebendes Interesse an der Erforschung der Stoffwechselwege von Krebszellen entstanden. Krebszellen weisen diverse Unterschiede bei der Energienutzung auf, wodurch sie eine schnelle und starke Proliferation zu erzielen. Des Weiteren, helfen diese Stoffwechsanpassungen Krebszellen in rauen Mikroumgebungsbedingungen zu überleben, wie begrenzte Nährstoffverfügbarkeit und Sauerstoffversorgung. Eine entscheidende Rolle im veränderten Stoffwechsel von Krebszellen spielt die erhöhte Ausschüttung an Wachstumsfaktoren und onkogenen Signalen. Krebsmedikamente, die diese Faktoren beeinflussen haben oftmals einen veränderten zellulären Metabolismus zur Folge. In diesem Zusammenhang wurden verschiedene Medikamente entwickelt oder umfunktioniert, um die Stoffwechselprozesse in Krebszellen zu stören. In der vorliegenden Dissertation werden Untersuchungen zur Fähigkeit von 1,25-Dihydroxyvitamin D_3 [$1,25(OH)_2D_3$] Stoffwechselwege in verschiedene Krebsmodelle zu beeinflussen präsentiert. $1,25(OH)_2D_3$ ist die hormonell aktive Form von Vitamin D und wird auch als Calcitriol bezeichnet. Unter Verwendung von Prostatakrebszelllinien mit verschiedenen Androgensensitivitäten und zwei molekularen Subtypen von Brustkrebszellen, konnte nachgewiesen werden, dass $1,25(OH)_2D_3$ ein Hauptregulator der Energienutzung und Glukosewahrnehmung Krebszellen ist. Die mit Biosensortechnologie, GC / MS-basierter Metabolomik, Genexpressionsanalysen mit RT-qPCR, enzymatischen Aktivitätsassays, FACS-Analysen und Immunoblotting, erhaltenen Daten, zeigen klar den Einfluss von $1,25(OH)_2D_3$ auf den Glukosestoffwechselweg und verschiedene Energie-Signalmoleküle wie der AMP-aktivierte Proteinkinase und dem Thioredoxin-interagierende Protein (TXNIP). Überraschender Weise, konnte entgegen der langjährig etablierten Assoziation zwischen TXNIP und Calcitriol gezeigt werden, dass TXNIP nicht in allen Krebszelllinien verschiedener Gewebeursprünge universell durch Calcitriol reguliert wird sondern vor allem in Abhängigkeit der Verfügbarkeit von Glukose reguliert wird. Letztendlich schlage ich vor, dass sich ein Teil der Anti-Krebs-Wirkung von Calcitriol durch die Regulation des Onko-Metabolismus erklären lässt und weitere Forschung in dies Richtung neue Wege aufzeigen kann, wie das therapeutische Potenzial von Calcitriol besser genutzt werden kann.

IV. List of abbreviations

1,25(OH)$_2$D$_3$	*1,25-dihydroxyvitamin D$_3$*
2-NBDG	*2-[N-(7-nitrobenz-2-oxa-1,3-diazol-4-yl) amino]-2-deoxy-D-glucose*
5-FU	*5-Fluorouracil*
α-KG	*Alpha-ketoglutarate*
ACACA	*Acetyl CoA carboxylase alpha*
ACC	*Acetyl CoA carboxylase*
ACLY	*ATP citrate lyase*
AML	*Acute myeloid leukemia*
AMPK	*AMP-activated protein kinase*
AR	*Androgen receptor*
BAPTA-AM	bis-(o-aminophenoxy)-ethane-N,N,N,N′-tetraacetic acid/tetra(acetoxymethyl)-ester
BECN1	*Beclin 1*
BSA	*Bovine serum albumin*
CAMKK2	*Calcium/calmodulin-dependent kinase kinase 2*
CHX	*Cycloheximide*
COX5B	*Cytochrome c oxidase subunit 5B*
CPT1	*Carnitine palmitoyl-transferase 1*
CYP	*Cytochrome P450*
CYTC	*Cytochrome c*
DDIT4	*DNA damage inducible transcript 4*
DHCR7	*7-dehydrocholesterol reductase*
DHE	*Dihydroethidium*
DHEA	*Dehydroepiandrosterone*
DMEM	*Dulbecco's Modified Eagle Medium*
DMSO	*Dimethyl sulfoxide*
D-PBS	*Dulbecco's Phosphate-Buffered Saline*
EDTA	*Ethylenediaminetetraacetic acid*
ER	*Estrogen receptor*
ECL	*Enhanced chemiluminescence*
FACS	*Fluorescence-activated cell sorting*

FASN	*Fatty acid synthase*
FCS	*Fetal calf serum*
GC	*Group-specific component*
GC/MS	*Gas chromatography/mass spectrometry*
G6P	*Glucose-6-phosphate*
G6PD	*Glucose-6-phosphate dehydrogenase*
GLS	*Glutaminase*
GLUT1	*Glucose transporter 1*
GOT1	*Glutamic-oxaloacetic transaminase 1*
GOx	*Glucose oxidase*
HEPES	*4-(2-hydroxyethyl)-1-piperazineethanesulfonic acid*
HIF1a	*Hypoxia-inducible factor 1a*
HKII	*Hexokinase II*
HRP	*Horseradish peroxidase*
IDH	*Isocitrate dehydrogenase*
KLK3	*Kallikrein-3 or prostate specific antigen*
LDHA	*Lactate dehydrogenase A*
LKB1	*Liver-kinase B1*
MLX	*Max-like protein X*
mTOR	*Mammalian target of rapamycin*
NC	*Negative control*
NDUFA1	*NADH ubiquinone oxidoreductase subunit A1*
OGDH	*Oxoglutarate dehydrogenase*
PAGE	*Polyacrylamide gel electrophoresis*
PDHA1	*Pyruvate dehydrogenase E1 component alpha 1 subunit*
PDK or PDHK	*Pyruvate dehydrogenase kinase*
PEP	*Phosphoenolpyruvate*
PGC1A	*Peroxisome proliferator-activated receptor gamma coactivator 1-alpha*
PHGDH	*Phosphoglycerate dehydrogenase*
PI3K	*Phosphatidylinositol 3-kinase*
PIP3	*Phosphatidylinositol-3,4,5-triphosphate*
PKM2	*Pyruvate kinase M2*
PMSF	*Phenylmethane sulfonyl fluoride*
PPP	*Pentose phosphate pathway*

PTEN	*Phosphatase and tensin homolog*
PTH	*Parathyroid hormone*
PVDF	*Polyvinylidene fluoride*
PUMA	*p53 upregulated modulator of apoptosis*
RANKL	*Receptor activator of nuclear factor kappa-B ligand*
RM	*Running medium*
RPMI	*Roswell Park Memorial Institute*
RXR	*Retinoid X receptor*
ROS	*Reactive oxygen species*
SD	*Standard deviation*
SDHC	*Succinate dehydrogenase complex subunit C*
SDS	*Sodium dodecyl sulfate*
SDRs	*SensorDish® Readers*
SEM	*Standard error of the mean*
SNPs	*Single nucleotide polymorphisms*
SRB	*Sulforhodamine B*
SREBP1c	*Sterol regulatory element-binding protein 1*c
SSP	*Serine synthesis pathway*
TCA cycle	*Tricarboxylic acid cycle*
TEMED	*Tetramethylethylenediamine*
TFAM	*Transcription factor A, mitochondrial*
TIGAR	*TP53-inducible glycolysis and apoptosis regulator*
TRPV6	*Transient receptor potential cation channel, subfamily V, member 6*
TSC	*Tuberous sclerosis complex*
TXNIP	*Thioredoxin-interacting protein*
VDR	*Vitamin D receptor*
VDRE	*Vitamin D response element*
VDUP1	*Vitamin D_3 upregulated protein 1*
VEGF	*Vascular endothelial growth factor*

V. List of figures

VI. List of tables

1. INTRODUCTION

1.1. Vitamin D and human health

Our understanding of vitamin D and its effects on humans has gone a long way since the investigations early in the twentieth century that aimed at discovering the anti-rachitic component of cod liver oil. Although the German steroid chemist Adolf Windaus was awarded the Nobel prize in Chemistry for his work on the "*constitution of sterols and their connection with vitamins*" in 1928 [1], research in the vitamin D field had stagnated for years before a series of landmark discoveries brought the molecule back in the limelight (**Figure 1**).

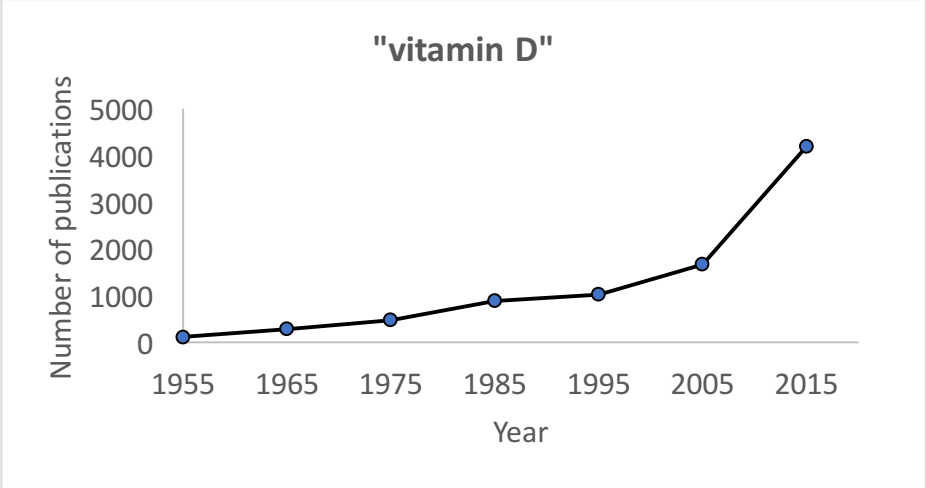

Figure 1: PubMed/MEDLINE search using "vitamin D" as a keyword. *An exponential increase in the number of publications on vitamin D is observed towards the end of the twentieth century, with the number of publications on this topic surpassing doubling between 2005 and 2015.*

Despite the classification as a vitamin, adequate and regular exposure to sunlight, precisely UV-B, is proposed to provide humans with sufficient vitamin D levels without the need for dietary supplementation [2]. Vitamin D is a fat-soluble vitamin that exists in two forms, D_3 (cholecalciferol) and D_2 (ergocalciferol) [3]. Bound to its binding protein, vitamin D is transported to the liver, the site of the first hydroxylation step, occurring at the 25-position [4]. The identity of the enzyme catalyzing this step has been contentious, however, recent evidence

has illustrated that the cytochrome P450 (CYP) 2R1 enzyme is a major vitamin D-25-hydroxylase [5]. The resulting metabolite, 25-hydroxyvitamin D, is the major circulating metabolite, and is currently used as the biomarker for vitamin D status in the clinic [6]. The second metabolizing/activating step takes place mainly in the kidneys, and is catalyzed by the 25-hydroxyvitamin D-1-hydroxylase, CYP27B1, which yields the bioactive form of the vitamin, 1,25-dihydroxyvitamin D [$1,25(OH)_2D_3$], also known as calcitriol [4]. Subsequently, the molecule binds to the nuclear vitamin D receptor (VDR) present in target cells, triggering its hetero-dimerization with retinoid X receptor (RXR), leading to binding to vitamin D response elements (VDRE) on promoters of target genes, including those involved in calcium homeostasis [4]. An increase in the levels of calcitriol induces the expression of CYP24A1, the catabolizing enzyme that converts the molecule to reduced activity metabolites [7].

In view of this, vitamin D had been mainly thought of as a major regulator of skeletal health, however, recent findings have reshaped this classical notion, including the identification of VDRs as well as the enzymatic machinery required for vitamin D metabolism and bio-activation in diverse types of cells [3]. In other words, in addition to acting in an endocrine fashion, vitamin D also works in an autocrine manner [4]. It is therefore conceivable that the molecule plays multiple roles in these non-classical target cells. Additionally, besides genomic effects, an increasing number of studies has demonstrated that $1,25(OH)_2D_3$ also induces rapid, non-genomic effects, such as rapid calcium absorption (transcaltachia), as well as insulin secretion [8].

Further supporting the proposed extra-skeletal effects of vitamin D are the epidemiological data demonstrating a correlation between suboptimal vitamin D levels and a myriad of chronic diseases, including cardiovascular disease, autoimmune diseases, and cancers [3, 4]. Based on this evidence, researchers worldwide have initiated numerous clinical trials to assess the therapeutic utility of the molecule against these diseases [9]. Of interest is the fact that guidelines for vitamin D supplementation as well as vitamin D status classification, issued by the Institute of Medicine and the Endocrine Society are different [9].

1.2. Vitamin D and cancer

1.2.1. Epidemiology

Over the years, many studies have linked vitamin D deficiency to increased incidence and poor prognosis of cancer [3, 4, 9]. Reports highlighting this potential date back to the 1980s [10], in which investigators observed an inverse correlation between UV radiation and the incidence of cancer. Since then, plentiful observational studies have demonstrated an inverse correlation between vitamin D status and different cancers [4, 9]. However, randomized-controlled trials evaluating the usefulness of vitamin D in reducing cancer risk have been so far inconclusive, at least in part due to insufficient dosing used [11]. Moreover, limitations of many conducted clinical trials include: i) associating health outcomes with vitamin D intake rather than circulating concentrations of 25(OH)D, ii) assuming that the clinical trial is the only source of the molecule for the subjects, which is typically the case with pharmaceuticals, and iii) recruiting subjects independent of baseline 25(OH)D levels, i.e. subjects may not be vitamin D deficient in the first place [11].

Despite this, several clinical trials have reported beneficial outcomes with vitamin D supplementation, an example of which is the Women's Health Initiative, in which the investigators described reduced incidence of total, as well as breast and invasive breast cancers, in women receiving vitamin D and calcium supplement, provided they did not initially receive personal vitamin D and calcium supplementation [12].

A recently conducted genome-wide association study has demonstrated a connection between single nucleotide polymorphisms (SNPs) in genes involved in the vitamin D pathway and 25-hydroxyvitamin D levels in subjects of European descent [13]. Genes implicated in these studies include *DHCR7* (7-dehydrocholesterol reductase), *GC* (group-specific component), and *CYP2R1* [13]. The first gene encodes an enzyme that converts 7-dehydrocholesterol to cholesterol, which is the last step in the cholesterol biosynthetic pathway [13]. Since 7-dehydrocholesterol is the starting molecule for vitamin D_3 photosynthesis in the skin, a clear connection between polymorphisms in the *DHCR7* gene and 25-hydroxyvitamin D levels could be drawn, on the basis that an altered enzymatic activity associated with a particular genetic

variant may influence the levels of its substrate available for vitamin D_3 production. The *GC* gene on the other hand encodes the vitamin D binding protein, which functions as a transporter of vitamin D and its metabolites [13]. SNPs in this gene have been shown to influence the affinity of the protein to its cargo molecules, as well as overall levels of the protein, thus impacting total and bioavailable/free 25-hydroxyvitamin D levels [14]. Given the correlation of SNPs in these genetic loci with vitamin D status, several studies have explored their association with different diseases including cancers, however, such investigations have reported conflicting associations with cancer risk [15-17].

In addition to genetic polymorphisms, alterations in the expression level of vitamin D genes, such as the *VDR*, *CYP27B1*, and *CYP24A1* genes, have been reported [9]. For example, CYP24A1 amplification has been observed in cancer cells, which may influence the efficacy of vitamin D-based therapies [9]. Treatment of tumor cells with CYP inhibitors in combination with calcitriol has been shown to enhance the latter's anti-cancer potential [18, 19], however, it should be noted that inhibiting the degradation of vitamin D metabolites may also augment unwanted calcemic effects. Alterations in the expression of CYP27B1 on the other hand have been shown to be influenced by the tumor grade and the extent of cellular differentiation [20]. Moreover, elevated VDR expression in prostate [21], breast [22], and colorectal cancer [23] cells has been linked to better prognosis in patients.

1.2.2. Molecular mechanisms

The discovery of calcitriol's ability to exert anti-cancer effects originates from two articles published in 1981, in which the authors of the first report described the anti-proliferative effect of the molecule in malignant melanoma cells [24], and the induction of differentiation in myeloid leukemia cells in the second one [25].

The now known anti-cancer effects calcitriol and its analogs induce in tumor cells are diverse, and new properties are frequently reported in the literature [7, 9]. Vitamin D compounds have been shown to modulate different pathways aberrantly regulated in cancers, including cell cycle control and proliferation, as well as differentiation and inflammation [9]. Additionally, calcitriol possesses a myriad of tissue-specific anti-cancer effects, such as induction of differentiation in myeloid leukemia and prostate cancer cells, hampering of estrogen signaling

in breast cancer cells, and inhibition of the Wnt/ β-catenin signaling pathway in colon cancer cells [9].

Other more "general" effects have also been observed in multiple tumor types such as induction of the cell cycle inhibitor p21, and reduction in the MYC oncogene, both of which are reported vitamin D target genes [26, 27]. Furthermore, with regards to apoptotic signaling, calcitriol has been shown to modulate the expression of members of the Bcl2 family of proteins, with the expression of anti-apoptotic members, for example Bcl2, downregulated in cancer cells with treatment, and pro-apoptotic members, namely BAX, induced [9].

Intriguingly, in cultured prostate cancer cells, calcitriol treatment has been shown to markedly induce androgen receptor (AR) expression [28, 29]. While this may appear counter-therapeutic since therapies used in prostate cancer management aim to inhibit androgen signaling [30], this induction in AR levels by calcitriol in LNCaP cells appears to be critical to the molecule's anti-tumor activities. Specifically, it has been shown that culturing these cells in medium supplemented with charcoal-stripped serum, or co-treating cells with the AR antagonist casodex in normal medium (i.e. supplemented with serum containing endogenous androgens), markedly limits calcitriol's growth-inhibiting effects [31], which altogether indicates that basal AR activity is necessary for such anti-tumor activities. Further analyses revealed that the androgen-induced, proliferation shutdown-associated gene, *AS3*, was induced by $1,25(OH)_2D_3$ in LNCaP cells, and that this induction was abrogated in the presence of casodex [32]. Therefore, these findings highlight the potential anti-tumor antagonism of calcitriol and casodex (or other AR antagonists), which are otherwise independently potent in androgen-dependent prostate cancer cells.

In colorectal cancer cells, the expression levels of the transcription factor SNAIL have been shown to influence the efficacy of calcitriol and its analogs, due to its ability to reduce the expression of VDR [33]. Moreover, an inverse correlation between SNAIL and VDR expression has been reported in human colon cancers, and that colon cancer cells overexpressing SNAIL resist EB1089's (a vitamin D analog) growth inhibiting effects [33]. Additionally, SNAIL has been shown to hamper calcitriol's ability to induce E-cadherin [33]. Therefore, SNAIL expression level has been proposed to be a determinant of the success of vitamin D compounds in colon cancer treatment [34].

1.2.3. Vitamin D in cancer treatment: analogs and combination chemotherapy

A clear setback in vitamin D-based chemotherapy is the supra-physiological doses required to elicit potent anti-tumor effects, which may lead to hypercalcemia [35]. To overcome this setback, numerous hypo-calcemic vitamin D analogs have been developed with similar, or even more potent transactivation potential compared to the parent molecule, in normo-calcemic doses [35]. Several analogs have successfully made their way to the clinic, such as calcipotriol, which is currently used to treatment psoriasis, the hyper-proliferative skin disorder [35].

Although not completely understood, several studies have aimed at elucidating the underlying mechanism of reduced calcemic effects of these vitamin D analogs, and few explanations have been provided so far, including: i) altered catabolism, leading to tissue selectivity, since different types of cells may promote specific catabolic pathways [35]; and ii) promoter selectivity [36], due to differential VDR-RXR stabilization by analogs at different kinds of VDREs. For instance, the vitamin D analog EB1089 has been shown to preferentially stabilize VDR-RXR at VDREs of the IP9-type, more than at the classical DR3-type [37]. While both binding motifs are characterized by two hexameric nucleotide sequences, these sequences are inverted palindromic and separated by 9 nucleotides in case of the former, whereas direct repeats and separated by 3 nucleotides in case of the latter [36]. Since EB1089 has been shown to exert more potent anti-cancer effects than calcitriol, for example in breast cancer cells [38], it is possible that genes associated with the molecule's anti-tumor effects harbor IP9-type VDREs. While this notion has not been proven, supporting this possibility is the fact that the cell cycle regulator p21, which is a vitamin D-target gene, harbors such motif [39].

A different approach, one that serves both vitamin D-based therapies as well as other chemotherapeutics, is combination chemotherapy. This strategy is widely used in oncological settings to enhance the efficacy as well as reduce the side effects of the drugs used. In colorectal cancer for instance, the use of the FOLFOX regimen, composed of folinic acid, 5-fluorouracil (5-FU), and oxaliplatin, has been shown to be therapeutically advantageous compared to mono-therapies [40]. Investigating the combination of vitamin D compounds with classical and repurposed chemotherapeutics is a recurring theme in vitamin D literature, with several combinations proposed to be more potent than the corresponding single entities. For example, a recent report has illustrated that in animal models of pancreatic ductal adenocarcinoma, calcipotriol induces profound transcriptional changes in the tumor stroma, that lead to improved

tumoral delivery of the drug gemcitabine, and enhanced survival in animals receiving both drugs [41]. Besides this study, numerous reports have combined different VDR activators with drugs with diverse mechanisms of action, such as anti-metabolites [42], platins [43], and tyrosine kinase inhibitors [44], with mainly beneficial outcomes reported.

1.3. Tumor metabolism: mechanisms and therapies

1.3.1. The Warburg effect and beyond

Early in the twentieth century, seminal findings by Otto Warburg demonstrated that rapidly proliferating cancerous cells exhibit a distinct metabolic phenotype compared to normal cells [45]. Transformed cells were found to ferment glucose to lactate independent of oxygen levels, an observation coined as the "Warburg effect" or "aerobic glycolysis" [45]. Paradoxically, cancer cells seemed to prefer a less efficient energy-generating process—glycolysis—over mitochondrial respiration. Warburg initially proposed that mitochondrial defects in cancer cells dictated their metabolic "possibilities", however, it is now known that mitochondrial functions are not impaired in tumors, and that other underlying mechanisms may account for the observed metabolic reprogramming [45]. Furthermore, it is now widely accepted that the metabolic requirements of cancer cells exceed the need for ATP. In other words, for one parent cell to produce two daughter cells, cellular contents need to be duplicated, and thus in rapidly dividing cells, metabolism is tailored to shunt glucose into both biomass- and ATP-producing pathways [45].

Over the years, investigations into this field have spawned a wealth of knowledge on the cancer type-specific metabolic aberrations, as well as possible contributors. For example, in prostate cells, malignancy-driven metabolic rewiring leads to inhibition of zinc accumulation, thereby relieving aconitase inhibition, and enabling complete citrate oxidation [46]. Moreover, in advanced castration-resistant prostate cancers, in addition to alterations in glucose metabolism, the disease is characterized by a lipogenic phenotype [47]. In breast cancers, studies have suggested that estrogen receptor (ER)-positive and –negative subtypes exhibit different metabolic phenotypes, where ER-positive cells have been described to adopt more typical Warburg metabolism, whereas ER-negative cells exhibit a higher dependence on glutamine

metabolism [48], a phenomenon known as "glutamine addiction". Additionally, it has been shown that ER-negative breast cancer cells exhibit increased expression of the key de novo serine synthesis enzyme phosphoglycerate dehydrogenase (PHGDH) compared to ER-positive cells [49].

1.3.2. Regulation of onco-metabolism by oncogenes and tumor suppressors

While the consensus that cancer is a genetic disease remains, recent studies have argued that it is also a metabolic disease, since conditions such as obesity and insulin resistance are risk factors for cancer [50]. Recently, both schools of thought have been reconciled, with the demonstration that the genetic mutations in key tumor suppressors and proto-oncogenes that contribute to carcinogenesis also impact metabolic networks [51].

1.3.2.1. p53 and metabolism

Designated the "guardian of the genome", p53's canonical actions include cell cycle regulation and facilitation of DNA repair mechanisms, as well as regulation of apoptotic signaling [52]. The *TP53* gene, encoding the p53 protein, is the most highly mutated gene in cancers [53], with mutations not only leading to loss of wild-type functions, but also generation of the so-called "mutant p53", which is a pro-survival transcription factor [53]. Interestingly, the initial incorrect characterization of *TP53* as an oncogene resulted from the cloning of a mutated version of the gene [53].

Besides its well documented functions in maintaining genome integrity, recent studies have illustrated that p53 is a key metabolic regulator that works through influencing various arms of cellular energy production and utilization [54]. In tumor cells, wild-type p53 has been shown to dampen the Warburg effect and induce mitochondrial respiration, via modulating the expression of pivotal proteins, such as the glucose transporter 1 (GLUT1) and pyruvate dehydrogenase kinase (PDK) 2 [54], the enzyme responsible for phosphorylating the pyruvate dehydrogenase complex thus inhibiting its activity, which ultimately controls mitochondrial respiratory rate. p53 is also known to influence tricarboxylic acid (TCA) cycle anaplerosis, through inducing the expression of glutaminase (GLS) 2, which converts glutamine to glutamate, which can then be converted to alpha-ketoglutarate (α-KG) and incorporated into

the TCA cycle [54]. Furthermore, p53 has been shown to differentially modulate the pentose phosphate pathway (PPP) [54]. The nature of this regulation has been proposed to be subject to the degree of p53 activation, where activation in response to oxidative stress induces *TIGAR* (TP53-inducible glycolysis and apoptosis regulator), which leads to an increased flux through the PPP, essentially generating NADPH for oxidative defense [54]. TIGAR is a bisphosphatase that induces the conversion of fructose-2,6-bisphosphate, an allosteric activator of the rate-limiting glycolytic enzyme phosphofructokinase, to fructose-6-phosphate [54]. In this regard, the molecule limits glycolytic flux and increases shunting of metabolites into the PPP. On the other hand, p53 is known to bind to the rate-limiting PPP enzyme glucose-6-phosphate dehydrogenase (G6PD) thus inhibiting its activity [54], leading to an inhibition of flux through this pathway and possibly reducing the levels of building blocks necessary to sustain tumor survival. Moreover, p53 also influences fatty acid metabolism, through reducing fatty acid biosynthesis and inducing beta-oxidation [54]. The former effect is partially achieved through reducing the expression of SREBP1c (sterol regulatory element-binding protein 1c), a transcription factor known to drive the expression of key enzymes in fatty acid biosynthesis, such as fatty acid synthase (FASN), ATP citrate lyase (ACLY), and acetyl CoA carboxylase (ACC) [54]. With regards to fatty acid beta-oxidation, p53 has been shown to induce carnitine acetyltransferases expression levels, which transport fatty acids to the mitochondria [54].

1.3.2.2. PI3K/PTEN/Akt signaling

The PI3K (phosphatidylinositol 3-kinase) pathway is a central regulator of metabolic networks in cancerous cells [55]. PI3K activation produces PIP3 (phosphatidylinositol-3,4,5-triphosphate), a phospholipid which acts as an inducer of downstream targets, including Akt [55, 56]. This process is tightly regulated under normal conditions by the tumor suppressor PTEN (phosphatase and tensin homolog), which dephosphorylates PIP3, thereby inhibiting downstream pathways [55, 56]. In cancers however, activating and inhibiting mutations have been described in PI3K and PTEN, respectively, which deregulate the pathway, leading to the activation of Akt and triggering of metabolic transformation [55, 56]. Among the observed changes in cells' metabolic profile upon activation of oncogenic Akt signaling is a potent induction in glycolysis, mediated by an increase in glucose uptake and expression of key glycolytic genes such as hexokinase II (HKII) and lactate dehydrogenase [57]. Additionally,

Akt activation induces mammalian target of rapamycin (mTOR) signaling [57], which also impacts cellular nutrient availability and utilization [58].

1.3.2.3. c-Myc and HIF1a

c-Myc is an oncogene that is estimated to be overexpressed in 70% of cancers [59]. Similarly, HIF1a (hypoxia-inducible factor 1a) is known to be amplified in cancers due to intra-tumoral hypoxia [59]. Both moieties are transcription factors that regulate the expression of various transporters and enzymes involved in glucose metabolism [59]. Hyper-activation of both factors in transformed cells triggers a metabolic program, including induced glycolysis, which enables survival under hypoxic conditions [59].

1.3.2.4. LKB1/AMPK/mTOR signaling

AMP-activated protein kinase (AMPK) is a heterotrimeric complex that acts as an integral cellular metabolic sensor, responding to energetic stress (elevation in AMP:ATP ratio) through inhibiting and activating energy-depleting and –producing pathways, respectively [60]. In doing so, AMPK elevates ATP levels and prevents metabolic distress [60].

The mechanism of AMPK activation involves binding of AMP to the complex's gamma subunit, allosterically activating it, and enabling its further activation by its upstream kinase liver kinase B1 (LKB1), which phosphorylates threonine 172 on AMPK's alpha-subunit [60]. LKB1 is a well characterized tumor suppressor, with mutations in the *LKB1* gene implicated in different tumors, as well as in the genetic disorder Peutz-Jegher's syndrome, in which sufferers have a predisposition to the development of various tumor types [61]. Moreover, besides activation of AMPK as a result of energetic stress, an increase in intracellular Ca^{2+} levels induces the activity of CAMKK2 (calcium/calmodulin-dependent kinase kinase 2), AMPK's other activating kinase [60].

AMPK's metabolic effects are highly versatile, and include modulation of glucose uptake, glycolysis, gluconeogenesis, fatty acid metabolism, mitochondrial biogenesis, and finally, autophagy [60]. Additionally, AMPK activation leads to inhibition of the pro-survival mTOR pathway, thereby inhibiting protein synthesis [60]. In view of these effects, one is faced with the possibility that AMPK could acts as a tumor suppressor as well as an oncogene [62]. In

favor of the former is: i) the activation of this molecule by LKB1 (a tumor suppressor), ii) the resulting inhibition of mTOR, and finally, iii) phosphorylation and subsequently stabilization of tumor suppressor p53 by AMPK, leading to a metabolic cell cycle checkpoint. On the other hand, AMPK-mediated induction of energy-generating pathways, including glucose uptake, beta-oxidation of fatty acids, and autophagy, may enable cancer cells survive starvation.

1.3.3. Therapeutic approaches for cancer metabolism

Several reasons account for the clear emergence of cancer metabolism as a viable therapeutic target, including associations between aberrations in whole-body metabolism and cancer initiation and progression [50]. Furthermore, successful anti-cancer drugs that are currently in clinical use have either direct metabolic targets, such as 5-FU and methotrexate, which target thymidylate synthase and dihydrofolate reductase, respectively, or impact metabolic processes such as glucose uptake, which is the case of tyrosine kinase inhibitors [50]. The latter highlights the potential use of fluorodeoxyglucose-positron emission tomography as a predictor of response to chemotherapeutics that modulate signaling aberrations in cancer.

However, multiple challenges remain in this field, for example, identifying metabolic targets that are safe to "drug" in cancer cells, while having minimal effects on normal or rapidly proliferating non-malignant cells, i.e. selectivity [50]. Noteworthy is that besides aerobic glycolysis and glutamine addition, which are known to be exhibited by different cancers, cancer type-specific metabolic aberrations have been reported, which may enable the (semi)-selective targeting of metabolism in cancer patients. For example, some cancers, such as prostate cancer and hepatocellular carcinoma, have been shown to be deficient in argininosuccinate synthase 1, an important enzyme in de novo synthesis of the semi-essential amino acid arginine [63]. These tumors mainly rely on exogenous sources of arginine, making them "arginine auxotrophic" [63], and thus, depleting this extracellular supply, for example by using recombinant arginases [64], may impact tumor cell metabolism while having minimal effects on healthy cells' metabolism.

Moreover, cellular metabolism exhibits marked plasticity, which enables cells to bypass/overcome a metabolic insult induced by an anti-cancer drug targeting a particular metabolic enzyme, i.e. resistance [50]. In this regard, utilizing advanced technologies in

metabolic flux analyses will facilitate the tracing of these “escape routes” [50], and ultimately allow designing combinational strategies targeting different metabolic pathways simultaneously.

Table 1: List of promising novel and repurposed "metabolic" drugs that have demonstrated anti-tumor potential in cell-based and preclinical models. *Such drugs limit either nutrient availability (e.g. recombinant human arginase 1) or utilization (e.g. metformin).*

Drug	Target	Rationale	Experimental evidence	References
CBR-5884	PHGDH	PHGDH, which catalyzes the first step in de novo serine synthesis, has been shown to be overexpressed in various cancers, making its inhibition a therapeutic strategy.	This small molecule has been recently shown to be toxic to breast cancer cell lines more reliant on de novo serine synthesis, but not to those more dependent on exogenous sources.	[65]
CB-839	GLS	Cancer cells are known to exhibit "glutamine addiction", where studies have shown that glutamine is the second used nutrient in culture medium after glucose. GLS catalyzes the conversion of glutamine to glutamate, which can then contribute to TCA cycle anaplerosis.	In preclinical studies, treatment of triple-negative breast cancer models, as well as multiple myeloma xenografts with the drug yielded beneficial results. Clinical trials assessing the molecule's efficacy in breast cancer and renal cell carcinoma patients are underway.	[64, 66]
rhArg1-PEG	Arginine	Some tumor cells are arginine auxotrophic, therefore, depleting extracellular/serum arginine by recombinant arginases is therapeutically advantageous.	Treatment induces anti-tumor effects in in-vitro and in-vivo models of T-cell leukemia, and the molecule is currently in clinical trials of refractory lymphoma and leukemia.	[63]

2-Deoxyglucose	Hexokinase	Inhibition of glycolysis in cancer cells potentially leads to metabolic collapse and cell death.	Tumor cells treated with 2-Deoxyglucose undergo apoptosis and/or growth arrest. Clinical data however illustrate that toxic effects are associated with therapy.	[50]
AG-221	Isocitrate dehydrogenase (IDH) 2	*IDH 1* and *2* genes are the most frequently mutated metabolic genes in tumors. These mutants give rise to the onco-metabolite R-2-hydroxyglutarate, which alters cells' epigenetic profile and hampers cellular differentiation.	AG-221 has shown beneficial effects in ex-vivo and xenograft models of acute myeloid leukemia (AML), and is currently being tested in clinical trials against AML and solid tumors.	[67-69]
Metformin	Mitochondrial complex I	Inhibition of this target significantly reduces mitochondrial respiratory capacity, leading to substantial energetic stress and loss of cellular viability.	Preclinical data demonstrate the potential utility of this molecule against different tumors, and several clinical trials are currently underway to investigate the efficacy of metformin against cancer.	[70]
Orlistat	FASN	FASN has been shown to be overexpressed in different cancers, and is associated with poor prognosis and reduced disease-free survival in patients. Overexpression of FASN has also been linked to chemoresistance.	Orlistat has demonstrated anti-tumor potential in different cancer cell lines and preclinical models, most notably prostate cancer models.	[71]

Etomoxir	Carnitine palmitoyl-transferase 1 (CPT1)	Fatty acid oxidation is an essential pathway for cancer cells to obtain ATP as well as NADPH for anabolic and redox processes. CPT1, which conjugates fatty acids with carnitine enabling their transport into the mitochondria for further metabolism, has been shown to be overexpressed in tumors, making it a potential drug target.	Studies utilizing different human cancer cell lines, as well as a preclinical murine model of leukemia, demonstrated anti-cancer effects with etomoxir treatment. However, hepatotoxicity was observed in patients treated with the drug in a clinical trial.	[72-75]

1.4. Rationale and working hypothesis of the present research

In light of the aforementioned data on the skeletal and supra-skeletal effects of calcitriol, I proposed that the molecule may also regulate energy production and utilization pathways in cancer cells. Although this theme had not been thoroughly investigated, few groups have reported on the ability of $1,25(OH)_2D_3$ to influence cellular metabolism in different cell types, including transformed breast epithelial cells and dendritic cells [76, 77]. Furthermore, several pathways that are directly connected to nutrient metabolism and energetic stress have been shown to be impacted by $1,25(OH)_2D_3$ treatment. For example, in both normal and transformed cells, calcitriol and its analogs have been shown to induce autophagy [78-82], a pro-survival pathway that is activated in response to starvation [83], via directly influencing autophagy genes [82], or through inducing AMPK signaling [78]. Additionally, $1,25(OH)_2D_3$ has been shown to negatively regulate the expression of oncogenes implicated in tumor metabolism, namely c-Myc [27] and HIF1a [84]. Moreover, profound crosstalk between vitamin D and p53 signaling has been reported [85, 86], indicating that putative metabolic effects could be executed through this channel. Finally, the key glucose-metabolizing gene—G6PD—as well as the regulator of glucose homeostasis, thioredoxin-interacting protein (TXNIP), have been proposed to be direct targets of $1,25(OH)_2D_3$ [87, 88], which altogether served as the basis for the proposed research (**Figure 2**, modified from Abu el Maaty and Wölfl [89]). I focused on prostate and breast cancer cell lines in my work since studies have shown that $1,25(OH)_2D_3$ induces multi-faceted anti-cancer effects in both in-vitro and in-vivo models of both diseases [9]. Results of my investigations on prostate cancer cell lines have been recently published [90].

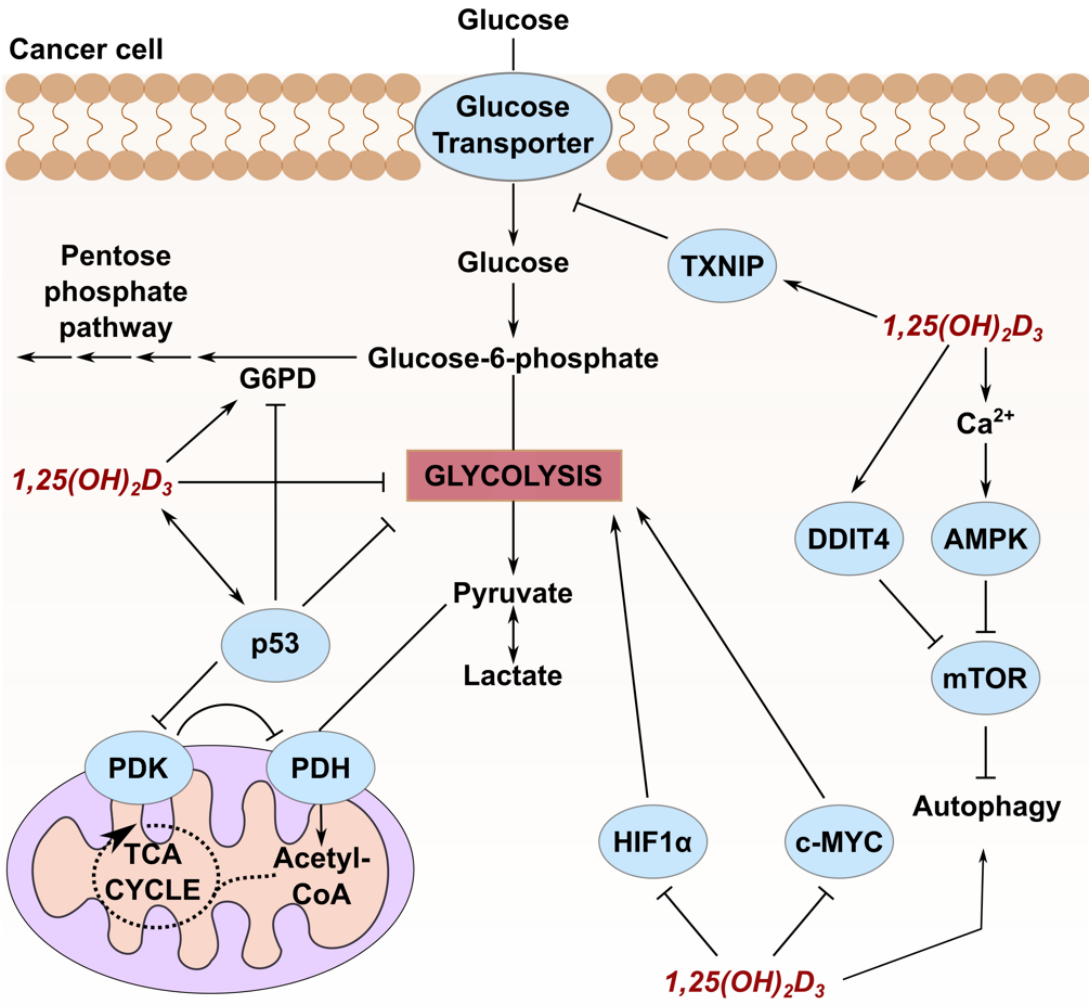

Figure 2: Potential regulation of metabolic networks by 1,25(OH)$_2$D$_3$ through influencing different metabolism-related tumor-suppressors, oncogenes, and signaling molecules. *Experimental evidence indicating calcitriol's potential effects on energy metabolism include: i) the ability of calcitriol to reduce the expression of the oncogenes c-Myc and HIF1a, which are known drivers of aerobic glycolysis, ii) activation of AMPK signaling and inhibition of the mTOR pathway by VDR activators, iii) crosstalk between VDR and p53 signaling, and iv) putative induction in G6PD and TXNIP expression by 1,25(OH)$_2$D$_3$. Figure modified from Abu el Maaty and Wölfl [89].*

2. RESULTS

2.1. Regulation of glucose-metabolizing pathways in prostate cancer cells by calcitriol.

2.1.1. 1,25(OH)$_2$D$_3$ induces diverse changes in glucose metabolism of prostate cancer cells.

The normal prostatic epithelium is known to exhibit a unique metabolic phenotype, characterized by a truncated TCA cycle due to an increase in intracellular Zn^{2+} levels, which inhibit the enzyme aconitase, leading to citrate accumulation [46]. Citrate is subsequently released in the seminal fluid to provide an energy source for sperm [91]. In malignant prostate cells, this phenotype is reversed, and citrate is further oxidized through the TCA cycle to yield reducing equivalents [46].

To investigate the ability of 1,25(OH)$_2$D$_3$ to regulate glucose metabolism in prostate cancer cells, I utilized the biosensor chip system BIONAS 2500 to simultaneously measure, in real-time, changes in glycolytic and respiratory rates, measured as extracellular acidification and oxygen consumption rates, respectively, as well as impedance, which provides information on the adherence/viability of cultured cells on the biosensor chip. To this end, I included in my study four prostate cancer cell lines of different androgen sensitivities: LNCaP and VCaP, representing androgen receptor (AR)-positive prostate cancer, as well as DU-145 and PC-3, representing AR-negative prostate cancer. Running medium (RM) not containing any treatment was first continuously introduced to the chips for 6h, after which either 1,25(OH)$_2$D$_3$- or dimethyl sulfoxide (DMSO)-treated RM was pumped for 72h, which was then followed by a recovery period of approximately 15h, in which cells were exposed to DMSO-treated RM. The three mentioned parameters were monitored throughout the course of the experiment.

Interestingly, I observed significant reductions in glycolytic and respiratory rates in response to 1,25(OH)$_2$D$_3$ treatment in all investigated cell lines, however, more potent changes were observed in the AR-positive cell lines LNCaP and VCaP (**Figure 3**).

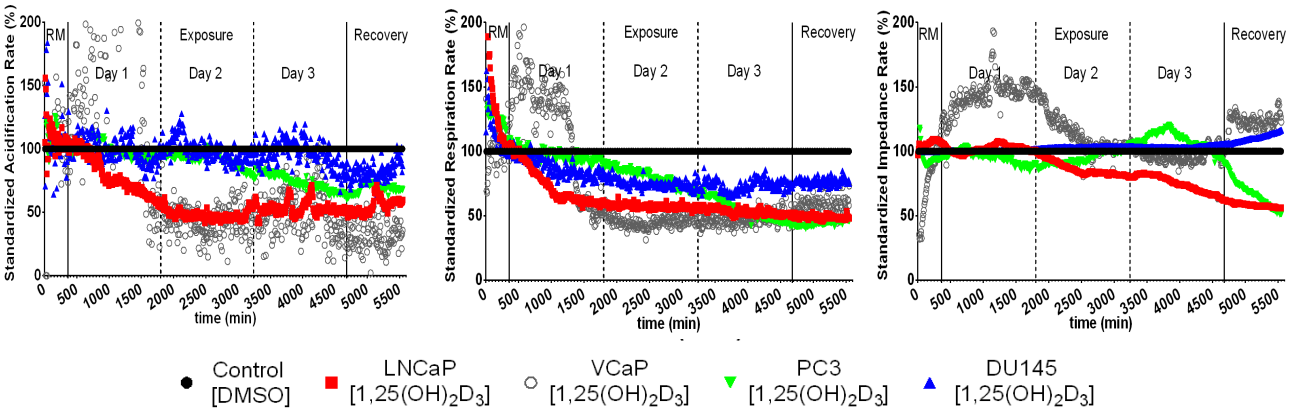

Figure 3: Real-time measurements of cellular bioenergetics in prostate cancer cell lines treated with 1,25(OH)$_2$D$_3$ (100 nM) using the Bionas 2500 biosensor chip system. *Measurements obtained from 1,25(OH)$_2$D$_3$ -treated cells were normalized to those from DMSO-treated ones of the same cell line, however the data pertaining to all cell lines are presented together. The AR-positive cell lines LNCaP and VCaP appeared to be more responsive, in terms of altering their glycolytic capacity, to 1,25(OH)$_2$D$_3$ treatment, since their extracellular acidification rates were found to be reduced within the first day of treatment. Respiratory capacity of all cell lines, on the other hand, was found to be reduced in response to 1,25(OH)$_2$D$_3$, within the first day of treatment, with varying degrees. With regards to cellular viability, illustrated by impedance rate, only LNCaP cells were found to be impacted by 1,25(OH)$_2$D$_3$ treatment, with impedance rate found to be reduced starting second day of treatment. Results are representative of two biological replicates. Figure obtained from Abu el Maaty et al. [90].*

Focusing on LNCaP cells, I performed thorough analyses to investigate the diversity of 1,25(OH)$_2$D$_3$'s metabolic effects. Since both extracellular acidification and oxygen consumption rates were clearly reduced by treatment in this cell line, I hypothesized that 1,25(OH)$_2$D$_3$ influences metabolic aberrations that are observed in different cancer types, e.g. enhanced glucose uptake, as well as prostate-specific metabolic aberrations, e.g. the previously mentioned reversal of TCA cycle truncation. To address these possibilities, I first studied changes in glucose uptake of LNCaP cells in response to 1, 2, and 3 days of treatment with calcitriol, by measuring the concentration of glucose in the culture medium of both 1,25(OH)$_2$D$_3$- and vehicle-treated cells, as well as by measuring the intracellular amount of 2-NBDG (2-[N-(7-nitrobenz-2-oxa-1,3-diazol-4-yl) amino]-2-deoxy-D-glucose), a fluorescently labelled glucose analog, using fluorescence-activated cell sorting (FACS) analysis. I observed

significantly higher levels of glucose in the medium of $1,25(OH)_2D_3$-treated cells, and lower intracellular levels of 2-NBDG, across the investigated time course (**Figure 4a,b**), demonstrating a clear reduction in the uptake of glucose from the culture medium. I postulated that these effects may be coupled to a reduction in GLUT1 expression. This protein has been shown to be overexpressed in different tumors, and that this expression correlates with clinical outcome [92]. Indeed, I found that GLUT1 protein expression was significantly reduced in LNCaP cells after 72h of treatment with $1,25(OH)_2D_3$ (**Figure 4c,d**).

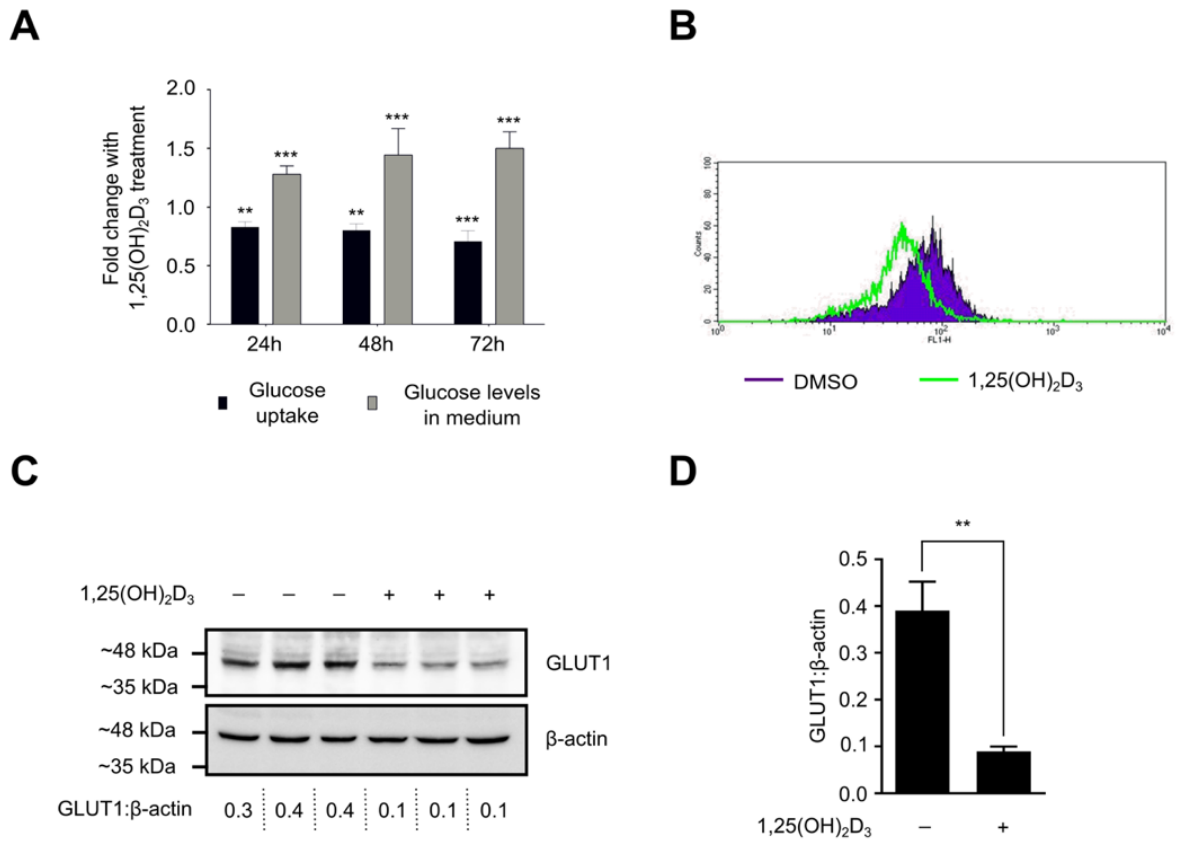

Figure 4: 1,25(OH)$_2$D$_3$ (100 nM) negatively influences glucose uptake in LNCaP cells. *(A) Glucose uptake by DMSO- and 1,25(OH)$_2$D$_3$-treated LNCaP cells was evaluated using the fluorescently labeled glucose analog 2-NBDG coupled with FACS analysis, whereas levels of glucose in the medium were evaluated by the glucose oxidase (GOx) assay. The significant reduction observed in glucose uptake with 1,25(OH)$_2$D$_3$ treatment is complemented by a significant increase in glucose levels in the culture medium of such cells. Results of 1,25(OH)$_2$D$_3$-treated cells of both experiments were normalized to their respective controls, and results are presented as fold change in the parameter investigated with treatment. Error bars ± standard deviation (SD) ; n=3. A two-tailed Student's t-test was used to compare the results of DMSO- and 1,25(OH)$_2$D$_3$-treated cells, with ** and *** depicting p-values less than or equal to 0.01 and 0.001, respectively. (B) Representative histogram plot obtained from FACS analysis of glucose uptake. A clear reduction in fluorescence emission is observed with 1,25(OH)$_2$D$_3$ treatment. Western blot (C) and associated densitometric analysis (D) of GLUT1 protein levels in LNCaP cells in response to 72h of treatment with 1,25(OH)$_2$D$_3$. A significant reduction in protein levels are observed. Values below the blot are obtained from densitometric analysis of the presented bands. Figure obtained from Abu el Maaty et al. [90].*

To investigate whether 1,25(OH)$_2$D$_3$ influences the TCA cycle or not, levels of the cycle's intermediates in LNCaP cells were analyzed using gas chromatography/mass spectrometry (GC/MS). A 72h treatment with 1,25(OH)$_2$D$_3$ resulted in a significant increase in citrate/isocitrate levels, and a decrease in other downstream intermediates (**Figure 5**), indicating a possible reversion to the metabolic phenotype of differentiated prostate cells. Although I did not thoroughly investigate this possibility, it is conceivable that 1,25(OH)$_2$D$_3$ truncates the TCA cycle in LNCaP cells by increasing intracellular levels of Zn^{2+}. In support of this is the induced mRNA expression of the Zn^{2+} transporter SLC39A1 by calcitriol in LNCaP cells (data not shown).

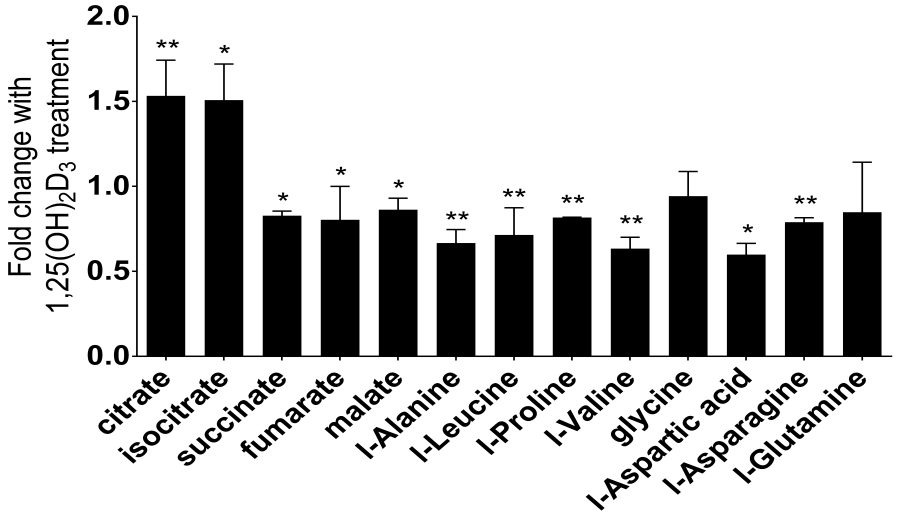

Figure 5: Quantification of TCA cycle intermediates and anaplerosis-related amino acids in 1,25(OH)$_2$D$_3$-treated LNCaP cells. *72h of treatment of LNCaP cells with 1,25(OH)$_2$D$_3$ (100 nM) significantly increases citrate/isocitrate levels and decreases levels of downstream metabolites. Levels of select amino acids are also influenced by 1,25(OH)$_2$D$_3$ treatment. A two-tailed Student's t-test was used to compare the results of DMSO- and 1,25(OH)$_2$D$_3$-treated cells, with * and ** depicting p-values less than or equal to 0.05 and 0.01, respectively. Error bars ± SD ; n=3. Figure obtained from Abu el Maaty et al. [90].*

Given the recognized role of the VDR as a transcription factor capable of regulating the expression of hundreds of genes [9], I postulated that significant changes in the mRNA expression of various metabolic genes would accompany, or partly explain the observed metabolic changes. I thus performed an mRNA expression analysis using RT-qPCR to investigate changes in the expression of genes encoding proteins involved in glucose, glutamine, and fatty acid metabolism. Surprisingly, the mRNA levels of all investigated metabolic genes were found to be reduced with 1,25(OH)$_2$D$_3$ treatment (**Figure 6**). I then aimed to confirm the down-regulation of the strongest hit—PDHK1 (pyruvate dehydrogenase kinase 1)—by immunoblotting, and observed a significant reduction in the enzyme's protein expression by treatment (**Figure 7**).

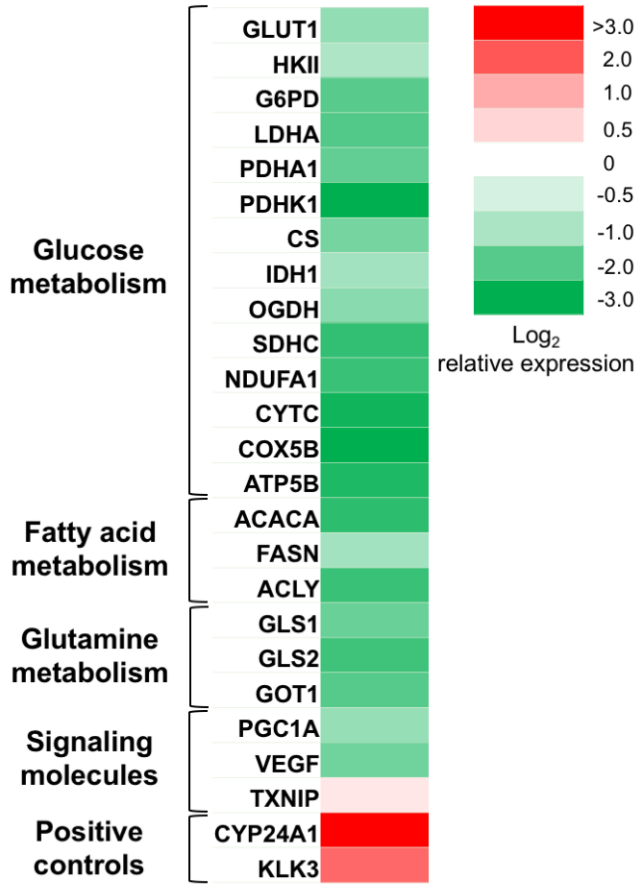

Figure 6: mRNA expression analysis of changes in metabolism-related genes in response to a 72h treatment with 1,25(OH)$_2$D$_3$ (100 nM) in LNCaP cells. *An overall downregulation in the various metabolic genes investigated is observed with treatment. Positive controls included are the vitamin D-catabolizing enzyme CYP24A1, as well as kallikrein-3/prostate specific antigen (KLK3), a differentiation marker that has been shown to be induced with 1,25(OH)$_2$D$_3$ treatment of prostate cancer cells. Relative expression is calculated using the ΔΔCt method, with vinculin as the housekeeping gene (n=3). Figure obtained from Abu el Maaty et al. [90].*

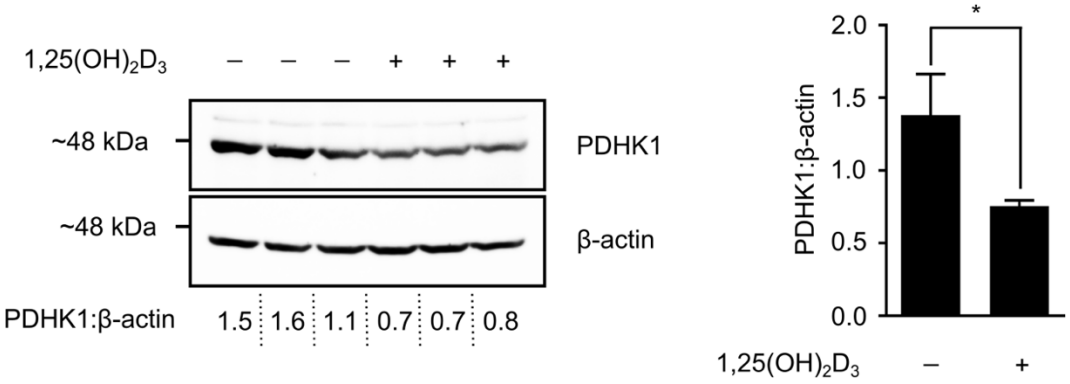

Figure 7: 1,25(OH)$_2$D$_3$ (100 nM) significantly reduces PDHK1 protein levels in LNCaP cells. *Western blot analysis of PDHK1 levels in 72h DMSO- and 1,25(OH)$_2$D$_3$-treated LNCaP cells (left), and the associated densitometric analysis (right). Values below blots are obtained from densitometric analysis of the presented bands. A two-tailed Student's t-test was used to compare the results of DMSO- and 1,25(OH)$_2$D$_3$-treated cells, with * depicting a p-value of less than or equal to 0.05. Error bars ± SD ; n=3. Figure obtained from Abu el Maaty et al. [90].*

Finally, to investigate the influence of treatment on overall energy status across different time points, intracellular ATP levels were studied using a commercially available ATP assay kit. While ATP levels were found to be significantly reduced with calcitriol treatment after 24 and 48h, they were not significantly affected by treatment in 72h (**Figure 8**). This is in line with the induction in mitochondrial mass and membrane potential observed after a 72h treatment with $1,25(OH)_2D_3$ (**Figure 8**).

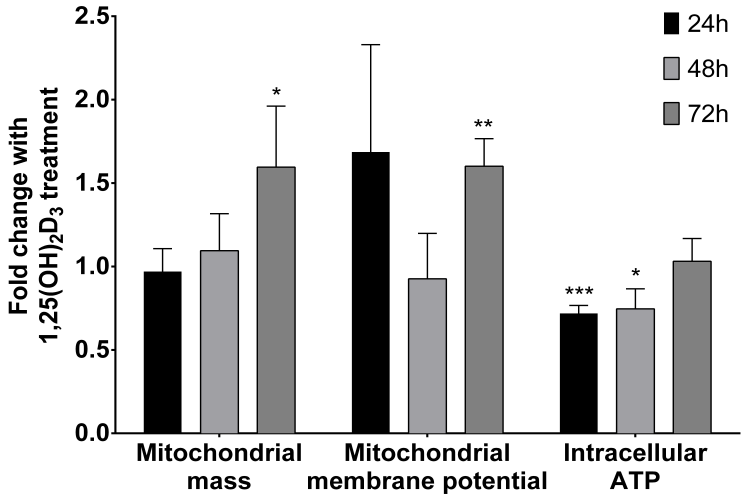

Figure 8: Analysis of changes in mitochondrial biogenesis/activity in LNCaP cells in response to 24, 48, and 72h of treatment with $1,25(OH)_2D_3$. *Intracellular ATP levels were found to be significantly reduced after 24 and 48h of treatment with $1,25(OH)_2D_3$ (100 nM), however, levels were normalized at the last time point, an observation coinciding with significantly elevated mitochondrial mass and membrane potential with $1,25(OH)_2D_3$ treatment. A two-tailed Student's t-test was used to compare the results of DMSO- and $1,25(OH)_2D_3$-treated cells, with *, **, and *** depicting p-values less than or equal to 0.05, 0.01, and 0.001, respectively. Error bars ± SD ; n=3. Figure obtained from Abu el Maaty et al. [90].*

2.1.2. TXNIP expression is reduced by $1,25(OH)_2D_3$, possibly due to an interplay between protein degradation and metabolic rewiring.

Based on the observed changes in the metabolic phenotype of LNCaP cells in response to $1,25(OH)_2D_3$, I postulated that treatment also affects energy-related signaling molecules. As mentioned in the introduction section, several clues pointed towards the ability of calcitriol to

influence metabolic signaling networks. On one hand, the activity of the intracellular energy-sensor AMPK has been shown to be induced by VDR activators [78]. On the other hand, the intracellular glucose-sensor TXNIP, has been initially characterized in AML (HL-60) cells as a gene that is induced by $1,25(OH)_2D_3$ treatment, thus termed the vitamin D_3 upregulated protein 1 (VDUP1) [88].

AMPK is a heterotrimeric complex, consisting of beta and gamma regulatory subunits, as well as an alpha catalytic subunit [60]. In response to energetic stress—an increase in AMP:ATP ratio—AMPK inhibits and activates energy-consuming and –producing pathways, respectively [60]. TXNIP, however, is known to be an integral part of cellular glucose sensing. An increase in intracellular levels of glycolytic intermediates is sensed by the transcriptional heterodimer MondoA/Max-like protein X (MLX), leading to its nuclear translocation and subsequent binding to carbohydrate response elements on the TXNIP promoter, inducing its expression [93]. TXNIP subsequently limits glucose uptake through reducing the expression and/or limiting the plasma membrane availability of GLUT1 [94]. Wu et al. [94] have demonstrated that TXNIP is also a component of AMPK signaling, one that is phosphorylated by AMPK, leading to its degradation, and ultimately, increased glucose uptake.

Considering this, I studied AMPK signaling activity, using phosphorylated ACC (S79) as a marker of the pathway's activation, as well as the expression levels of TXNIP, in response to $1,25(OH)_2D_3$ treatment, using immunoblotting. After 24, 48, and 72h of treatment, AMPK signaling and TXNIP expression were found to be consistently induced and reduced with treatment, respectively (**Figure 9** and **Figure 10**).

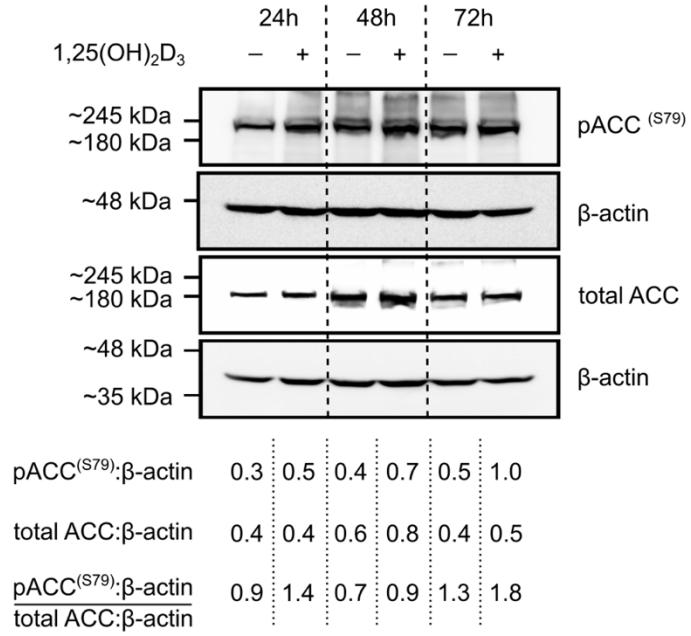

Figure 9: 1,25(OH)$_2$D$_3$ (100 nM) activates AMPK signaling in LNCaP cells. *pACC (S79) was found to be induced with treated across the investigated time points. Values below blots are obtained from densitometric analysis of the presented bands. Figure obtained from Abu el Maaty et al. [90].*

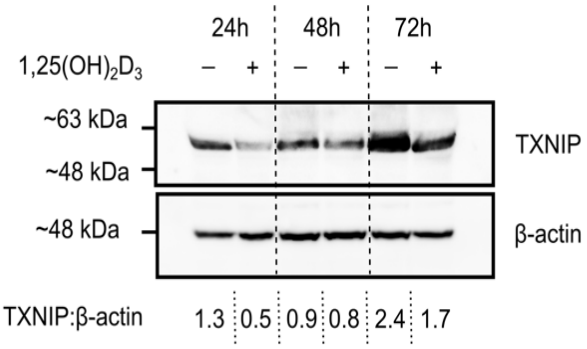

Figure 10: 1,25(OH)$_2$D$_3$ consistently reduces TXNIP expression in LNCaP cells. *Western blot analysis of TXNIP reveals a profound reduction in protein expression with 1,25(OH)$_2$D$_3$ (100 nM) treatment at the different time points investigated. Values below blots are obtained from densitometric analysis of the corresponding bands. Figure obtained from Abu el Maaty et al. [90].*

The latter observation was striking, given the long-assumed connection between the vitamin and the protein. However, noteworthy is that the canonical regulation of TXNIP expression by 1,25(OH)$_2$D$_3$ has only been observed on the mRNA level in HL-60 cells, and analysis of mouse VDUP1 gene promoter did not reveal the presence of VDRE [95]. Additionally, I observed a mild, yet significant induction in TXNIP mRNA levels in response to 1,25(OH)$_2$D$_3$ (**Figure 6**). To determine whether the canonical regulation occurs at earlier time points, I treated LNCaP cells with 1,25(OH)$_2$D$_3$ for 1, 3, 6, and 12h, and investigated TXNIP levels using immunoblotting. Not only was a clear induction in TXNIP protein level absent, but a reduction

in its expression level was also observed after 3 and 6h of treatment, and a marked decrease was observed after 12h of treatment (***Figure 11***).

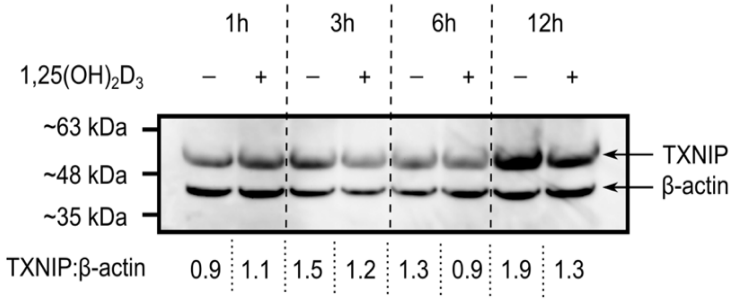

Figure 11: Canonical regulation of TXNIP by 1,25(OH)$_2$D$_3$ is not observed in short time points. *Western blot analysis of TXNIP levels in DMSO- and 1,25(OH)$_2$D$_3$ (100 nM)-treated LNCaP cells reveals a reduction in expression with treatment in as early as 3h. Values below blots are obtained from densitometric analysis of the corresponding bands. Figure obtained from Abu el Maaty et al. [90].*

To investigate this finding further, I hypothesized that the observed induction in AMPK led to TXNIP degradation. To address this possibility, I first sought to confirm TXNIP degradation by 1,25(OH)$_2$D$_3$. LNCaP cells were therefore treated with either DMSO or calcitriol for 66h, after which proteasomal and lysosomal inhibitors, MG-132 and leupeptin, respectively, were added to the conditioned medium for an additional 6h. Furthermore, as a positive control of TXNIP regulation, 2-Deoxyglucose, a non-metabolizable glucose analog, was similarly added to the conditioned medium 24h prior to the end of the intended treatment period with DMSO or 1,25(OH)$_2$D$_3$ (72h). 2-Deoxyglucose enters cells and is phosphorylated by hexokinase, but does not undergo further glycolytic steps. An accumulation of 2-Deoxyglucose-6-phosphate mimics elevated levels of glycolytic intermediates, which triggers the translocation of MondoA/MLX into the nucleus, thus inducing TXNIP expression. In the present setting, the possibility that the reduction in TXNIP levels is due to treatment-induced metabolic changes/reduced glycolytic flux, could be addressed using this experimental approach, since TXNIP would be potentially rescued by 2-Deoxyglucose in such case. All employed treatments were found to rescue TXNIP levels in the presence of 1,25(OH)$_2$D$_3$ (**Figure 12**).

With regards to the involvement of AMPK signaling in mediating calcitriol's effects on TXNIP degradation, I speculated that activation of this signaling pathway by 1,25(OH)$_2$D$_3$ might be

due to treatment-induced energetic stress and/or increased intracellular Ca^{2+} levels. The latter leads to AMPK activation through activating its upstream kinase CAMKK2 [60]. To investigate the role of these pathways, I treated LNCaP cells with an AMPK inhibitor (compound C) [60], or a CAMKK2 inhibitor (STO-609) [96], in the presence of either DMSO or $1,25(OH)_2D_3$. LNCaP cells were therefore treated for 48h with a vehicle or calcitriol, to ensure reduction in TXNIP levels, after which the different inhibitors were added to the conditioned medium for an additional 24h. Interestingly, STO-609, but not compound C, rescued TXNIP expression in the presence of $1,25(OH)_2D_3$ (**Figure 12**).

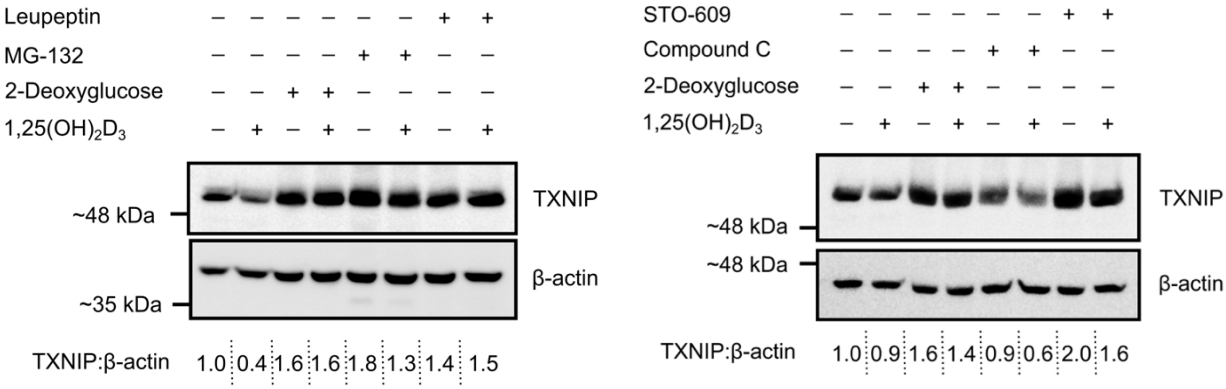

Figure 12: TXNIP is degraded in response to $1,25(OH)_2D_3$ treatment, possibly through activation of AMPK signaling. *(Left) Reduction of TXNIP protein levels with $1,25(OH)_2D_3$ (100 nM) treatment is rescued by the proteasomal and lysosomal inhibitors, MG-132 (5 μM) and leupeptin (20 μM), respectively, as well as by the positive control 2-Deoxyglucose (10 mM). Cells were initially treated with either DMSO or $1,25(OH)_2D_3$ for 66h, after which the inhibitors were added to the conditioned medium for an additional 6h. 2-Deoxyglucose was similarly added to the conditioned medium of cells, 48h after the initial treatment, for an additional 24h. (Right) The small molecule CAMKK2 inhibitor STO-609 (20 μM), but not compound C (5 μM), rescues TXNIP protein levels in the presence of $1,25(OH)_2D_3$. The molecules were added to the conditioned medium of 48h treated cells, for an additional 24h. Values below blots are obtained from densitometric analysis of the corresponding bands. Figure obtained from Abu el Maaty et al. [90].*

In addition to the described effects of $1,25(OH)_2D_3$ treatment on metabolism-related signaling molecules, previous studies have shown that the oncogene c-Myc is downregulated by calcitriol in prostate cancer cells [97]. As previously mentioned, c-Myc is implicated in the metabolic

reprogramming observed in tumors, through promoting the glycolytic pathway [59]. Additionally, Myc has been shown to either cooperate or compete with MondoA in mediating metabolic effects in different tumors [98]. For example, in triple-negative breast cancer, c-Myc has been shown to drive glycolysis through reducing TXNIP (a MondoA target) expression in breast cancer cells [99]. On the other hand, in neuroblastoma, N-Myc and MondoA were described as cooperatively regulating glutamine metabolism [100]. Although such relationship has not been described in prostate cancer, I aimed to investigate the possibility that the overall reduction in glucose metabolism with 1,25$(OH)_2D_3$ treatment in LNCaP cells is at least partly mediated through its reduction of c-Myc levels, which consequently leads to a reduction in TXNIP expression. To test this hypothesis, I first aimed to confirm the downregulation of c-Myc levels in LNCaP cells by calcitriol, which were indeed found to be reduced after 72h of treatment (**Figure 13**). I then added the Myc-Max hetero-dimerization and transactivation inhibitor 10058-F4 [101], to the conditioned medium of LNCaP cells treated for 48h with either DMSO or 1,25$(OH)_2D_3$, for an additional 24h. Similar to calcitriol's effects, 10058-F4 markedly reduced TXNIP expression in LNCaP cells (**Figure 13**), demonstrating that c-Myc inhibition decreases TXNIP levels through direct and/or indirect mechanisms. Directly, for example, through recruiting transcription repressing complexes to the TXNIP promoter, and indirectly, through reducing glycolytic flux thereby decreasing the levels of TXNIP-inducing glycolytic intermediates.

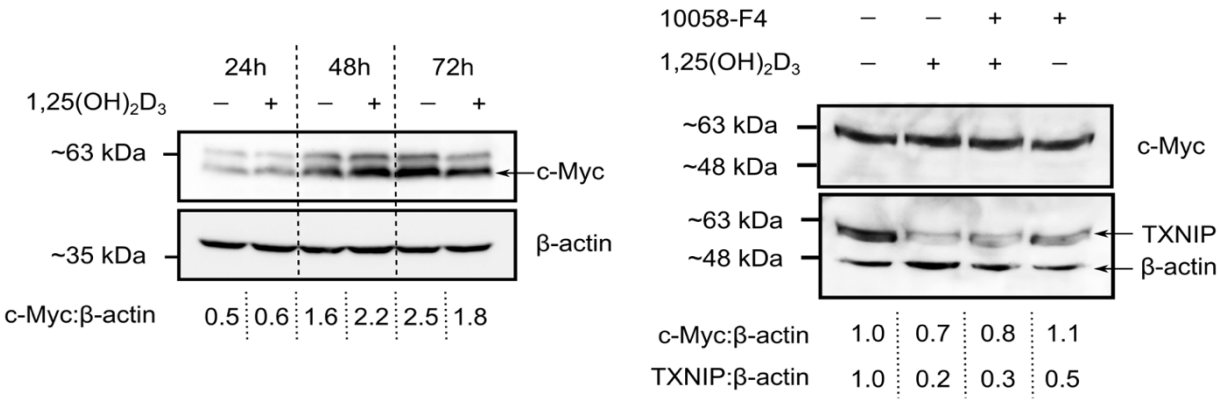

Figure 13: c-Myc potentially contributes to the regulation of TXNIP by 1,25(OH)$_2$D$_3$ in LNCaP cells. *(Left) Western blot analysis illustrating the reduction of c-Myc levels in LNCaP cells after 72h of treatment with 1,25(OH)$_2$D$_3$ (100 nM). (Right) The small molecule c-Myc inhibitor 10058-F4 (20 μM), added to the medium of 48h DMSO- or 1,25(OH)$_2$D$_3$-treated cells for an additional 24h, was found to markedly decrease TXNIP protein expression in LNCaP cells independent of 1,25(OH)$_2$D$_3$. Values below blots are obtained from densitometric analysis of the corresponding bands. Figure obtained from Abu el Maaty et al. [90].*

2.1.3. Metabolic regulation by 1,25(OH)$_2$D$_3$ in LNCaP cells is largely androgen receptor-independent.

Given the diversity and potency of calcitriol's metabolism-regulating activities in the AR-positive cell line LNCaP, I questioned the importance of the AR in mediating or facilitating these effects. The AR has been recently shown to influence glucose metabolizing pathways in prostate cancer cells [102], and extensive crosstalk between the AR and the VDR has been described [31, 103]. Firstly, I confirmed results of earlier reports demonstrating significant induction in AR expression in LNCaP cells with 1,25(OH)$_2$D$_3$ treatment (**Figure 14**) [28, 29].

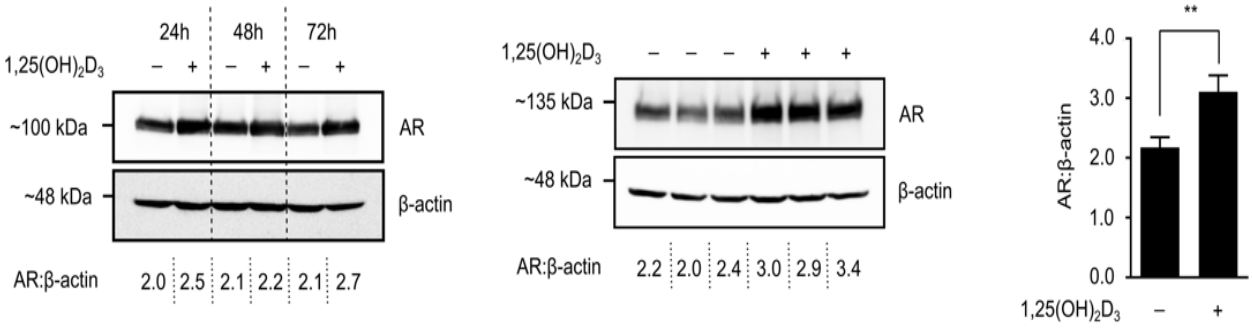

Figure 14: AR levels are consistently induced in LNCaP cells with 1,25(OH)$_2$D$_3$ treatment. *Western blot analysis of AR levels in LNCaP cells in response 1,25(OH)$_2$D$_3$ (100 nM) over a time course (left), as well as after 72h of treatment (middle). (Right) A significant increase in AR protein levels after 72h of 1,25(OH)$_2$D$_3$ treatment is illustrated by densitometric analysis of the corresponding bands (middle blot). A two-tailed Student's t-test was used to compare the AR protein levels in DMSO- and 1,25(OH)$_2$D$_3$-treated cells, and ** depicts a p-value of less than or equal to 0.01. Error bars ± SD ; n=3. Figure obtained from Abu el Maaty et al. [90].*

To examine the role of the AR in calcitriol's regulation of TXNIP expression, I transiently knocked-down AR levels in LNCaP cells and treated them with either DMSO or 1,25(OH)$_2$D$_3$. Results demonstrate a reduction in TXNIP expression in LNCaP cells by treatment independent of AR expression levels (**Figure 15**).

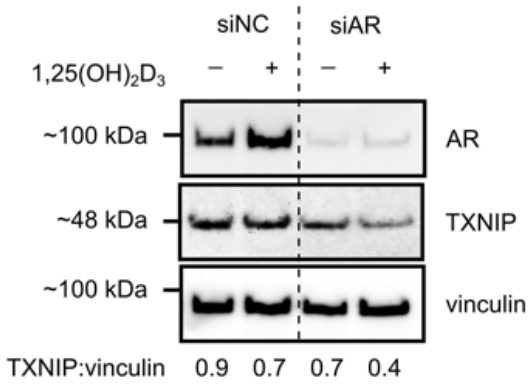

Figure 15: Knocking-down AR levels in LNCaP cells does not influence regulation of TXNIP by 1,25(OH)$_2$D$_3$ (100 nM). *Western blot analysis of TXNIP levels in DMSO- and 1,25(OH)$_2$D$_3$-treated LNCaP cells, transfected with anti-AR siRNA or a negative control (NC). Reduction in TXNIP levels after 24h of treatment is independent of AR levels. Values below the blot are obtained from densitometric analysis of the corresponding bands. Figure obtained from Abu el Maaty et al. [90].*

To further investigate the role of the AR in the observed metabolic changes, increasing concentrations of the AR agonist and antagonist, testosterone and casodex, respectively, were added to the conditioned medium of LNCaP cells treated for 48h with either DMSO or 1,25(OH)$_2$D$_3$, for an additional 24h, after which both TXNIP protein expression and glucose uptake levels were evaluated. Testosterone treatment led to a minor increase in TXNIP protein level, an effect that was accompanied by a reduction in glucose uptake (**Figure 16**). However, in the presence of calcitriol, testosterone treatment did not alter the reduction in TXNIP expression (**Figure 16**). On the other hand, while calcitriol induces AR expression and casodex is an AR antagonist, similar effects on TXNIP expression were observed, where a single high dose of casodex (100 μM) was found to deplete TXNIP levels (**Figure 16**). Noteworthy is that this dose did not appear to alter glucose uptake of LNCaP cells (**Figure 16**).

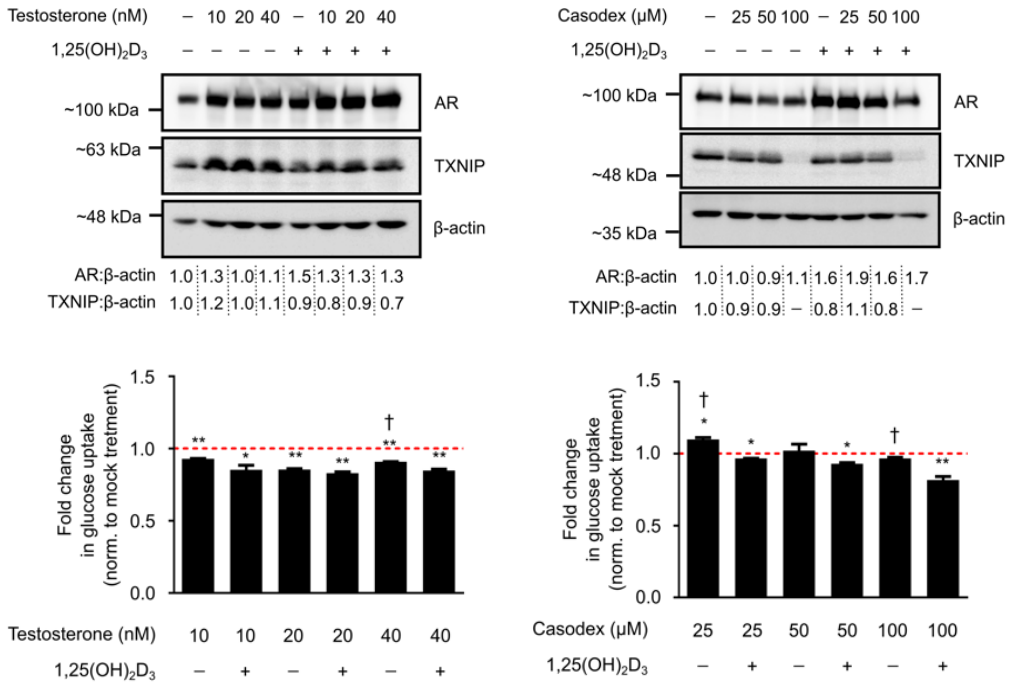

Figure 16: Pharmacological modulators of the AR do not influence 1,25(OH)$_2$D$_3$'s effects on TXNIP or glucose uptake in LNCaP cells. *Increasing concentrations of testosterone (10-40 nM) or casodex (25-100 μM), added to the conditioned medium of 48h DMSO- or 1,25(OH)$_2$D$_3$ (100 nM)-treated cells, for an additional 24h, do not diminish the negative regulation of TXNIP protein levels (top) or glucose uptake (bottom) by 1,25(OH)$_2$D$_3$. Values below blots are obtained from densitometric analysis of the corresponding bands. A two-tailed Student's t-test was used to compare the results of DMSO-treated cells and the different conditions, with * and ** depicting p-values less than or equal to 0.05 and 0.01, respectively. Statistical significance between the mono-treatments and the combination treatments is depicted by a dagger. Error bars ± SD ; n=2. Figure obtained from Abu el Maaty et al. [90].*

Since 1,25(OH)$_2$D$_3$ treatment was also found to transcriptionally regulate metabolic genes, I investigated whether AR stimulation or inhibition led to similar effects on the mRNA expression of select genes. The same treatment plan for the AR modulators as described in the previous section was employed, however a single dose of each molecule was used. While 1,25(OH)$_2$D$_3$-mediated transcriptional regulation of PDHK1 was mimicked by both testosterone and casodex, regulation of GLUT1 by the AR modulators was in opposing fashion to 1,25(OH)$_2$D$_3$'s effect (**Figure 17**). Moreover, the reduction of GLUT1, PDHA1 (pyruvate

dehydrogenase E1 component alpha 1 subunit), and PDHK1 mRNA expression by $1,25(OH)_2D_3$ was not observed in cells co-treated with casodex. Therefore, taking all the data together, I concluded that calcitriol's metabolic effects are largely AR-independent.

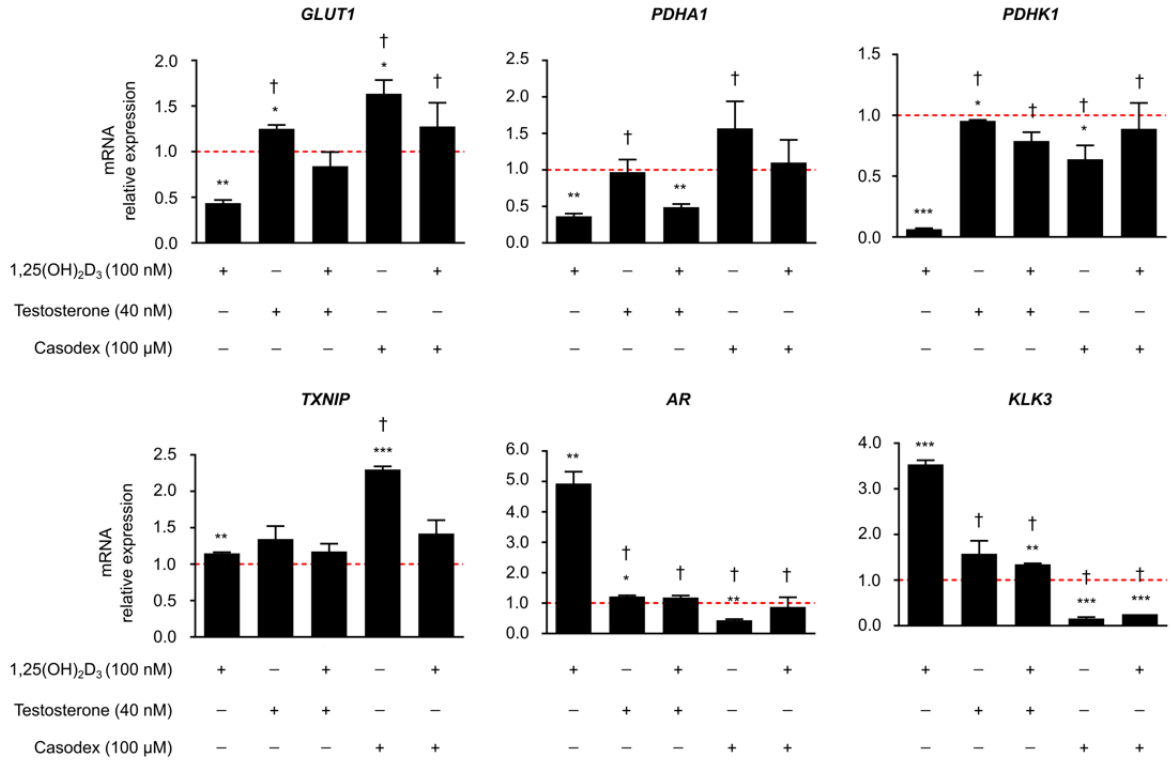

Figure 17: Effects of $1,25(OH)_2D_3$ on the mRNA expression of metabolic genes in LNCaP cells is partially AR-dependent. *While the effect of testosterone (40 nM) or casodex (100 µM) on PDHK1 mRNA levels mimicked that of $1,25(OH)_2D_3$ (100 nM), reduction in GLUT1 and PDHA1 mRNA levels in response to $1,25(OH)_2D_3$ appeared to be blocked in the presence of casodex. A two-tailed Student's t-test was used to compare the results of DMSO-treated cells and the different conditions, with *, ** and *** depicting p-values less than or equal to 0.05, 0.01 and 0.001, respectively. Statistical significance between the different conditions and $1,25(OH)_2D_3$ is depicted by a dagger Error bars ± SD ; n=2. Figure obtained from Abu el Maaty et al. [90].*

2.2. $1,25(OH)_2D_3$ impacts energy-generating and glucose-sensing networks in breast cancer cells.

2.2.1. Calcitriol treatment differentially regulates metabolic networks in luminal and basal breast cancer cells.

Encouraged by the demonstrated ability of $1,25(OH)_2D_3$ to induce diverse metabolic changes in prostate cancer cells, I wondered if similar effects could also be observed in experimental models of another endocrine-related cancer. As previously highlighted, studies have illustrated that $1,25(OH)_2D_3$ possesses multi-faceted anti-tumor effects in breast cancer models, including regulation of the cell cycle, apoptosis, and estrogen signaling [9]. I therefore sought to investigate the ability of the molecule to regulate metabolic processes in breast cancer cell lines representing different molecular subtypes. Using MCF-7 and MDA-MB-231 cells as representative models for luminal and basal breast cancers, respectively, I studied changes in glycolytic and respiratory rates using the BIONAS 2500 biosensor chip system mentioned in the previous section. In MCF-7 cells, $1,25(OH)_2D_3$ was found to gradually induce glycolytic rate over the course of three days, but did not impact respiratory rate in the same time frame (**Figure 18**). In contrast to these observations, respiratory, but not glycolytic rate in MDA-MB-231 cells was found to be reduced with $1,25(OH)_2D_3$ treatment (**Figure 18**).

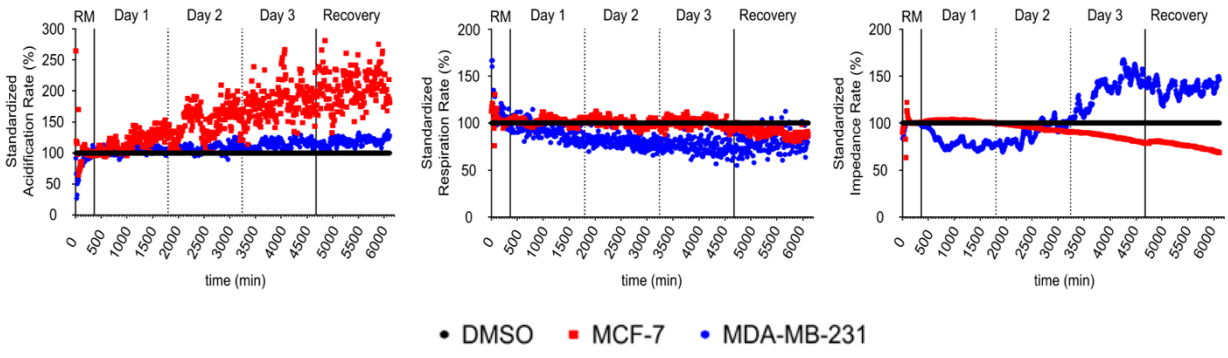

Figure 18: Simultaneous, real-time measurements of glycolytic, respiratory, and impedance rates in breast cancer cell lines treated with 1,25(OH)$_2$D$_3$ (100 nM). *In MCF-7 cells, 1,25(OH)$_2$D$_3$ treatment appeared to induce glycolytic rate, but not respiratory capacity. On the other hand, respiratory, but not glycolytic rate in MDA-MB-231 cells, was found to be reduced with 1,25(OH)$_2$D$_3$. Measurements obtained from 1,25(OH)$_2$D$_3$-treated cells were normalized to those from DMSO-treated ones of the same cell line, however the data pertaining to all cell lines are presented together. Data are representative of two biological replicates.*

To get a clearer view of 1,25(OH)$_2$D$_3$-mediated metabolic changes in the different cell lines, GC/MS-based metabolomics was performed to quantify TCA cycle intermediates as well as levels of select amino acids in response to treatment. I observed differential regulation of levels of TCA cycle metabolites by calcitriol in the different cell lines (**Figure 19**). In MCF-7 cells, 1,25(OH)$_2$D$_3$ treatment clearly reduced citrate levels as well as levels of downstream intermediates (**Figure 19**). In MDA-MB-231 cells however, the treatment led to a marked increase in citrate and α-KG levels (**Figure 19**). Strikingly, I observed a profound induction in intracellular serine levels in MCF-7 cells with treatment (**Figure 19**). This observation was of interest since numerous recent studies have focused on the importance of this non-essential amino acid to cancer cell survival [104].

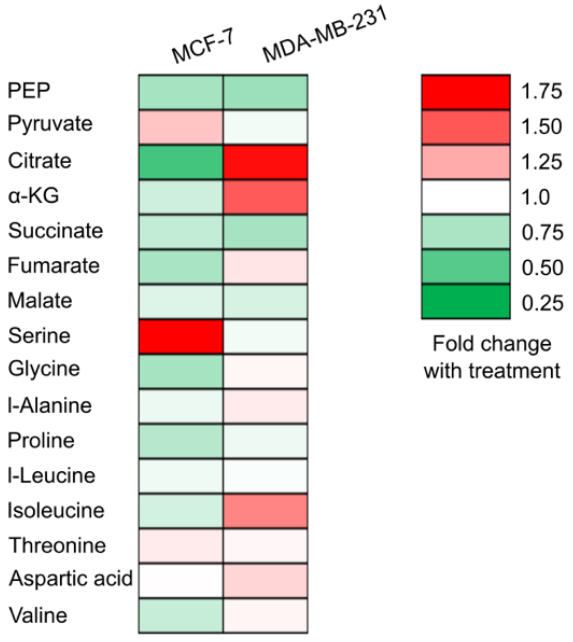

Figure 19: GC/MS-based quantification of TCA cycle metabolites and amino acids in breast cancer cells treated with 1,25(OH)$_2$D$_3$ (100 nM). *In MCF-7 cells, levels of citrate as well as other downstream TCA cycle metabolites were reduced in response to a 72h treatment with 1,25(OH)$_2$D$_3$. In MDA-MB-231 cells, however, an accumulation in citrate and α-KG is observed. A profound increase in intracellular serine levels in 1,25(OH)$_2$D$_3$-treated MCF-7 cells is also observed. Results are the average of two biological replicates.*

Additionally, I postulated that calcitriol treatment may majorly regulate the expression of various metabolic genes in breast cancer cells in a manner similar to that observed in LNCaP cells. I thus aimed to evaluate the expression of not only genes related to glucose, glutamine and fatty acid metabolism, but also those involved in p53- and autophagy-signaling, since the two investigated cell lines exhibit different p53 variations—wild-type (MCF-7) and mutant (MDA-MB-231)—as well as because recent reports demonstrated the ability of VDR activators to trigger autophagy in breast tumor cells [82, 105]. Contrary to the findings in LNCaP cells, the mRNA expression levels of most investigated genes were not significantly reduced with calcitriol treatment (**Figure 20**). Furthermore, the mRNA expression of the G6PD gene was found to be clearly induced by treatment in both cell lines (**Figure 20**). This enzyme is responsible for catalyzing the first reaction of the PPP, which provides cells with precursors for biosynthetic pathways as well as NADPH for anti-oxidant defense [106, 107]. Furthermore, studies have illustrated that G6PD is overexpressed in different cancer types [106], making it a potential oncogene.

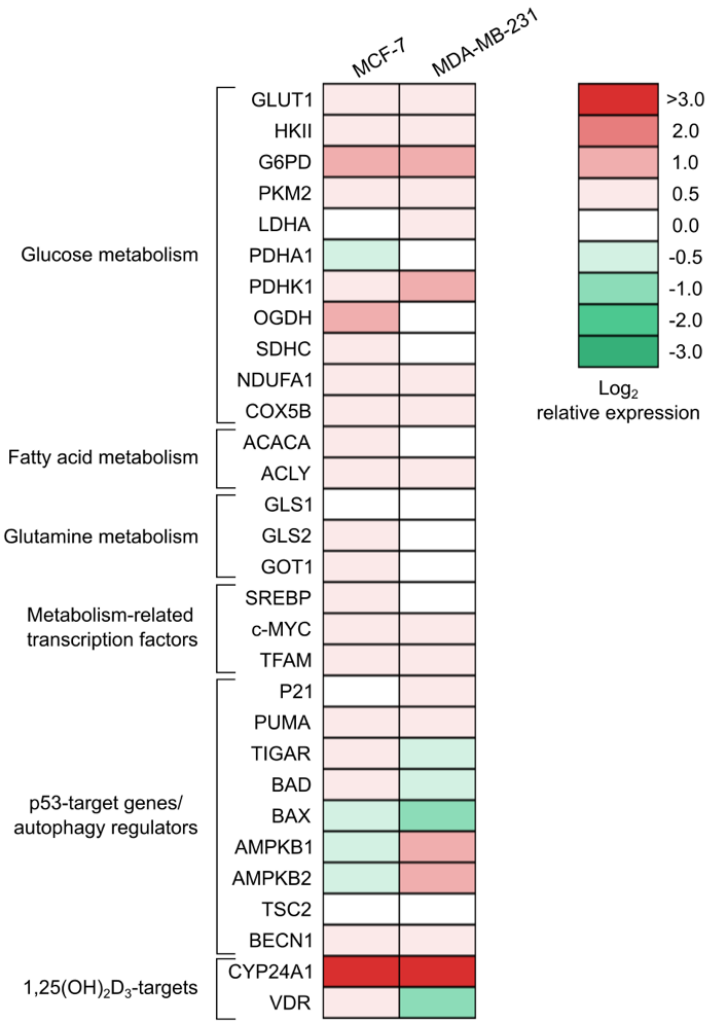

Figure 20: Analysis of mRNA expression of metabolic genes in breast cancer cells treated for 72h with 1,25(OH)$_2$D$_3$ (100 nM). *While most genes were found to be mildly regulated by treatment in both cell lines, the G6PD gene was found to be induced by 1,25(OH)$_2$D$_3$ in MCF-7 and MDA-MB-231 cells. Relative expression was calculated using the ΔΔCt method, with vinculin as the housekeeping gene. Data presented are the average of two biological replicates.*

To assess the overall energy status of breast cancer cells, the previously mentioned ATP assay was utilized to quantify intracellular ATP levels in response to 24, 48, and 72h of treatment with calcitriol. While treatment led to a significant reduction in ATP levels in MCF-7 cells at the latest investigated time point, the opposite effect was observed for MDA-MB-231 cells (**Figure 21**).

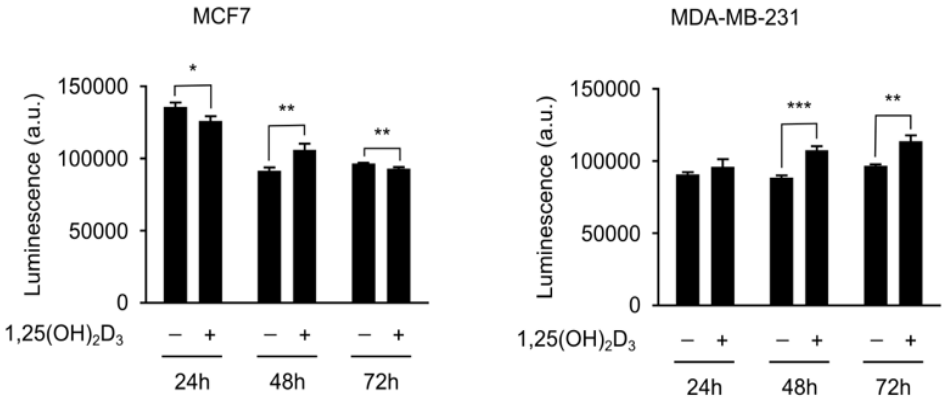

Figure 21: Assessment of overall energy levels in DMSO- and 1,25(OH)$_2$D$_3$ (100 nM)-treated breast cancer cells. *Luminescence values, correlating with cellular ATP levels, were normalized to cellular protein content. A two-tailed Student's t-test was used to compare the results of DMSO- and 1,25(OH)$_2$D$_3$-treated cells, with *, ** and *** depicting p-values less than or equal to 0.05, 0.01 and 0.001, respectively. Error bars ± SD ; n=3.*

2.2.2. 1,25(OH)$_2$D$_3$ induces TXNIP degradation in MCF-7 cells.

Following the characterization of 1,25(OH)$_2$D$_3$-induced metabolic changes in breast cancer cells, I investigated the regulation of AMPK signaling and TXNIP expression by treatment, employing the same strategy adopted for LNCaP cells. While 72h of treatment with calcitriol led to a clear induction in AMPK activity and a significant reduction in TXNIP levels in MCF-7 cells, minor effects were observed in MDA-MB-231 cells (**Figure 22**).

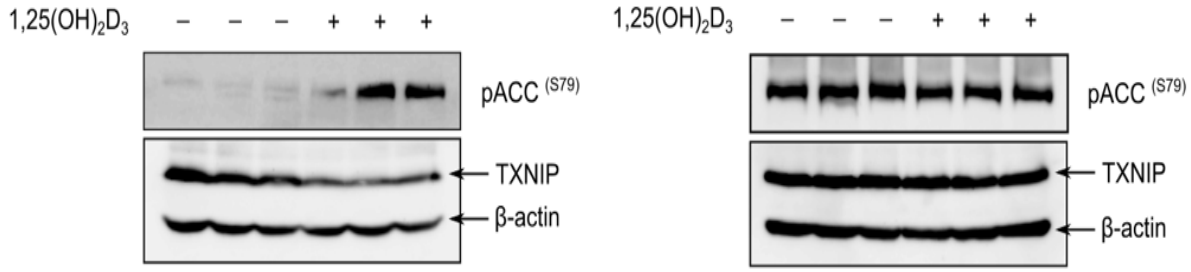

Figure 22: Western blot analysis of changes in TXNIP levels and AMPK signaling activation in breast cancer cells in response to 72h of 1,25(OH)$_2$D$_3$ (100 nM) treatment. *Levels of TXNIP and pACC (S79) appeared to be differentially regulated by 1,25(OH)$_2$D$_3$ in MCF-7 cells (left) and MDA-MB-231 (right).*

Motivated by similar non-canonical regulation in prostate cancer cells, I aimed to characterize the nature of TXNIP regulation by 1,25(OH)$_2$D$_3$ in MCF-7 cells. I started by employing a thorough time course, comprising both short and long time points (1-72h), and studying the 1,25(OH)$_2$D$_3$-mediated regulation of TXNIP mRNA and protein expression. I observed an initial induction in TXNIP mRNA levels at the early time points (1-3h), however, this was largely ablated at the later time points (6-72h) (**Figure 23**). Protein levels on the other hand appeared to be unaffected by treatment at early time points, but a clear reduction in expression levels was observed starting at 12h (**Figure 23**).

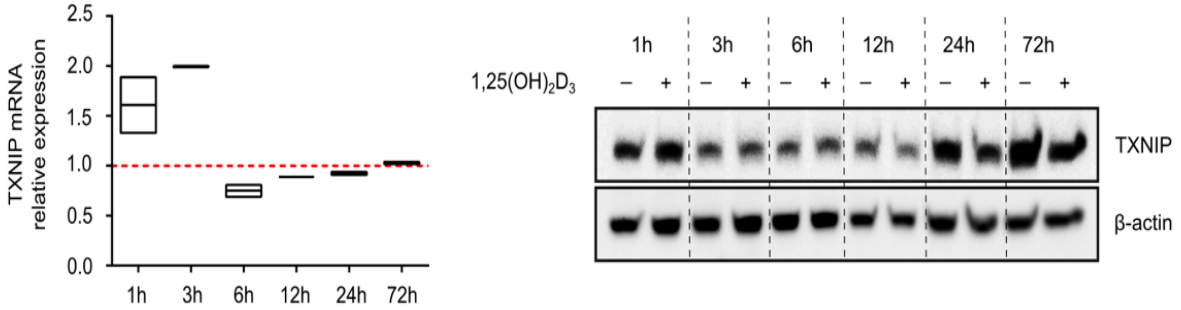

Figure 23: Time-dependent evaluation of changes in TXNIP mRNA (left) and protein (right) levels in MCF-7 cells in response to 1,25(OH)$_2$D$_3$ (100 nM) treatment. *Relative expression was calculated using the ΔΔCt method, with vinculin as the housekeeping gene. The lines in the middle of the floating bars represent the mean of two biological replicates, and the upper and lower ends of the bars represent the highest and lowest values, respectively.*

Since TXNIP is involved in both glucose and redox homeostasis [93, 108, 109], I assessed glucose uptake and intracellular ROS levels in 1,25$(OH)_2D_3$-treated MCF-7 cells. While intracellular ROS levels were found to be insignificantly affected by treatment in the investigated time points, glucose uptake was found to be reduced after 24 but not 72h of treatment (**Figure 24**).

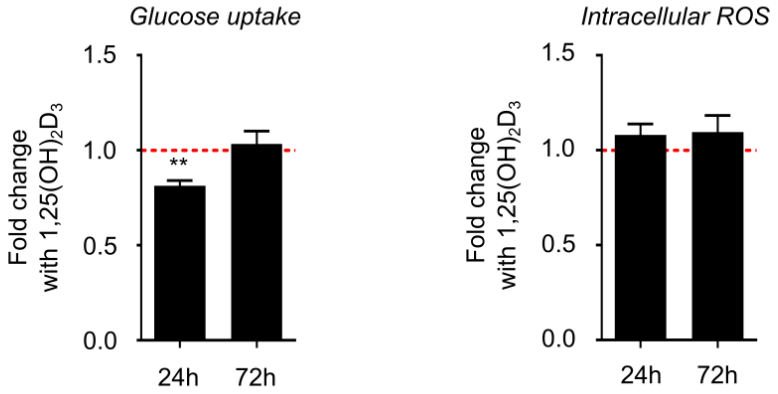

Figure 24: Changes in glucose uptake and intracellular ROS levels in response to treatment of MCF-7 cells with 1,25(OH)$_2$D$_3$ (100 nM). *24h of treatment was found to significantly reduce glucose uptake, an effect that was not observed after 72h. Intracellular ROS levels were found to be unaltered by calcitriol in the investigated time points. A two-tailed Student's t-test was used to compare the results of DMSO- and 1,25(OH)$_2$D$_3$-treated cells, with ** depicting p-values less than or equal to 0.01. Error bars ± SD ; n=3.*

I then posited that 1,25$(OH)_2D_3$-mediated metabolic reprogramming might have reduced the levels of TXNIP-inducing glycolytic intermediates—thereby hampering the initial rise in TXNIP mRNA levels—and/or led to TXNIP degradation via AMPK induction. Therefore, I devised an experiment in which MG-132 or 2-Deoxyglucose are added to the conditioned medium of MCF-7 cells, treated for 72h with either DMSO or 1,25$(OH)_2D_3$, 2 and 24h before the 72h-treatment period was over, respectively. While I observed complete rescuing of TXNIP expression in response to 1,25$(OH)_2D_3$ treatment by 2-Deoxyglucose, MG-132 only partially rescued the molecule's expression (**Figure 25**). To further confirm this, I treated MCF-7 cells with 1,25$(OH)_2D_3$ for 72h, during which MG-132 was added to the culture medium at different time points prior to the end of the 1,25$(OH)_2D_3$ treatment period. The presence of calcitriol was found to delay TXNIP rescuing by MG-132 (**Figure 25**).

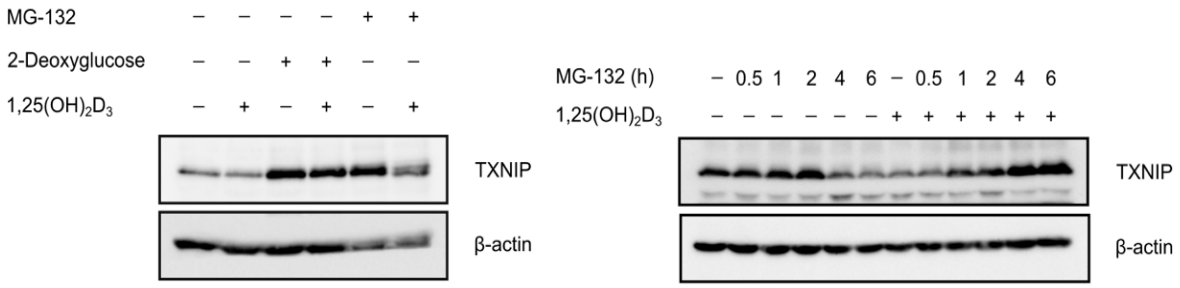

Figure 25: 1,25(OH)$_2$D$_3$ (100 nM) induces TXNIP degradation in MCF-7 cells. *(Left) MG-132 (5 μM) added to the culture medium of DMSO- or 1,25(OH)$_2$D$_3$-treated MCF-7 cells 2h prior to the end of the treatment period (72h), only partially rescues the reduction in TXNIP protein levels by 1,25(OH)$_2$D$_3$. (Right) MG-132, added to the medium of cells treated with either DMSO or 1,25(OH)$_2$D$_3$ for different periods before the end of the initial treatment (72h), induces delayed rescuing of TXNIP protein expression in 1,25(OH)$_2$D$_3$-treated cells.*

While TXNIP degradation as a result of AMPK activation remained a possibility, I proposed that treatment might have also regulated the expression/activity of TXNIP-degrading machinery. Recent studies, reviewed thoroughly by Álvarez-Díaz et al. [110], illustrated the ability of vitamin D to modulate the expression of diverse protein degradation players. Since Zhang et al. [111] have recently shown that ITCH, an E3 ubiquitin ligase, is responsible for marking TXNIP for proteasomal degradation, I tested whether 1,25(OH)$_2$D$_3$ leads to TXNIP degradation through inducing ITCH expression. Indeed, treatment was found to significantly induce both ITCH mRNA and protein levels (**Figure 26**). To assess the possible extent of this induction on TXNIP degradation, I treated MCF-7 cells with the de novo protein synthesis inhibitor cycloheximide (CHX), both in the presence and absence of 1,25(OH)$_2$D$_3$. Similar to the MG-132 experiment described above, CHX was added to the conditioned medium of cells at different time points before the end of the 72h treatment period with either DMSO or calcitriol. While CHX treatment led to a time-dependent reduction in TXNIP half-life in DMSO-treated cells, rescuing of TXNIP levels was observed in 1,25(OH)$_2$D$_3$-treated cells at the latest CHX time point (**Figure 26**), highlighting the possibility that induction in the expression of ITCH—or other TXNIP-degrading machinery—contributed to TXNIP degradation by treatment.

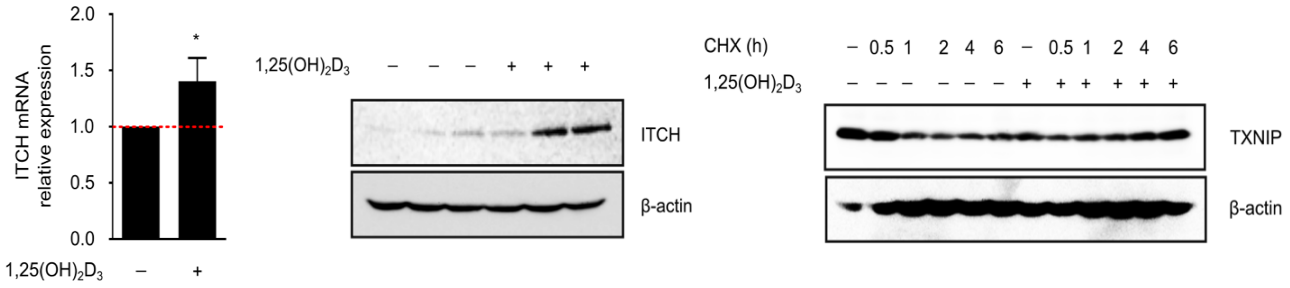

Figure 26: 1,25(OH)$_2$D$_3$ induces ITCH expression in MCF-7 cells. *72h of treatment with 1,25(OH)$_2$D$_3$ (100 nM) induces ITCH mRNA (left) and protein (middle) levels. ITCH mRNA relative expression is calculated using ΔΔCt method with vinculin as the housekeeping gene. A two-tailed Student's t-test was used to compare the results of DMSO- and 1,25(OH)$_2$D$_3$-treated cells, with * depicting p-values less than or equal to 0.05. Error bars ± SD ; n=2. (Right) CHX (10 μM), added to the medium of DMSO- or 1,25(OH)$_2$D$_3$-treated cells at different time points before the end of the 72h treatment period, reduces TXNIP protein half-life and rescues TXNIP protein levels in DMSO- and 1,25(OH)$_2$D$_3$-treated cells, respectively, in a time-dependent manner.*

To investigate the involvement of AMPK signaling in TXNIP regulation by 1,25(OH)$_2$D$_3$, AMPKα1 was knocked-down in MCF-7 cells using siRNA. Cells were subsequently treated with either DMSO or 1,25(OH)$_2$D$_3$ for 24 and 72h, after which TXNIP expression was assessed by immunoblotting. Knocking-down AMPKα1 levels appeared not to influence the reduction in TXNIP expression by 1,25(OH)$_2$D$_3$ at either time point (**Figure 27**).

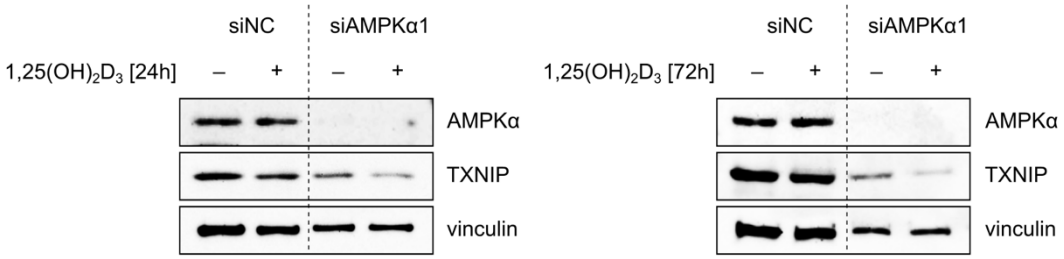

Figure 27: Reduction of TXNIP protein expression by 1,25(OH)$_2$D$_3$ (100 nM) in MCF-7 cells is AMPK-independent. *24 (left) and 72h (right) of treatment with 1,25(OH)$_2$D$_3$ negatively regulate TXNIP levels in cells transfected with either anti-AMPKα1 siRNA or NC.*

To further confirm the lack of involvement of AMPK signaling in $1,25(OH)_2D_3$'s regulation of TXNIP expression, I sought to limit the possibility of the treatment activating this pathway by increasing intracellular Ca^{2+} levels. I therefore treated MCF-7 cells for 24h with either the low-calcemic VDR activator calcipotriol [35], or $1,25(OH)_2D_3$, the latter in the presence and absence of the cell permeable Ca^{2+} chelator bis-(o-aminophenoxy)-ethane-N,N,N,N'-tetraacetic acid/tetra(acetoxymethyl)-ester (BAPTA-AM) [78], added to the condition medium for the last 2h of treatment. Calcipotriol treatment elicited similar effects on TXNIP expression as $1,25(OH)_2D_3$, whereas the addition of BAPTA-AM to $1,25(OH)_2D_3$-treated MCF-7 cells did not attenuate TXNIP's regulation by treatment (**Figure 28**).

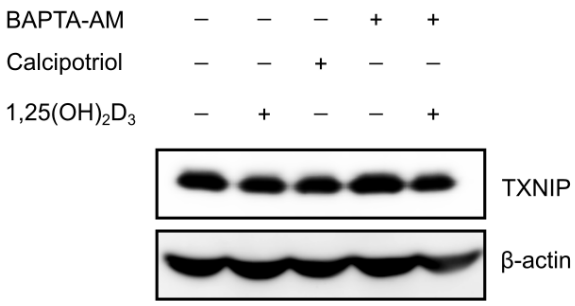

Figure 28: $1,25(OH)_2D_3$'s regulation of TXNIP expression in MCF-7 cells is independent of its calcemic effects. *Treatment of cells for 24h with calcipotriol (100 nM) reduces TXNIP proteins levels in a manner similar to that observed with $1,25(OH)_2D_3$ (100 nM). Addition of BAPTA-AM (20 μM) to the conditioned medium of DMSO- or $1,25(OH)_2D_3$-treated cells, 2h before the end of the treatment period, does not alter $1,25(OH)_2D_3$'s regulation of TXNIP.*

2.2.3. Metabolic adaptation to $1,25(OH)_2D_3$ possibly contributes to TXNIP regulation.

I then decided to revisit the possibility that certain metabolic changes provoked by treatment contributed to the observed reduction in TXNIP expression. Based on the observation that the increase in TXNIP mRNA expression was found to be transient and short-lived, I speculated that certain metabolic changes reduced the levels of glycolytic metabolites capable of inducing the nuclear translocation of MondoA/MLX. Based on the previous findings that MCF-7 cells treated for 72h with calcitriol exhibit higher mRNA expression of G6PD (**Figure 20**), as well as increased serine levels compared to DMSO-treated cells (**Figure 19**), I posited that two

glycolytic side branches—namely the PPP and the serine synthesis pathway (SSP)—might be induced by calcitriol, essentially diverting metabolites away from the glycolytic pathway. Additionally, the increased extracellular acidification rate observed in MCF-7 cells with calcitriol treatment (**Figure 18**) might also be indicative of reduced levels of glycolytic metabolites.

I therefore decided to focus on calcitriol's regulation of G6PD expression, as well as lactate production, as potential contributors to the observed TXNIP regulation. In this regard, I first aimed to confirm the induction in G6PD expression by $1,25(OH)_2D_3$ on both the protein and activity levels, as well as elucidate the time point at which mRNA levels are first induced. G6PD mRNA levels were found to be induced by treatment in as early as 6h (**Figure 29**), i.e. the time point at which the ablation in TXNIP mRNA induction by calcitriol was first observed (**Figure 23**). Additionally, a significant induction in G6PD protein expression was observed after 72h of treatment (**Figure 29**). Complementary data was obtained for the enzyme's activity, which was found to be strongly induced after 72h of treatment (**Figure 29**).

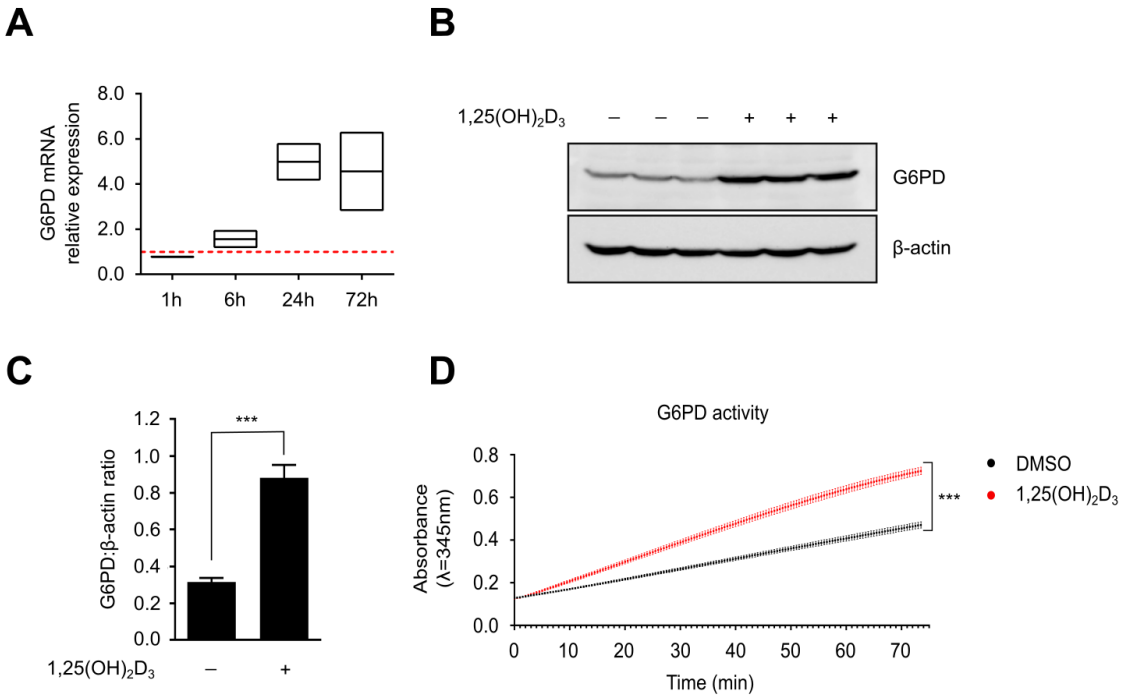

Figure 29: 1,25(OH)$_2$D$_3$ (100 nM) induces G6PD expression and activity in MCF-7 cells. *(A) G6PD mRNA levels are induced with 1,25(OH)$_2$D$_3$ in a time-dependent manner. Relative expression was calculated using the ΔΔCt method, with vinculin as the housekeeping gene. Upper, lower, and middle lines of the floating bars represent the highest, lowest, and the average value of two biological replicates, respectively. (B,C) Western blot and associated densitometric analysis of G6PD levels in 72h DMSO- and 1,25(OH)$_2$D$_3$-treated MCF-7 cells. A two-tailed Student's t-test was used to compare the results of DMSO- and 1,25(OH)$_2$D$_3$-treated cells, with *** depicting p-values less than or equal to 0.001. (D) Kinetic measurements of the increase in absorbance associated with the reduction of NADP+ to NADPH by G6PD in DMSO- and 1,25(OH)$_2$D$_3$-treated MCF-7 crude lysates. The rate of reduction was found to be significantly higher with 1,25(OH)$_2$D$_3$ treatment indicating increased enzymatic activity of G6PD.*

Increasing concentrations of the non-competitive G6PD inhibitor dehydroepiandrosterone (DHEA) [112] were then added to the conditioned medium of MCF-7 cells treated for 48h with calcitriol or a vehicle, for an additional 24h. Independent of 1,25(OH)$_2$D$_3$, DHEA treatment reduced TXNIP expression in a dose-dependent manner (**Figure 30**). A similar experimental setup was repeated using the lactate dehydrogenase inhibitor Na oxamate [113]. In the absence of calcitriol, Na oxamate was found to minorly modulate TXNIP levels, whereas in the presence of calcitriol, a dose-dependent decrease in expression levels was observed (**Figure 30**). In view of these results, I propose that inhibiting the flow of metabolites through a particular pathway, e.g. through the PPP using DHEA, or glycolysis using Na oxamate, prompts metabolites to be shunted into other "activated" pathways in 1,25(OH)$_2$D$_3$ treated cells. In other words, while inhibiting the PPP in 1,25(OH)$_2$D$_3$-treated cells might prevent the flux of metabolites through this pathway, other pathways induced by 1,25(OH)$_2$D$_3$ treatment may provide free channels—for example glycolysis—for these metabolites to enter.

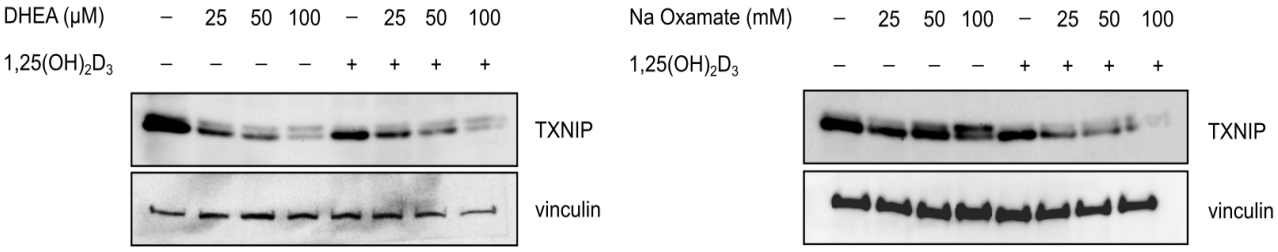

Figure 30: Inhibition of G6PD or lactate dehydrogenase does not rescue TXNIP protein expression in 1,25(OH)$_2$D$_3$-treated cells. *Western blot analysis of TXNIP expression in MCF-7 cells treated with increasing concentrations of DHEA (25-100 μM) or Na Oxamate (25-100 mM), added to the conditioned medium of cells treated for 48h with either DMSO or 1,25(OH)$_2$D$_3$ (100 nM), for an additional 24h. Results illustrate a dose-dependent decrease in TXNIP levels independent and dependent of 1,25(OH)$_2$D$_3$, in the case of DHEA and Na Oxamate, respectively.*

2.2.4. Pharmacological targeting of metabolic "weak points" in 1,25(OH)$_2$D$_3$-treated breast cancer cells.

Although the anti-tumor effects of calcitriol in MCF-7 cells have been reported in many publications [114, 115], a number of observations described above question the therapeutic efficacy of calcitriol in luminal breast cancers. To further clarify, several metabolic changes triggered with treatment appear to be survival-promoting in nature. For example, induction in lactate production and intracellular serine levels (onco-metabolites), as well as G6PD expression (a potential oncogene) by 1,25(OH)$_2$D$_3$ treatment in MCF-7 cells are seemingly undesirable "metabolic side-effects" that could hamper the molecule's therapeutic potential. I postulated that this metabolic adaptation to calcitriol treatment is either a resistance mechanism that enables cells to withstand the molecule's anti-tumor effects, or simply an unwanted vitamin D effect, similar to treatment-induced hypercalcemia. Either way, targeting these potential metabolic "weak points" may enhance calcitriol's therapeutic efficacy.

To address this issue, I first treated MCF-7 cells for 72h with increasing concentrations of the G6PD inhibitor DHEA, in the presence and absence of calcitriol, and assessed the proliferation of cells. A combination of both molecules was found to induce more profound anti-proliferative effects compared to mono-treatment with DHEA (**Figure 31**).

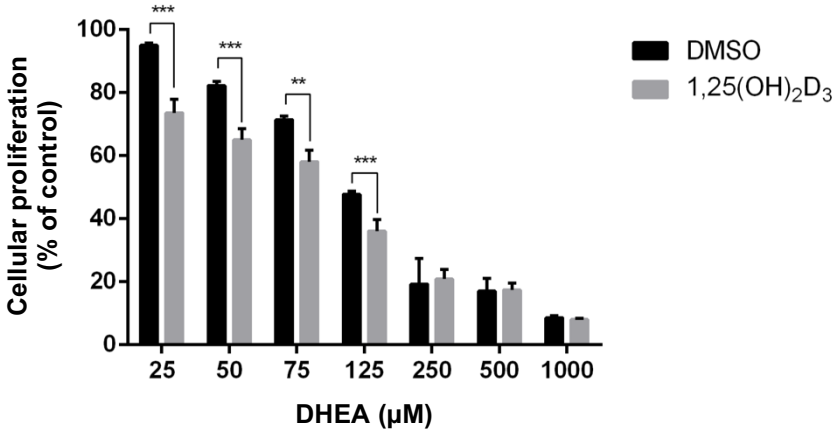

Figure 31: Sulforhodamine B (SRB) assay evaluating the influence of 1,25(OH)$_2$D$_3$ on the anti-proliferative effects of DHEA in MCF-7 cells. *DHEA treatment (72h) was found to clearly reduce proliferation rate in a dose-dependent manner, an effect that was augmented in the presence of 1,25(OH)$_2$D$_3$ (100 nM). Results obtained from the different treatments are normalized to those of DMSO-treated cells. A two-tailed Student's t-test was used to compare the results of mono- and co-treatments, with ** and *** depicting p-values less than or equal to 0.01 and 0.001, respectively. Error bars ± SD ; n=2.*

With regards to the increased serine levels observed with treatment, I hypothesized that 1,25(OH)$_2$D$_3$ reduces the cellular uptake of the amino acid, prompting an increase in its de novo synthesis. Supporting this possibility is the reduction in SLC1A5 (a serine transporter) expression by calcitriol in transformed breast epithelial cells reported by Zhou et al. [116]. CBR-5884 is a novel small molecule inhibitor of the SSP enzyme PHGDH [65]. This molecule has been shown to impact the survival of cancer cells relying more on de novo serine synthesis than uptake [65]. Thus, in the postulated setting of reduced serine uptake with 1,25(OH)$_2$D$_3$ and the compensatory induction in the SSP, calcitriol treatment would prime MCF-7 cells to be more susceptible to CBR-5884's anti-tumor effects. Indeed, treating MCF-7 cells for 72h with a combination of 1,25(OH)$_2$D$_3$ and various concentrations of CBR-5884 led to more potent anti-proliferative effects compared to CBR-5884 alone (**Figure 32**).

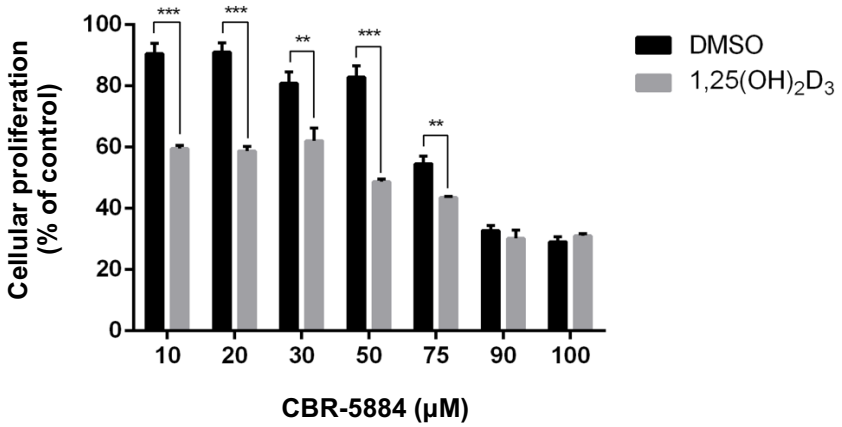

Figure 32: 1,25(OH)$_2$D$_3$ (100 nM) markedly potentiates the anti-proliferative effects of CBR-5884 in MCF-7 cells. *SRB assay reveals a significant reduction in the proliferation of MCF-7 cells treated for 72h with a combination of 1,25(OH)$_2$D$_3$ and CBR-5884, compared to cells treated with the latter alone. Results obtained from the different treatments are normalized to those of DMSO-treated cells. A two-tailed Student's t-test was used to compare the results of mono- and co-treatments, with ** and *** depicting p-values less than or equal to 0.01 and 0.001, respectively. Error bars ± SD ; n=2.*

To investigate whether the observed calcitriol-mediated serine accumulation—through contributing to the folate cycle and thymidine synthesis—may hamper the efficacy of anti-metabolites such as 5-FU, MCF-7 cells were treated for 72h with increasing concentrations of 5-FU, in the presence of either DMSO or 1,25(OH)$_2$D$_3$, and cellular proliferation was evaluated. The presence of calcitriol consistently led to a significant reduction in cellular proliferation with 5-FU, compared to cells treated with 5-FU alone (**Figure 33**).

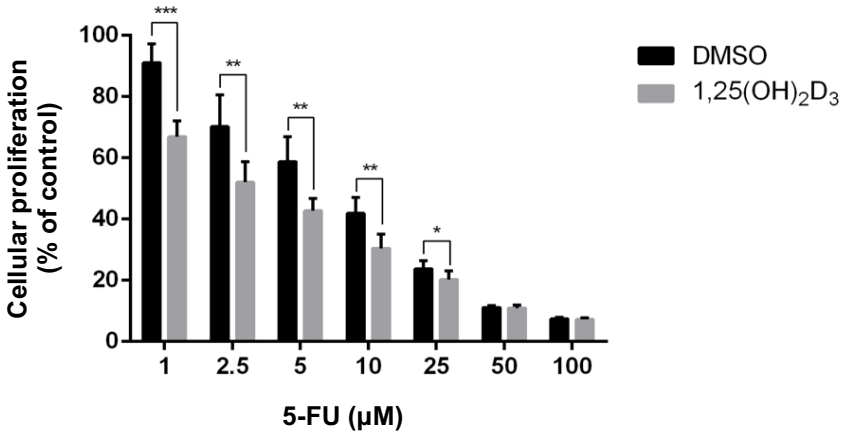

Figure 33: Observed potentiation of 5-FU's anti-proliferative effects in MCF-7 cells upon co-treatment with 1,25(OH)$_2$D$_3$ (100 nM). *72h of treatment with the 5-FU-1,25(OH)$_2$D$_3$ combination exhibits increased efficacy compared to treatment with 5-FU alone, as illustrated by the SRB assay data. Results obtained from the different treatments are normalized to those of DMSO-treated cells. A two-tailed Student's t-test was used to compare the results of mono- and co-treatments, with *, **, and *** depicting p-values less than or equal to 0.05, 0.01, and 0.001, respectively. Error bars ± SD ; n=2.*

2.3. Regulation of the putative vitamin D target gene—TXNIP—by calcitriol.

2.3.1. 1,25(OH)$_2$D$_3$ treatment differentially regulates TXNIP levels in diverse cancer cell lines.

Results of the above-mentioned investigations elucidated the possibility that in cancers, calcitriol treatment may not universally lead to an upregulation in the expression of the putative tumor suppressor TXNIP. In LNCaP and MCF-7 cells, 1,25(OH)$_2$D$_3$ was found to substantially reduce TXNIP protein levels, whereas in MDA-MB-231 cells, treatment does not profoundly alter its expression levels (**Figure 10** and **Figure 22**). In view of this, I aimed to address the question of whether TXNIP really is a vitamin D upregulated protein, and whether the canonical regulation is observed in cancer cell lines besides HL-60 cells. Noteworthy is that this regulation has only so far been described in HL-60 cells [88, 117], and that promoter analysis did not identify VDRE in the mouse VDUP1 [95]. On the other hand, another report identified putative VDRE in the TXNIP promoter using in-silico transcription factor binding prediction software, however the functionality of this site has not been tested [118]. My investigations into this theme have been recently published [119].

I thus first aimed to screen the regulation of this gene on the protein level in response to a 72h treatment with calcitriol in different cell lines of diverse tissue origins. Cell lines derived from hematological (HL-60, Jurkat, U937), liver (HepG2, HLE, SK-HEP-1), breast (MDA-MB-231, MCF-7), prostate (LNCaP, DU145, PC3), pancreatic (AsPC-1, BxPC-3, PC3), and colorectal (HCT116, HT-29) cancers were included in the study, and changes in TXNIP protein expression in response to treatment were evaluated by immunoblotting.

The different cell lines exhibited varying degrees of basal TXNIP expression, with certain cell lines exhibiting very low or undetectable protein levels (**Figure 34**). In cell lines with seemingly silenced TXNIP expression, such as Jurkat, DU145, and PC3 cells, calcitriol treatment did not induce its expression (**Figure 34**). On the other hand, in cell lines expressing detectable TXNIP protein levels, its expression was found to be either induced, reduced, or unchanged with $1,25(OH)_2D_3$ treatment, demonstrating that the canonical increase in TXNIP protein level by calcitriol is not present in all cell lines (**Figure 34**).

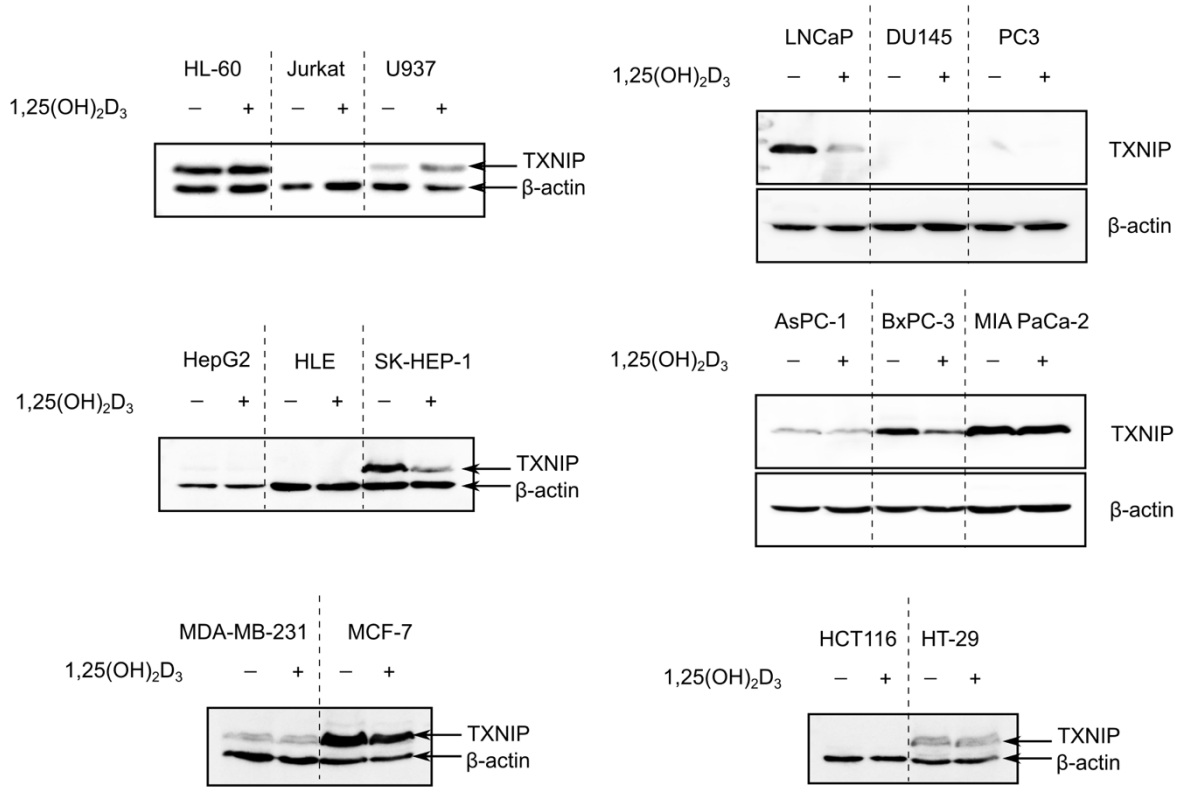

Figure 34: Differential regulation of TXNIP expression by 1,25(OH)$_2$D$_3$ (100 nM) in cancer cell lines of various tissue origins. *Western blot analysis of TXNIP expression in cells treated for 72h with 1,25(OH)$_2$D$_3$. Canonical induction with treatment is only observed in hematological cancer cell lines (U937 and HL-60), whereas non-canonical regulation is observed in LNCaP, SK-HEP-1, BxPC-3, and MCF-7. Lack of regulation is also observed in cell lines with and without basal TXNIP expression, such as HT-29 and HCT116, respectively. Figure obtained from Abu el Maaty et al. [119].*

In view of these findings, I decided to take a closer look at 1,25(OH)$_2$D$_3$'s regulation of TXNIP expression in the cell line in which it was first discovered, HL-60. Since the original report by Chen and Deluca only described the regulation on the mRNA level [88], I sought to replicate their findings, as well as add additional late time points, to get a clearer picture of whether this induction in mRNA expression is transient or sustained. I therefore treated HL-60 cells with calcitriol for 1, 3, 6, 24, 72, and 96h, and analyzed TXNIP mRNA levels using RT-qPCR. Interestingly, while the expected induction in mRNA levels was observed with treatment in the early time points (up to 24h of treatment), the induction in mRNA levels was not only hampered at the later time points, but also mildly reduced with treatment (**Figure 35**).

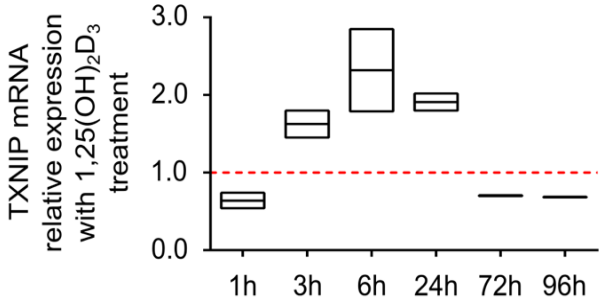

Figure 35: TXNIP mRNA levels are only transiently induced in 1,25(OH)$_2$D$_3$-treated HL-60 cells. *The increase in TXNIP mRNA expression with calcitriol (100 nM) treatment is observed at earlier time points (≤ 24h), and is succeeded by an apparent reduction at later time points. Relative expression was calculated using the ΔΔCt method, with vinculin as the housekeeping gene. Upper, lower, and middle lines of the floating bars represent the highest, lowest, and the average value of two biological replicates, respectively. Figure obtained from Abu el Maaty et al. [119].*

I then studied the regulation of TXNIP protein expression across similar time points. A mild increase in TXNIP protein expression was observed after 24h of treatment with calcitriol, whereas a more profound induction was observed after 96h. Additionally, basal TXNIP expression displayed treatment-independent temporal fluctuations (**Figure 36**). I speculated that at the latest investigated time point (96h), the observed increase in TXNIP protein levels with $1,25(OH)_2D_3$ stemmed from the reduced availability of glucose in the culture medium in vehicle-treated cells, leading to a reduction in intracellular glycolytic intermediates and consequently basal TXNIP expression.

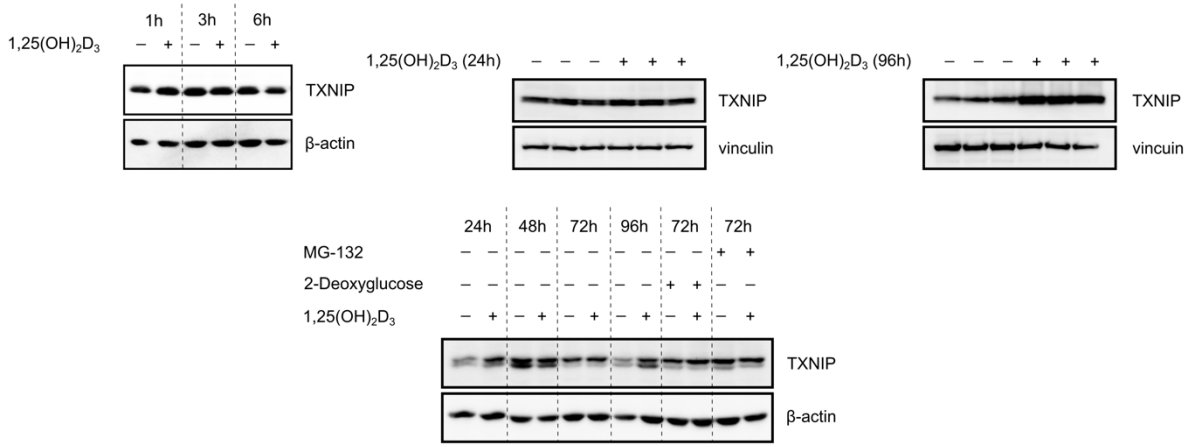

Figure 36: Increase in TXNIP protein levels with $1,25(OH)_2D_3$ is only observed in HL-60 cells at the latest investigated time point. *Western blot analysis of time-dependent regulation of TXNIP expression by $1,25(OH)_2D_3$ (100 nM). While TXNIP protein expression was found to exhibit temporal fluctuations independent of $1,25(OH)_2D_3$, a clear induction in the protein's level is observed after 96h of treatment. 2-Deoxyglucose (10 mM) and MG-132 (5 µM) were included as positive controls, added to the culture medium of cells 24 and 6h prior to the end of the treatment period (72h) with either DMSO or $1,25(OH)_2D_3$, respectively. Figure obtained from Abu el Maaty et al. [119].*

To investigate the possibility that depletion in glucose levels contributed to the reduced basal TXNIP expression at the last time point, I measured the concentration of glucose in the medium of HL-60 cells treated with either DMSO or $1,25(OH)_2D_3$, over a 4-day time course. Although the level of glucose in the culture medium of DMSO-treated cells was significantly lower compared to that of $1,25(OH)_2D_3$-treated cells—possibly due to inhibition of cellular proliferation with the latter—levels were not found to be depleted even at the latest time point (**Figure 37**), which indicates that the observed temporal fluctuations in TXNIP protein

expression reflect the engagement of TXNIP in normal glucose homeostasis rather than critical reduction in glucose availability.

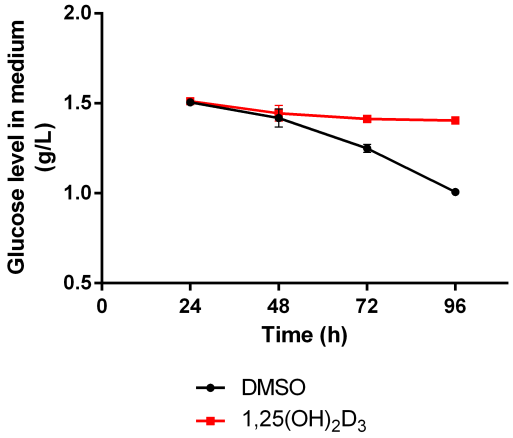

Figure 37: Analysis of changes in glucose concentrations in the culture medium of HL-60 cells treated with either DMSO or 1,25(OH)$_2$D$_3$ over time. *The time-dependent decrease in glucose levels in the medium of vehicle-treated cells is not observed with 1,25(OH)$_2$D$_3$ (100 nM) treatment, possibly due to the reduction in cellular proliferation. Glucose levels are not depleted in either experimental condition at the latest time point. Error bars ± SD ; n=3. Figure obtained from Abu el Maaty et al. [119].*

Furthermore, I studied the potential functional consequences of TXNIP expression, by examining changes in intracellular ROS and glucose uptake with calcitriol treatment, across a time course spanning short and long time points. Intracellular ROS levels were found to be insignificantly influenced by calcitriol at most investigated time points, except at 96h, in which levels were found to be markedly induced with treatment (**Figure 38**). Glucose uptake, on the other hand, was found to be significantly induced and reduced with treatment, after 6 and 72h (**Figure 38**), respectively, highlighting the possible contribution of intracellular glucose/glycolytic metabolites to TXNIP mRNA regulation by 1,25(OH)$_2$D$_3$ (**Figure 35**).

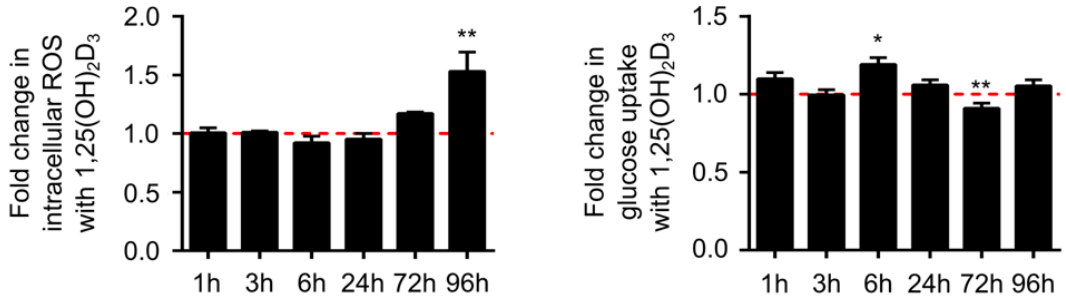

Figure 38: Changes in intracellular ROS levels and glucose uptake in HL-60 cells in response to 1,25(OH)$_2$D$_3$ (100 nM). *While differential regulation of glucose uptake was observed with treatment at the different time points, a significant induction in intracellular ROS levels with 1,25(OH)$_2$D$_3$ was only observed after 96h of treatment. A two-tailed Student's t-test was used to compared the results of DMSO- and 1,25(OH)$_2$D$_3$-treated cells, with * and ** depicting p-values less than or equal to 0.05 and 0.01, respectively. Error bars ± SD ; n=3. Figure obtained from Abu el Maaty et al. [119].*

2.3.2. 1,25(OH)$_2$D$_3$ increases TXNIP expression in HL-60 cells through transcriptional induction and protein stabilization.

Although looking at glucose concentrations in the culture medium did not point towards TXNIP protein stabilization by calcitriol per se, the observed minor reduction in TXNIP mRNA levels after 96h of treatment was indicative of the lack/minimal contribution of transcriptional/translational induction to the clear increase in protein levels with 1,25(OH)$_2$D$_3$ at this time point. To confirm this, HL-60 cells were treated with either DMSO or calcitriol for 96h, and CHX was added to the conditioned medium at different time points before the end of the 96h treatment period. In DMSO-treated cells, CHX treatment led to a profound decrease in TXNIP protein half-life in a time-dependent manner (**Figure 39**). On the other hand, in 1,25(OH)$_2$D$_3$-treated cells, CHX treatments did not significantly decrease TXNIP protein levels (**Figure 39**), demonstrating the lack of involvement of de novo protein synthesis in TXNIP protein induction by a 96h calcitriol treatment.

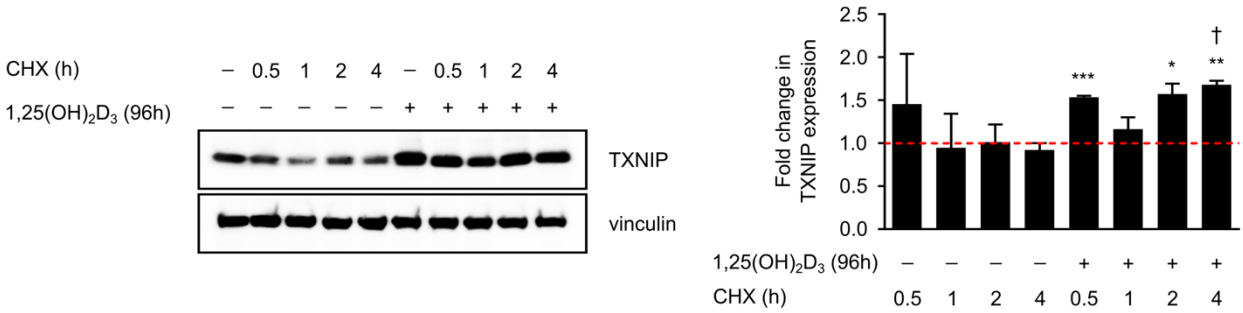

Figure 39: CHX (10 µM) reduces TXNIP protein half-life in 96h DMSO-, but not 1,25(OH)$_2$D$_3$ (100 nM)-treated HL-60 cells. *(Left) Representative western blot analysis of the time-dependent decrease in TXNIP protein expression with CHX, observed in cells treated with DMSO, but not in those treated with 1,25(OH)$_2$D$_3$. CHX treatments were performed in the culture medium of treated HL-60 cells at multiple time points before the end of the DMSO/1,25(OH)$_2$D$_3$ treatment period (96h). (Right) Densitometric analysis of two similar western blot experiments. A two-tailed Student's t-test was used to compare the results of DMSO-treated cells and the different conditions. *, **, and *** depict p-values less than or equal to 0.05, 0.01, and 0.001, respectively. A dagger depicts significance between mono- and co-treatment. Error bars ± standard error of the mean (SEM). Figure obtained from Abu el Maaty et al. [119].*

I then repeated the same experimental setup for a time point at which TXNIP mRNA levels were induced with treatment (24h). The addition of CHX was found to reduce TXNIP protein half-life in both DMSO- and 1,25(OH)$_2$D$_3$-treated HL-60 cells (**Figure 40**), demonstrating the differential modes of TXNIP regulation by treatment (transcriptional/translational induction in 24h, and protein stabilization in 96h).

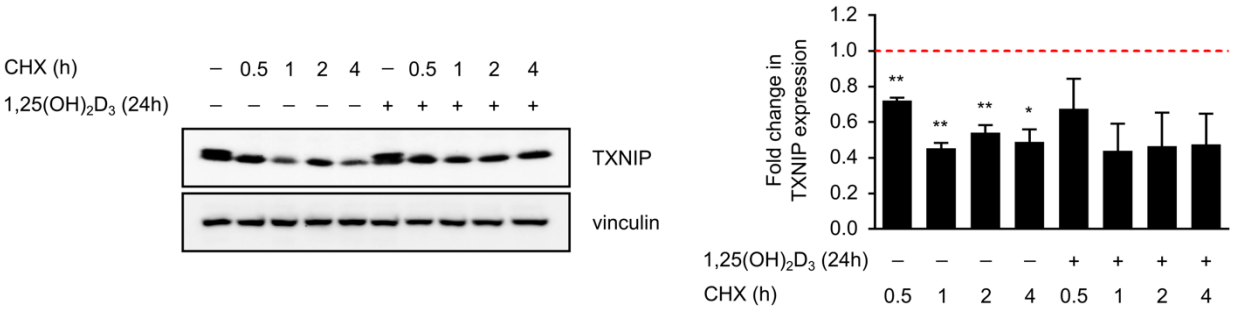

Figure 40: CHX (10 µM) reduces TXNIP half-life in HL-60 cells treated for 24h with DMSO or 1,25(OH)$_2$D$_3$ (100 nM). *Representative western blot (left) and densitometric analysis (right) of two similar experiments. CHX treatments were performed in the culture medium of treated HL-60 cells at multiple time points before the end of the DMSO/1,25(OH)$_2$D$_3$ treatment period (24h). A two-tailed Student's t-test was used to compared the results of DMSO-treated cells and the different conditions. * and ** depict p-values less than or equal to 0.05 and 0.01, respectively. Error bars ± SEM. Figure obtained from Abu el Maaty et al. [119].*

Subsequently, I postulated that similar to the observations in MCF-7 cells, 1,25(OH)$_2$D$_3$ may impact TXNIP protein stability in HL-60 cells through regulating ITCH expression. Although 24 and 96h of treatment with calcitriol significantly reduced ITCH mRNA levels in HL-60 cells, protein expression was unchanged with treatment (**Figure 41**).

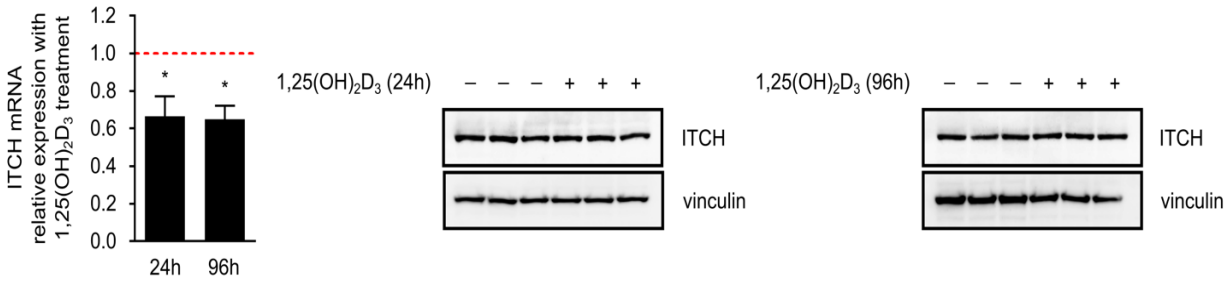

Figure 41: 1,25(OH)$_2$D$_3$ (100 nM) regulates ITCH mRNA but not protein expression in HL-60 cells. *(Left) 24 and 96h of treatment with 1,25(OH)$_2$D$_3$ reduce ITCH mRNA levels in HL-60 cells. Relative expression was calculated using the ΔΔCt method with vinculin as the housekeeping gene. A two-tailed Student's t-test was used to compare the results of DMSO- and calcitriol-treated cells. * depicts p-values less than or equal to 0.05. Error bars ± SD ; n=2. 1,25(OH)$_2$D$_3$ treatment, however, does not regulate ITCH protein levels in HL-60 cells after 24 (middle) or 96h (right). Figure obtained from Abu el Maaty et al. [119].*

2.3.3. Regulation of TXNIP expression by 1,25(OH)$_2$D$_3$ in HL-60 cells possibly involves glucose-sensing networks, but is not a consequence of glucose metabolism reprogramming.

Given the well-defined role of the glucose-sensing transcription heterodimer MondoA/MLX in regulating TXNIP expression [93], I hypothesized that regulation by 1,25(OH)$_2$D$_3$ may be dependent on the functionality of this pathway. I therefore cultured HL-60 cells in glucose-free medium and investigated TXNIP mRNA expression after 24 and 96h of 1,25(OH)$_2$D$_3$ treatment. Indeed, the induction and reduction in the mRNA expression of TXNIP observed in HL-60 cells after 24 and 96h of calcitriol treatment, respectively, were diminished in the absence of glucose (**Figure 42**). However, the vitamin D catabolizing enzyme CYP24A1 was found to be induced by treatment independent of glucose levels (**Figure 42**).

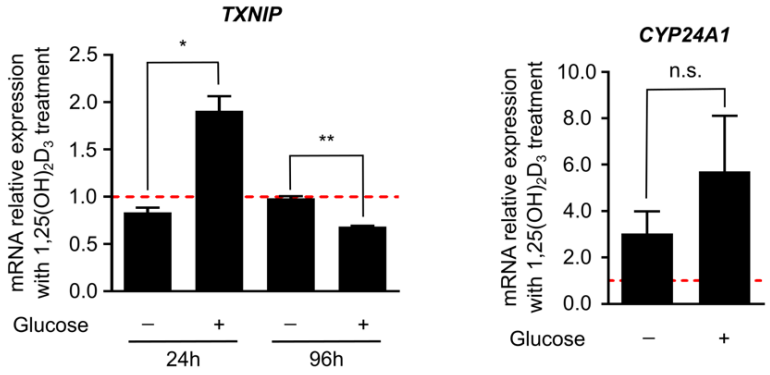

Figure 42: Regulation of TXNIP mRNA expression in HL-60 cells by 1,25(OH)$_2$D$_3$ (100 nM) is glucose-dependent. *Bi-directional regulation of TXNIP mRNA expression by 1,25(OH)$_2$D$_3$ is not present in cells cultured in glucose-free medium. However, the regulation of CYP24A1 mRNA expression in HL-60 cells by 96h of treatment with 1,25(OH)$_2$D$_3$ was found to be independent of glucose levels in the medium. Relative expression is calculated using the ΔΔCt method with vinculin as the housekeeping gene. A two-tailed Student's t-test was used to compare the results of the different conditions. * and ** depict p-values less than or equal to 0.05 and 0.01, respectively. n.s.=non-significant. Error bars ± SD ; n=2. Figure obtained from Abu el Maaty et al. [119].*

Furthermore, I investigated the regulation of TXNIP protein levels by 1,25(OH)$_2$D$_3$ in HL-60 cells cultured in either full medium or medium lacking glucose. Under glucose-free conditions, TXNIP protein levels were found to be strongly depleted, and their levels unaltered by

1,25(OH)$_2$D$_3$ treatment (**Figure 43**). Similarly, in the presence of the glucose transporter inhibitor phloretin [120], calcitriol was incapable of inducing TXNIP protein levels (**Figure 43**), which altogether highlight the necessity of both glucose in the medium, and a functioning glucose transport system, for 1,25(OH)$_2$D$_3$ to induce TXNIP expression. Additionally, the induction in intracellular ROS levels after 96h of treatment of HL-60 cells with 1,25(OH)$_2$D$_3$ was also diminished in the absence of glucose (**Figure 44**). However, the anti-proliferative effects of 1,25(OH)$_2$D$_3$ were observed in HL-60 cells cultured in full medium and glucose-free medium (**Figure 45**).

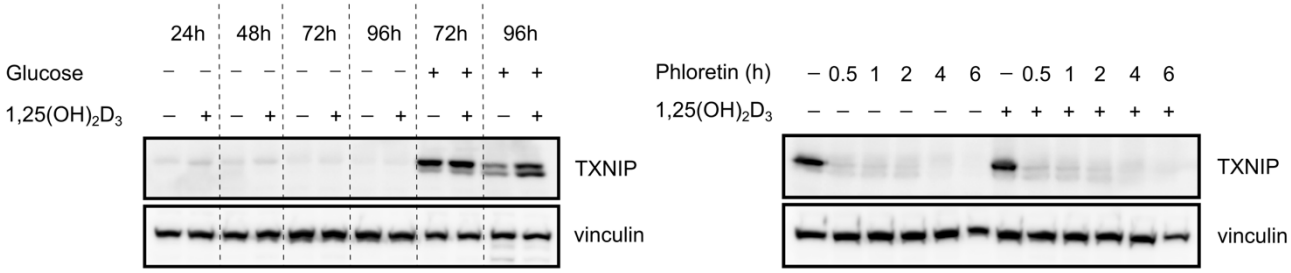

Figure 43: Regulation of TXNIP protein expression in HL-60 cells by 1,25(OH)$_2$D$_3$ depends on glucose-availability, and a functioning glucose transport system. *(Left) Western blot analysis of TXNIP levels in cells treated with either DMSO or 1,25(OH)$_2$D$_3$ (100 nM), cultured in either glucose-free or full medium. (Right) A single high concentration of phloretin (200 µM), added to culture medium containing either DMSO or 1,25(OH)$_2$D$_3$, at multiple time points before the end of the 24h treatment period, inhibits 1,25(OH)$_2$D$_3$'s regulation of TXNIP. Figure obtained from Abu el Maaty et al. [119].*

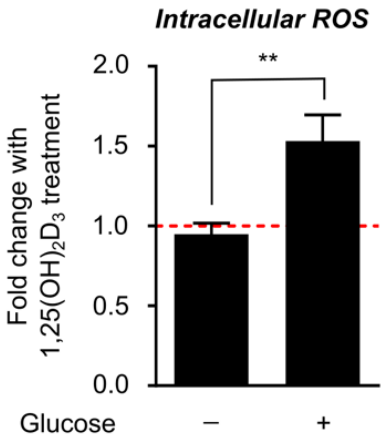

Figure 44: Induction of intracellular ROS by 1,25(OH)$_2$D$_3$ in HL-60 cells is glucose-dependent. *96h of treatment with 1,25(OH)$_2$D$_3$ (100 nM) induces ROS in HL-60 cells cultured in full medium, but not in those cultured in glucose-free medium. Significance between the different experimental conditions is calculated using a two-tailed Student's t-test, with ** depicting a p-value less than or equal to 0.01. Error bars ± SD ; n=3. Figure obtained from Abu el Maaty et al. [119].*

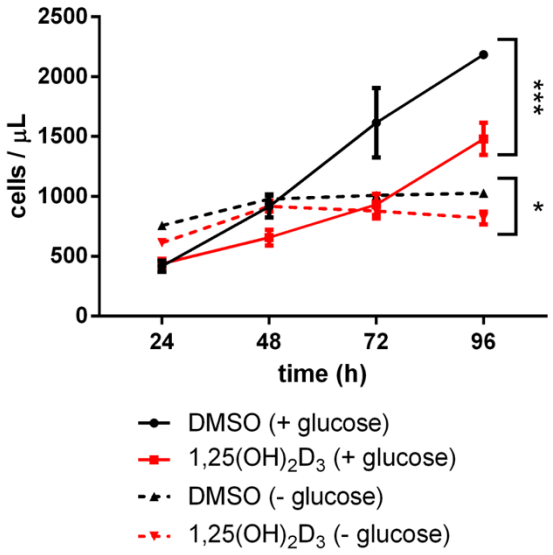

Figure 45: 1,25(OH)$_2$D$_3$ (100 nM) reduces proliferation of HL-60 cells cultured in full medium or glucose-free medium. *A two-tailed Student's t-test was used to compare the results of the different conditions at the latest time point, with * and *** depicting p-values less than or equal to 0.05 and 0.001, respectively. Error bars ± SD ; n=3. Figure obtained from Abu el Maaty et al. [119].*

Since I have previously observed that TXNIP regulation by 1,25(OH)$_2$D$_3$ in prostate and breast cancer cells is linked to metabolic reprogramming, I sought to investigate the metabolic effects calcitriol induces in HL-60 cells. Real-time measurements of culture medium pH and levels of dissolved oxygen, reflecting glycolytic and respiratory rates, respectively, were performed in response to 1,25(OH)$_2$D$_3$ treatment over a course of 4 days. Calcitriol treatment appeared not to induce major differences in the metabolic parameters investigated (**Figure 46**).

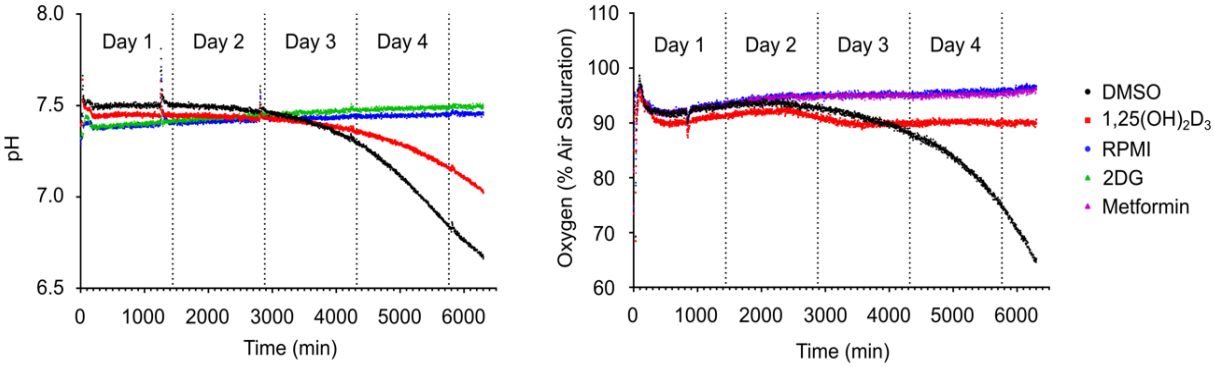

Figure 46: 1,25(OH)$_2$D$_3$ (100 nM) does not markedly influence glucose metabolism in HL-60 cells. *Continuous monitoring of changes in the pH of the culture medium and levels of dissolved oxygen demonstrate lack/minimal influence of 1,25(OH)$_2$D$_3$ on either parameter. Differences in the measurements observed between DMSO and 1,25(OH)$_2$D$_3$ treatments in the fourth day are possibly attributed to the effect of the latter on cellular proliferation. Controls used for oxygen and pH measurements include metformin (2 mM) and 2-Deoxyglucose (10 mM), respectively, as well as culture medium not containing cells (RPMI: Roswell Park Memorial Institute). Figure obtained from Abu el Maaty et al. [119].*

Despite this, calcitriol was found to induce significant alterations in the overall energy status of HL-60 cells, assessed using an ATP assay (**Figure 47**). In 24h, $1,25(OH)_2D_3$ significantly reduced cellular ATP levels, whereas in 48 and 72h, levels were significantly elevated with treatment (**Figure 47**). However, activation of the metabolic stress-related signaling pathway AMPK, was neither observed after 24 nor 96h of treatment (**Figure 47**), which altogether illustrate that treatment-induced metabolic rewiring is an unlikely contributor to TXNIP regulation by $1,25(OH)_2D_3$ in HL-60 cells.

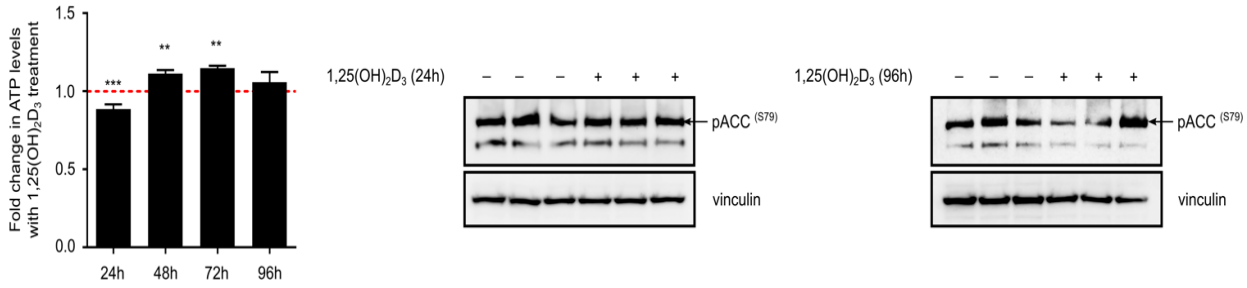

Figure 47: $1,25(OH)_2D_3$ (100 nM) treatment does not induce AMPK signaling in HL-60 cells. *Although $1,25(OH)_2D_3$ was found to differentially alter cellular ATP levels across different time points (left), induction in ACC (S79) phosphorylation was neither observed after 24 (middle) nor 96h (right) of treatment. ATP measurements were normalized to cell count, and are presented as fold change with $1,25(OH)_2D_3$ treatment. Statistical significance is assessed using a two-tailed Student's t-test, with ** and *** depicting p-values less than or equal to 0.01 and 0.001, respectively. Error bars ± SD ; n=3. Figure obtained from Abu el Maaty et al. [119].*

3. DISCUSSION

Prior to the completion of the work presented in this thesis, the appreciated anti-cancer roles of $1,25(OH)_2D_3$ and its analogues were diverse, however, did not include modulation of energy metabolism. The results presented in this thesis illustrate previously uncharacterized effects of calcitriol on distinct metabolic networks in different cancer models. Additionally, data challenge the previously unquestioned notion of TXNIP being a vitamin D upregulated protein. In the following subsections, I discuss in depth the newly recognized role of vitamin D as a potent modulator of onco-metabolism, the potential underlying causes and consequences of TXNIP's non-canonical regulation by $1,25(OH)_2D_3$, and finally, provide an outlook on the future of vitamin D-based chemotherapy, in view of the new findings.

3.1. $1,25(OH)_2D_3$-mediated regulation of metabolic networks in tumor cells.

Based on the results described in this thesis, calcitriol clearly modulates glucose metabolizing pathways in endocrine-related cancers, namely in prostate and breast cancer cell lines (**Figure 3** and **Figure 18**). I demonstrate that $1,25(OH)_2D_3$ regulates the expression of various genes implicated in tumoral glucose metabolism, such as GLUT1 (**Figure 4**), PDHK1 (**Figure 7**), and G6PD (**Figure 29**), as well as energy-related signaling molecules, including AMPK and TXNIP (**Figure 9**, **Figure 10**, **Figure 22**).

Although these $1,25(OH)_2D_3$-mediated metabolic effects are less studied compared to the anti-proliferative and pro-apoptotic ones, I argue that such investigations shed light on ways to enhance the molecule's anti-tumor potential, and that a better understanding of calcitriol's effect on energy metabolism would enable the harnessing of its beneficial effects, while suppressing the potentially counter-therapeutic ones. For example, in MCF-7 cells, $1,25(OH)_2D_3$ triggers versatile metabolic events that typically support tumor growth, including induction of G6PD expression and activity (**Figure 29**), accumulation of serine (**Figure 19**), and enhanced lactate production (**Figure 18**). Even though proliferation of MCF-7 cells was found to be markedly inhibited by $1,25(OH)_2D_3$ (data not shown), it is possible that a subset of these metabolic responses represents a resistance mechanism adopted by cells. Thus, inhibition

of such escape routes through genetic or pharmacological means may potentiate calcitriol's anti-cancer effects. For instance, I demonstrate that pharmacological inhibition, using CBR-5884, of the SSP, which is proposed to be induced in $1,25(OH)_2D_3$-treated MCF-7 cells, enhances the overall treatment's efficacy (**Figure 32**). Similarly, based on their findings that calcitriol induces autophagy—which plays both tumor inhibiting and promoting roles—in luminal breast cancer cells, Tavera-Mendoza et al. [82] illustrated that co-treating mice grafted with MCF-7, or MCF-7 cells in-vitro, with calcitriol and an inhibitor of autophagosome degradation (chloroquine or hydroxychloroquine), leads to a toxic accumulation of autophagosomes, and ultimately, potentiation of calcitriol's anti-tumor effects. Such approach may improve the efficacy of VDR activators in other cancer types, since vitamin D compounds have been shown to induce autophagy in different cancer models [79, 80].

In addition to inducing metabolic changes in tumor cells, calcitriol may elicit similar effects in stromal cells, in view of recent findings illustrating beneficial effects of VDR activation in cancer-associated fibroblasts [41, 121]. For example, Sherman et al. [41] recently showed that calcipotriol induces profound genetic changes in pancreatic stellate cells—the most prevalent fibroblastic type of cells in the pancreatic tumor microenvironment—which induce their conversion from "activated" to "quiescent". This effect enhances the tumoral delivery of gemcitabine, leading to an improved survival in mice receiving both calcipotriol and gemcitabine, compared to animals receiving gemcitabine alone [41]. A different study by Ferrer-Mayorga et al. [121] demonstrated that increased VDR expression in fibroblasts of the tumor stroma positively correlates with overall survival in patients with colorectal cancer. The authors also illustrated that treatment of cancer-associated fibroblasts with $1,25(OH)_2D_3$ induces a gene signature that correlates with improved overall- as well as disease free-survival in patients [121]. Since metabolic crosstalk has been demonstrated between tumor and stromal cells [122], it would be interesting to investigate the potential role of vitamin D signaling in influencing this symbiosis.

Besides reprogramming glucose metabolism in tumor cells, the influence of calcitriol on fatty acid and amino acid metabolism remains a possibility. Based on the data obtained from initial metabolic screens on prostate and breast cancer cells, $1,25(OH)_2D_3$ treatment modulates overall levels of different amino acids (**Figure 5** and **Figure 19**), as well as the mRNA expression of glutamine- and fatty acid-metabolizing enzymes (**Figure 6**). In transformed breast epithelial cells, studies have illustrated that $1,25(OH)_2D_3$ treatment reduces glutamine uptake and lipid

accumulation, due to a reduction in SLC1A5 (a vital glutamine transporter) expression [116], and fatty acid synthesis [123], respectively.

Despite accumulating evidence highlighting vitamin D's extra-skeletal activities, the molecule is still mainly viewed as a regulator of calcium homeostasis. Nonetheless, it is possible that such classical role may underscore new roles in transformed cells, both oncogenic and tumor suppressing. In other words, aberrations in calcium signaling are becoming increasingly linked to tumorigenesis, where studies have illustrated increased expression of various calcium channels, such as TRPV6 (transient receptor potential cation channel, subfamily V, member 6), in breast and prostate cancer [124]. Interestingly, the *TRPV6* gene, whose expression correlates with prostate cancer severity [125], is a direct target of the VDR [8]. Moreover, in LNCaP cells, TRPV6 has been linked to enhanced survival and resistance to apoptosis, and with regards to calcitriol, paradoxically, has been shown to be induced by treatment, and to confer resistance to apoptotic induction by calcitriol as well [126]. Regarding regulation of metabolic processes, overexpression of various calcium channels in cancers may lead to diverse signaling events, such as activation of AMPK, through activating its upstream kinase CAMKK2, potentially leading to autophagy induction. Such model may explain the constitutive activation of AMPK, observed by Park et al. [127] in prostate cancer cell lines and human tissues. Similar to the counter-therapeutic induction of TRPV6 in LNCaP cells reported by Lehen'kyi et al. [126], activation of AMPK signaling by $1,25(OH)_2D_3$ in the same cell line illustrated in this thesis, may dampen the molecule's therapeutic potential/efficacy, by inducing pro-survival pathways, namely autophagy. Although I observed metabolic reprogramming and a reduction in cellular energy levels which may lead to AMPK activation (**Figure 3**, **Figure 8**, **Figure 9**), it is conceivable that the latter observation be achieved by $1,25(OH)_2D_3$-mediated induction in intracellular calcium levels, due to increased expression of TRPV6.

Conversely, regulation of calcium homeostasis by vitamin D might involve non-classical mechanisms, namely influencing energy metabolism. $1,25(OH)_2D_3$ elevates circulating Ca^{2+} levels through increasing its renal and intestinal absorption, as well as by inducing osteoclast formation [3]. The latter mechanism, involves induction of RANKL (receptor activator of nuclear factor kappa-B ligand) expression in osteoblasts, which binds to its receptor RANK on pre-osteoclasts, inducing their maturation to osteoclasts, which in turn increase serum levels of phosphorus and calcium by removing them from bones [3]. Recent studies have illustrated that metabolic alterations occur during osteoclast differentiation [128], with both glycolysis and

oxidative phosphorylation reported to be induced during RANKL-mediated osteoclast differentiation [129]. Similarly, mitochondrial dysfunction through deletion of Ndufs4—an essential subunit of mitochondrial complex I—was found to disrupt differentiation of osteoclasts [130]. On the other hand, osteoblasts have also been shown to exhibit a unique metabolic profile, which similar to cancer cells, is characterized by increased glycolysis even in the presence of oxygen [128]. Interestingly, a recent study by Esen et al. [131] illustrated that parathyroid hormone (PTH), which stimulates bone formation as well as $1,25(OH)_2D_3$ renal production, triggers profound metabolic changes in osteoblast-lineage cells, through inducing insulin-like growth factor-1/mTOR complex 2 signaling. The authors illustrated that PTH treatment induces aerobic glycolysis in cells, and that pharmacological induction of mitochondrial metabolism dampens PTH's anabolic effect on bones [131]. Therefore, taken together, these studies demonstrate that cellular metabolism is critical to both bone resorption and formation. Given $1,25(OH)_2D_3$'s direct and indirect roles in regulating bone health [132], as well as its negative feedback regulation of PTH production and secretion [3], it is possible that metabolic changes underlie vitamin D-mediated bone remodeling. A better understanding of such mechanisms would lead to the optimal use of vitamin D compounds in diseases such as osteoporosis.

3.2. TXNIP: a bystander, a "conditional" tumor suppressor, or a potential oncogene?

An unexpected result in the early investigations of this thesis was the strong reduction in TXNIP protein expression with $1,25(OH)_2D_3$ treatment in LNCaP cells (**Figure 10**). The initial hypothesis was that the decrease in glucose uptake in calcitriol-treated LNCaP cells was mediated through increased TXNIP expression, given the protein's first identification as the VDUP1 and its role as a negative regulator of glucose uptake [88, 93]. However, it appeared that TXNIP protein levels are negatively regulated by $1,25(OH)_2D_3$ due to possible hampering of transcriptional induction on one hand, and protein degradation on the other. Similar effects were observed in MCF-7 breast cancer cells (**Figure 22**), demonstrating the occurrence of this regulation in experimental systems previously used to advocate vitamin D's anti-cancer effects [114, 115, 133]. Moreover, in other cell lines, calcitriol treatment had no effect on TXNIP protein levels (**Figure 34**), which not only questions the identity of the protein as one that is

upregulated by vitamin D treatment, but also its importance in mediating the anti-cancer effects of $1,25(OH)_2D_3$.

The view of TXNIP as a putative tumor suppressor originates from in-vitro, pre-clinical and clinical studies that demonstrate that: i) its expression is reduced/silenced in different tumor types, and ii) its expression induces oxidative stress-mediated apoptosis, cell cycle arrest, and inhibits mTOR signaling [108, 109]. While these are convincing arguments for TXNIP's tumor suppressing roles, the protein's influence on redox status could also be viewed from a pro-survival perspective, since targeting ROS homeostasis in cancer treatment is bi-directional [134]. In other words, cancer cells are known to exhibit higher levels of ROS compared to their non-cancerous counterparts [134], making them more susceptible to ROS-modulating drugs. Therefore, targeting this homeostasis by anti-oxidants (e.g. TXNIP inhibitors) or pro-oxidants (e.g. TXNIP inducers) inhibits tumor cell survival [134].

In this regard, I posit that inhibition of TXNIP may also be a viable therapeutic option, particularly in cancer cells that maintain the protein's expression, as well as have particularly high ROS levels secondary to tissue-specific hormone- or growth factor-signaling. For example, numerous studies have demonstrated the involvement of AR-signaling in the oxidative stress observed in hormone-dependent prostate cancer [135]. In this regard, different studies have shown that treatment of LNCaP cells with androgens induces intracellular ROS levels [136, 137], whereas Pathak et al. [138] illustrated that dihydrotestosterone induces oxidative DNA damage in LNCaP cells (hormone-dependent), but not in DU145 or PC3 cells (hormone-independent). Additionally, the authors demonstrated that treating LNCaP-grafted mice with the anti-androgen flutamide significantly reduces oxidative DNA damage [138]. Similarly, in a study conducted by Miyake et al. [139], prostate cancer patients receiving hormonal therapy exhibited lower urinary levels of 8-hydroxy-2'-deoxyguanosine—a marker of oxidative DNA damage—compared to the levels observed before commencement of treatment. Despite these results, a clear mechanistic link connecting the AR to ROS homeostasis is missing.

In this thesis, I show that LNCaP cells, which are AR-positive/hormone-sensitive prostate cancer cells, exhibit detectable TXNIP protein levels under basal conditions (**Figure 10**), and that genetic or pharmacological inhibition of the AR leads to a reduction in TXNIP protein expression (**Figure 15** and **Figure 16**). Although I did not experimentally link AR modulation

to ROS homeostasis in my studies, I propose that regulating the activity/expression of members of the thioredoxin system, such as TXNIP, may be a mechanism through which AR-signaling aberrations drive cancer growth and proliferation.

The other example of reduction in TXNIP protein expression by calcitriol is MCF-7 cells (**Figure 22**), which are luminal breast cancer cells, i.e. express ER and respond to hormone therapy, e.g. tamoxifen. Of note, is that estrogen and its metabolites, similar to androgens, have been shown to induce intracellular ROS levels, an effect known to contribute to the transformation and survival of breast cancer cells [140]. Given vitamin D's well-characterized role as an anti-estrogen signaling molecule, via reducing ER alpha and aromatase expression [9], it is possible that the calcitriol-mediated reduction in TXNIP expression, and potentially ROS levels, serves as an additional mechanism dampening estrogen signaling. Additionally, at least in MCF-7's case, the induction in G6PD expression and activity by calcitriol (**Figure 29**), may also lead to enhanced cellular anti-oxidant capacity, due to the increase in NADPH generation. Evidence supporting the inhibition of TXNIP as an anti-cancer strategy comes from the study by Song et al. [141], who demonstrated that reduction in VDUP1 expression using antisense cDNA, reduces intracellular ROS levels as well as inhibits proliferation of in-vitro and in-vivo melanoma models.

These notions are intriguing and certainly warrant additional investigations, since results of studies investigating the efficacy of various antioxidants in cancer therapy have been so far contradicting. On one hand, N-acetylcysteine and vitamin C have been shown to inhibit tumor growth in preclinical models [142]. On the other hand, results of the Selenium and Vitamin E Cancer Prevention Trial (SELECT) illustrated that dietary vitamin E supplementation significantly increases the risk of prostate cancer in men [143].

Furthermore, I propose that TXNIP's role in glucose-sensing traps it in a crossfire between potential anti-cancer agents that limit glucose uptake or activate AMPK signaling, such as phloretin and metformin, respectively, and those that induce TXNIP levels, such as suberoylanilide hydroxamic acid, the histone deacetylase inhibitor [118]. It would therefore be exciting to study the effect of combining such TXNIP "activators" and "inhibitors" on anti-cancer activities.

Inhibition of TXNIP has also been shown to possess beneficial effects in other diseases, such as diabetes, where studies have illustrated elevated TXNIP expression in muscles of pre-diabetic and diabetic individuals on one hand [144], as well as induction of pancreatic beta cell apoptosis [145], an important step in type 1 and type 2 diabetes development [117], by the protein on the other. Moreover, it has been shown that TXNIP and insulin negatively regulate each other's expression [146, 147], and that genetic/pharmacological inhibition of TXNIP in pancreatic beta cells protects from both type 1 and type 2 diabetes [117]. Furthermore, verapamail, a calcium channel blocker, has been shown to reduce TXNIP expression and beta cell apoptosis, elevate endogenous levels of insulin, and finally, protect mice from streptozotocin-induced diabetes [148]. Considering the established epidemiological link between diabetes and cancer [149], it is tempting to link diabetes-associated TXNIP induction to tumorigenesis. Interestingly, hyperinsulinemia, which is proposed to be one of the underlying molecular mechanisms linking diabetes to cancer [149], does not appear to impede diabetic hyperglycemia-induced TXNIP induction [117], highlighting the possibility that repeated and sustained post-prandial elevation in blood glucose levels, typically observed in pre-diabetics, may lead to a consistent, long-term increase in TXNIP levels, which may override, in terms of TXNIP regulation, the hyperinsulinemia observed in some type 2 diabetics. Furthermore, metformin, which is the most widely prescribed drug for type 2 diabetics and a putative anti-cancer drug [70], is known to exert beneficial effects via insulin-dependent and –independent mechanisms [70], which may have contrasting effects on TXNIP expression. As an inhibitor of mitochondrial respiratory chain complex I [70], metformin increases cellular AMP:ATP ratio leading to AMPK activation, which induces TXNIP phosphorylation and subsequent degradation [94]. Additionally, metformin induces cellular glucose uptake and inhibits gluconeogenesis, thus lowering blood glucose levels and improving insulin resistance [70]. Although this has not been investigated, the subsequent lowering of circulating insulin levels in response to metformin treatment may lead to stabilization of cellular TXNIP levels, however, it should be noted that normal/basal levels of TXNIP are not linked to dysfunctional beta cells, but rather enhanced expression [117]. Thus, normalization—but not depletion—of TXNIP levels is proposed to be beneficial to diabetes therapy [117].

With regards to TXNIP regulation by vitamin D, the data presented here clearly illustrate that the anticipated positive regulation of TXNIP expression by $1,25(OH)_2D_3$ is not universal (**Figure 34**). However, it remains a possibility that the TXNIP gene contains functional VDRE, and that their accessibility by the VDR-RXR heterodimer is subject to chromatin architecture.

Although promoter analysis of the mouse VDUP1 gene failed to show the presence of VDRE [95], a different study predicted putative VDRE in the human TXNIP gene, however, the functionality of this site has not been shown [118].

Moreover, a clear distinction should be made between potential transcriptional regulation of the TXNIP gene by $1,25(OH)_2D_3$ treatment, and actual elevation/stabilization in protein expression. Stambolsky et al. [86] demonstrated that mutant p53 converts the VDR from a tumor suppressor into a survival-promoting agent. In cells harboring mutant p53, the authors illustrated that calcitriol treatment reduces mRNA levels of TXNIP, a pro-apoptotic molecule [86]. On a similar note, the negative regulation of c-Myc by calcitriol shown in different publications [27, 97], could lead to differential regulation in TXNIP mRNA levels. Thus, transcriptional regulation of the TXNIP gene in cancer cells by calcitriol is subject to the cells' genetic background. On the other hand, assuming transcriptional induction by $1,25(OH)_2D_3$ as a prelude to increased TXNIP protein levels, the stability/activity of this protein is subject to diverse processes also influenced by vitamin D compounds, such as various protein degradation machinery [110], as well as by different kinases, namely AMPK and Akt [7, 78]. Moreover, TXNIP mRNA stability may also be targeted by vitamin D compounds post-transcriptionally, since microRNA expression has been shown to be regulated by vitamin D treatment [150]. Of interest, is that microRNA-17, which has been shown to inhibit TXNIP expression [117], has also been shown to be reduced in LNCaP cells by calcitriol treatment [133], indicating the possible stabilization of TXNIP mRNA levels by $1,25(OH)_2D_3$, possibly leading to an increase in protein levels.

Moreover, the functional consequences of putative TXNIP activation by $1,25(OH)_2D_3$ may be subject to its cellular localization, which may be dictated by other effects of the treatment. For example, it has been recently shown that TXNIP, which had been repeatedly identified as a cytoplasmic protein, resides in the nucleus of pancreatic beta cells under basal conditions, and shuttles to the mitochondria in response to oxidative stress, where it binds to thioredoxin-2, disrupting its association with apoptosis signal-regulating kinase 1, leading to the latter's activation and ultimately mitochondrial-dependent apoptosis [151]. In light of vitamin D's regulation of redox-related genes [87, 152, 153], such mechanism may underscore the functional outcome of TXNIP induction by calcitriol, where mitochondrial localization of the protein in response to treatment-induced oxidative stress may dampen its role in glucose-sensing.

3.3. Concluding remarks and future perspectives.

This thesis clearly demonstrates previously unrecognized effects of calcitriol in transformed cells. Demonstrating the regulation of energy metabolism in tumor cells by treatment undoubtedly contributes to the evidence linking vitamin D to cancer treatment. However, despite encouraging in-vitro and pre-clinical results that continue to accumulate, extrapolation of vitamin D-based therapies to the clinic is in a stalemate. I propose that an improved, or perhaps a broader understanding of vitamin D's cellular effects would lead to its optimal exploitation clinically. As a start, a strong distinction needs to be made between the "vitamin D-transcriptome" and the "vitamin D-proteome", since vitamin D-regulated genes may be subject to either treatment-induced post-translational modifications—potentially altering protein stability and/or function—or simply not translated to proteins in the first place. The former possibility is tightly linked to vitamin D's non-genomic effects on cell signaling [8], in which modulation of the activity of various signaling molecules by treatment, may lead to altered activity and stability of vitamin D-target genes. Moreover, effects of vitamin D on the expression levels of proteins may be largely independent of the classical transcriptional induction. To further clarify, vitamin D may alter the expression of putative target genes post-transcriptionally, for example, through regulating the expression of mRNA-stabilizing or –destabilizing non-coding RNAs like microRNAs, which have been shown to be regulated by vitamin D treatment [150]. Additionally, VDR activators may influence target protein stability and activity through inducing post-translational modifications, as previously mentioned, by: i) regulating the activity of various kinases, such as AMPK [78], which would lead to target protein phosphorylation, and/or ii) by inducing the expression of different E3 ligases [110], such as ITCH, which would enhance the ubiquitination and subsequent degradation of target proteins. Through these mechanisms, vitamin D treatment may indirectly influence the protein expression of numerous genes that had previously been undetected by classical cDNA microarray screens. A good example of such regulation is that of TXNIP by $1,25(OH)_2D_3$ in prostate and breast cancer cell lines described in this thesis.

Furthermore, I posit that hypercalcemia and tissue mineralization associated with the supra-physiological doses of calcitriol may not be the sole side effects hampering the molecule's use. For example, AMPK signaling induction by $1,25(OH)_2D_3$, secondary to either increases in AMP:ATP ratio or intracellular Ca^{2+} levels, may impede the overall anti-cancer outcome, since this may lead to the activation of survival-promoting pathways such as autophagy [60]. These

possibilities should not discourage the use of calcitriol in oncological settings, but rather prompt further investigations into the different options enabling the bypassing or targeting of these pathways. An example of such approach is the use of an inhibitor of de novo serine synthesis in combination with $1,25(OH)_2D_3$ to counteract the possible compensatory increase in serine synthesis in response to calcitriol's effect on serine uptake in breast cancer cells. Therefore, a clearer picture of vitamin D's cellular effects, both "the good" and "the bad", would substantially increase the chances of success of vitamin D-based chemotherapies in clinical trials.

In the context of this thesis, I propose that studying the metabolic effects of $1,25(OH)_2D_3$ on different tumor types would elucidate ways to enhance the molecule's efficacy. For example, in the case of prostate cancer cells, where calcitriol treatment was found to activate AMPK signaling, which is known to promote survival in such cells [127], either potentiating or counteracting this effect pharmacologically may enhance the molecule's efficacy. Noteworthy is that this pathway appears not to be activated by $1,25(OH)_2D_3$ in all investigated cancer cell lines, since it was not observed in experiments performed on MDA-MB-231 and HL-60 cells, as described in previous sections (**Figure 22** and **Figure 47**). This does not tightly correlate with a lack of metabolic rewiring induced by treatment, as is the case in HL-60 cells, since MDA-MB-231 cells exhibited clear metabolic changes in response to $1,25(OH)_2D_3$, nor does it correlate with the presumed canonical increase in intracellular Ca^{2+} levels—and subsequent signaling events—by calcitriol treatment. I hypothesize that AMPK signaling activation by VDR activators is largely dependent on cells' genetic background, for example, p53 status. Within the scope of the investigations described in this thesis, AMPK induction was observed in cancer cells harboring wild-type p53 (MCF-7 and LNCaP), but not in those with a mutant form (MDA-MB-231) or those lacking p53 (HL-60). This possibility is intriguing and warrants further investigations, since p53 has been shown to trans-activate AMPK β1/2 [154], and AMPK has been shown to phosphorylate p53 at serine 15, inducing its stabilization [155]. Therefore, in wild-type p53-harboring cells, putative increases in intracellular Ca^{2+} levels in response to $1,25(OH)_2D_3$ treatment could lead to a clearer, more sustained activation of AMPK, due to the bidirectional regulation of AMPK and p53.

4. MATERIALS AND METHODS

4.1. Materials

4.1.1. Chemicals

Table 2: List of chemicals used in the described experiments.

CHEMICAL	SUPPLIER
$1,25(OH)_2D_3$	Cayman Chemical, Biomol GmbH, Germany
10058-F4	Sigma-Aldrich, Germany
2-Deoxyglucose	Fluka-Sigma-Aldrich, Germany
4-(2-hydroxyethyl)-1-piperazineethanesulfonic acid (HEPES)	Carl Roth GmbH, Germany
5-FU	Fluka, Sigma-Aldrich, Germany
AICAR	Adipogen, Biomol GmbH, Germany
Ammonium persulfate	AppliChem, Germany
Aprotinin	AppliChem, Germany
BAPTA-AM	Cayman Chemical, Biomol GmbH, Germany
Bovine serum albumin (BSA)	Carl Roth GmbH, Germany
Bromophenol blue	AppliChem, Germany
Calcipotriol	Cayman Chemical, Biomol GmbH, Germany
Casodex	Santa Cruz Biotechnology, Heidelberg, Germany
CBR-5884	Cayman Chemical, Biomol GmbH, Germany

Chloroform	Zentralbereich Theoretikum Chemikalienlager, Heidelberg University.
CHX	Fluka-Sigma-Aldrich, Germany
Compound C	Calbiochem, Germany
DHEA	Cayman Chemical, Biomol GmbH, Germany
DMSO	Sigma-Aldrich, Germany
Ethanol	VWR Chemicals, Germany
Ethylenediaminetetraacetic acid (EDTA)	Merck, Germany
Glucose	Sigma-Aldrich, Germany
Glucose-6-phosphate (G6P)	Sigma-Aldrich, Germany
Glycerol	Sigma-Aldrich, Germany
Glycine	Sigma-Aldrich, Germany
Isopropanol	Zentralbereich Theoretikum Chemikalienlager, Heidelberg University.
KCl	AppliChem, Germany
L-Glutamine	Gibco, Germay
Leupeptin	AppliChem, Germany
Metformin HCl	Sigma-Aldrich, Germany
Methanol (absolute)	Sigma-Aldrich, Germany
MG-132	Sigma-Aldrich, Germany
$MgCl_2$	Sigma-Aldrich, Germany
Milk	Carl Roth GmbH, Germany
Na Oxamate	Cayman Chemical, Biomol GmbH, Germany
Na_3VO_4	AppliChem, Germany
$Na_4P_2O_7$	AppliChem, Germany
NaCl	AppliChem, Germany
NADP+	Sigma-Aldrich, Germany
NaF	AppliChem, Germany
o-dianisidine	Sigma-Aldrich, Germany
Pepstatin	AppliChem, Germany
Phenol red	Sigma-Aldrich, Germany

Phenylmethane sulfonyl fluoride (PMSF)	AppliChem, Germany
Phloretin	Sigma-Aldrich, Germany
Rotiphorese® Gel 30/ Acrylamide mix	Carl Roth GmbH, Germany
Sodium dodecyl sulfate (SDS)	Merck, Germany
ß-mercaptoethanol	Merck, Germany
STO-609	Cayman Chemical, Biomol GmbH, Germany
Testosterone	Sigma-Aldrich, Germany
Tetramethylethylenediamine (TEMED)	Carl Roth GmbH, Germany
Trichloroacetic acid	VWR Chemicals, Germany
Tris	Carl Roth GmbH, Germany
Tris-HCl	Carl Roth GmbH, Germany
Triton X-100	Carl Roth GmbH, Germany
Tween 20	Carl Roth GmbH, Germany
Urea	Carl Roth GmbH, Germany

4.1.2. Commercially-available reagents, kits, and consumables

Table 3: List of commercially-available reagents, kits, and consumable used in the described experiments.

ITEM	**SUPPLIER**
2-NBDG	Cayman Chemical, Biomol GmbH, Germany
Acid-washed glass beads (diameter 425-600 µm)	Sigma-Aldrich, Germany
ATPlite™ 1 step kit	Perkin Elmer, Germany
BD FACSFlow™	Becton Dickinson, Germany
BD™ FACSclean	Becton Dickinson, Germany
Black 96-well microplate (clear bottom)	Costar®, Corning Incorporated, USA
Bradford Reagent	Sigma-Aldrich, Germany
Cell culture flasks (T-25, -75, -175)	Greiner Bio-One, Germany
Cell culture petri-dishes	Greiner Bio-One, Germany

Cell culture plates (6-, 12-, 24-, 48-, and 96- well plates)	Greiner Bio-One, Germany
Dihydroethidium (DHE)	Cayman Chemical, Biomol GmbH, Germany
DMEM (without $NaHCO_3$ and glucose)	Pan-Biotech GmbH, Germany
Dulbecco's Modified Eagle Medium (DMEM)-GlutaMAX™	Gibco, Germay
Dulbecco's Phosphate-Buffered Saline (D-PBS)	Gibco, Germay
Eppendorf tubes (1.5 and 2.0 mL)	Greiner Bio-One, Germany
FACS tubes	Becton Dickinson, Germany
Falcon/Centrifuge tubes	Greiner Bio-One, Germany
Fetal Calf Serum (FCS)	Gibco, Germay
GOx	Sigma-Aldrich, Germany
Horseradish peroxidase (HRP)	Sigma-Aldrich, Germany
HydroDish®	PreSens Precision Sensing GmbH, Germany
JC-1	Sigma-Aldrich, Germany
LightCycler® 480 SYBR Green I Master	Roche, Germany
Lipofectamine® 3000	Thermo Fischer, Germany
MitoTracker Green	Thermo Fischer, Germany
Opti-MEM Reduced Serum Medium	Gibco, Germany
OxoDish®	PreSens Precision Sensing GmbH, Germany
PageRuler™ Prestained Protein Ladder	Nippon Genetics Europe GmbH, Germany
Parafilm® M	Sigma-Aldrich, Germany
Penicillin-streptomycin	Gibco, Germay
Polyvinylidene fluoride (PVDF) membranes	GE Healthcare, Germany
Ponceau S	Sigma-Aldrich, Germany
ProtoScript® II first strand cDNA synthesis kit	New England Biolabs, Germany
QIAzol lysis reagent	Qiagen, Germany
RPMI 1640 without glucose	Gibco, Germany
RPMI 1640-GlutaMAX™	Gibco, Germany

Sensorchips SC1000	Bionas, Rostock, Germany
Serological pipettes (2.0, 5.0, 10.0, 25.0 mL)	Costar corning incorporated
SRB sodium salt	Santa Cruz Biotechnology, Germany
Syringe filters (0.2 µm pore size)	GE Healthcare, Germany
Syringes (50 mL)	Becton Dickinson, Germany
TrypLE™ Express	Gibco, Germay
Western Lightning™ Plus-ECl	Perkin Elmer, Germany
Whatman™ 3mm CHR (45x57 cm)	GE Healthcare, Germany

4.1.3. Instruments

Table 4: List of instruments used to perform the described experiments.

INSTRUMENT	**SUPPLIER**
AccuBlock Tm Digital Dry Bath	Labnet International, Inc., NJ, USA
Analytical balance 440-33N	Kern und Sohn, Balingen, Germany
BIONAS 2500	Bionas, Rostock, Germany
BlueFlash-L	SERVA Electrophoresis GmbH, Germany
Centrifuge 5415R	Eppendorf, Germany
Centrifuge 5702	Eppendorf, Germany
Centrifuge 5804	Eppendorf, Germany
Enduro™ Power Supplies	Labnet International, Inc., NJ, USA
FACS Calibur	Becton Dickinson, Germany
Hemocytometer	Brand, Wertheim, Germany
HERA cell 150i incubator	Thermo Scientific, Germany
LAS3000 Imaging System	FujiFilm, Germany
Micropipettes (10, 20, 100, 200, 1000 µL)	Eppendorf, Germany
Microscope CKX41	Olympus Life Science, Germany
Miltidrop Combi	Thermo scientific, Germany
Mixer mill MM 300	Retsch, Germany
Multichannel pipettes (100 and 200 µL)	Eppendorf, Germany

NanoDrop 2000 spectrophotometer	Thermo scientific, Germany
Orbital shaker/Belly Dancer	Stovall Life Science Inc., NC, USA
Pipetboy	Integra Biosciences, Germany
Power Station 200	Labnet International, Inc., NJ, USA
Problot hybridization oven	Labnet International, Inc., NJ, USA
Real-time thermal cycler qTower	Analytik Jena AG, Germany
Roller mixer SRT6	Stuart, Germany
SensorDish® Readers (SDRs)	PreSens Precision Sensing GmbH, Germany
Spectrafuge Mini	Labnet International, Inc., NJ, USA
Tecan Infinite F200 Pro	Tecan, Germany
Tecan Ultra plate reader	Tecan, Germany
Thermomixer comfort	Eppendorf, Germany
Vacuum pump	ZM Engineering, Apolda, Germany
VIAFLO ASSIST automated multi-channel pipettes	Integra Biosciences, Germany
Vortex-Genie®2	Scientific Industries, Inc., NY, USA
Water bath	GFL, Germany

4.1.4. Buffers and solutions

Table 5: List/recipes of buffers/solutions used in the described experiments.

Buffer/solution	**Ingredient**	**Concentration**
Bionas RM	Glucose	1 g/L
	L-Glutamine	2 mM
	Penicillin	100 U/mL
	Streptomycin	100 µg/mL
	HEPES	1 mM
	FCS	0.1 %
	Phenol red	15 µg/L
		-

	DMEM (without $NaHCO_3$ and glucose)	
Lysis buffer for SDS-Polyacrylamide gel electrophoresis (PAGE)	Urea EDTA Triton X-100 NaF Pepstatin Leupeptin Aprotinin PMSF Na_3VO_4 $Na_4P_2O_7$ in D-PBS	6 M 1 mM 0.5 % 5 mM 10 µg/mL 10 µg/mL 3 µg/mL 100 µM 1 mM 2.5 mM -
5X Gel loading buffer	SDS ß-mercaptoethanol Bromophenol blue Glycerol Tris HCl in distilled water	4% 200 mM 0.2% 20 % 10 mM -
SDS-PAGE running buffer	Tris HCl Glycine SDS in distilled water	25 mM 250 mM 0.1% -
Tris-glycine SDS-Polyacrylamide gel (10%)	30% Acrylamide mix 1.5 M Tris (pH 8.8) 10% SDS 10% Ammonium persulfate TEMED Water	33% 25% 1% 1% 0.04% 40%

Stacking gel for Tris-glycine SDS-polyacrylamide gel (5%)	30% Acrylamide mix 1.0 M Tris (pH 6.8) 10% SDS 10% Ammonium persulfate TEMED Water	17% 12.5% 1% 1% 0.1% 68%
Anode buffer	Methanol Tris HCl in distilled water	10 % 0.3 M -
Cathode buffer	Methanol Tris HCl in distilled water	10 % 25 mM -
TBS/Tween	NaCl KCl Tris HCl Tween 20 in distilled water	8 g/L 0.2 g/L 3 g/L 0.1 % -
GOx enzyme mix	GOx Tris pH 8.0 HRP o-dianisidine	50 mg/L 250 mM 40 mg/L 100 mg/L
G6PD enzyme mix	KCl Tris HCl $MgSO_4$ in distilled water	100 mM 50 mM 5 mM -
Lysis buffer for crude extracts	HEPES EDTA $MgCl_2$ KCl in distilled water	20 mM 1 mM 5 mM 100 mM -

4.1.5. Computer software

Table 6: List of computer software used in performing experiments/analyzing data.

SOFTWARE	SUPPLIER
BIONAS analysis software	Bionas, Rostock, Germany
CellQuest Pro Analysis Software	Beckton Dickinson, NJ, USA
GraphPad PRISM	GraphPad Software Inc., CA, USA
Image Reader LAS-3000	Fujifilm, Germany
ImageJ	National Institutes of Health, Maryland, USA
Microsoft Excel	Microsoft, WA, USA
NanoDrop 2000 software	Thermo Scientific, Germany
qPCRsoft 3.1	Analytik Jena, Germany
SDR_v38 software	PreSens Precision Sensing GmbH, Germany

4.1.6. Cell lines

Table 7: List of all cell lines used in the described experiments.

CELL LINE	SUPPLIER
LNCaP (human prostate cancer)	ATCC, Manassas, USA
VCaP (human prostate cancer)	ATCC, Manassas, USA
DU145 (human prostate cancer)	ATCC, Manassas, USA
PC3 (human prostate cancer)	ATCC, Manassas, USA
MCF-7 (human breast cancer)	ATCC, Manassas, USA
MDA-MB-231 (human breast cancer)	ATCC, Manassas, USA
HL-60 (human acute promyelocytic leukemia)	ATCC, Manassas, USA
Jurkat (human acute T cell leukemia)	ATCC, Manassas, USA
U937 (human histiocytic lymophoma)	ATCC, Manassas, USA
HCT116 (human colorectal cancer)	ATCC, Manassas, USA
HT-29 (human colorectal cancer)	ATCC, Manassas, USA
HepG2 (human hepatocellular cancer)	ATCC, Manassas, USA

HLE (human hepatocellular cancer)	Kind gift from Prof. Dr. Steven Dooley (Heidelberg University)
SK-HEP-1 (human hepatocellular cancer)	ATCC, Manassas, USA
AsPC-1 (human pancreatic cancer)	ATCC, Manassas, USA
BxPC-3 (human pancreatic cancer)	ATCC, Manassas, USA
MIA PaCa-2 (human pancreatic cancer)	ATCC, Manassas, USA

4.1.7. Antibodies

Table 8: List of all antibodies used in immunoblotting experiments.

TARGET	**VENDOR**
Anti-AR	Cell Signaling Technology, New England Biolabs®, Frankfurt am Main, Germany
Anti-c-Myc	Cell Signaling Technology, New England Biolabs®, Frankfurt am Main, Germany
Anti-G6PD	Abgent, Inc. San Diego, CA, USA
Anti-GLUT1	Cell Signaling Technology, New England Biolabs®, Frankfurt am Main, Germany
Anti-ITCH	Cell Signaling Technology, New England Biolabs®, Frankfurt am Main, Germany
Anti-pACC (S79)	Cell Signaling Technology, New England Biolabs®, Frankfurt am Main, Germany
Anti-AMPKα	Santa Cruz Biotechnology, Heidelberg, Germany
Anti-PDHK1	Cell Signaling Technology, New England Biolabs®, Frankfurt am Main, Germany
Anti-ß-actin	Santa Cruz Biotechnology, Heidelberg, Germany
Anti-TXNIP (VDUP1)	MBL International Corporation, Woburn, MA, USA
Anti-Vinculin	Santa Cruz Biotechnology, Heidelberg, Germany
HRP-linked anti-mouse IgG	Cell Signaling Technology, New England Biolabs®, Frankfurt am Main, Germany

HRP-linked anti-rabbit IgG	Cell Signaling Technology, New England Biolabs®, Frankfurt am Main, Germany

4.1.8. Primers

Table 9: List of primers, all of which were synthesized by Eurofins Genomics (Germany), used for RT-qPCR experiments described in this thesis. Lyophilized primers obtained were dissolved in defined volumes of nuclease-free water, indicated by the manufacturer, to obtain a final concentration of 100 pmol/µL. For RT-qPCR, primers were further diluted (1:20) in water.

PRIMER NAME	PRIMER SEQUENCE
ACACA-For	5'-GATTCGTTGTCATGGTCACACC-3'
ACACA-Rev	5'-GTTGTTGTTTGGTCCTCCAGG-3'
ACLY-For	5'-GCATCTATGCCACCCGAGAAG-3'
ACLY-Rev	5'-CCAACAAGCAGCTTCTGGGC-3'
AMPKb1-For	5'-GTCGCTGAGGGGTGGTGAAG-3'
AMPKb1-Rev	5'-CTCGCAATCGCGCTTTACCTG-3'
AR-For	5'-ACATGGTGAGCGTGGACTTT-3'
AR-Rev	5'-GAGCTGGGGTGGGGAAATAG-3'
ATP5B-For	5'-GGAGTCTAGAGGATCCACAGC-3'
ATP5B-Rev	5'-CCCTGCCCCTGCTACTACG-3'
BAD-For	5'-CGGAGGATGAGTGACGAGTT-3'
BAD-Rev	5'-CCAAGTTCCGATCCCACCAG-3'
BAX-For	5'-GGGGACGAACTGGACAGTAA-3'
BAX-Rev	5'-CAGTTGAAGTTGCCGTCAGA-3'

BECN1-For	5'-GCTGAAGACAGAGCGATGGTA-3'
BECN1-Rev	5'-GGACGTCTTAGACCCTTCCA-3'
COX5B-For	5'-CCAGCGTCGTCTGGTTTTGG-3'
COX5B-Rev	5'-GCTCAGTGTGCCAGCTGCT-3'
CS-For	5'-CTCAAAAGAGTGGGCAAAGAGG-3'
CS-Rev	5'-CTGCACTGAGCTGAGACATGG-3'
CYP24A1-For	5'-TGGGGCTGGGAGTAATACTGA-3'
CYP24A1-Rev	5'-GAACGCAATTTCATGGGAGGC-3'
CYTC-For	5'-GAAGTGTTCCCAGTGCCACAC-3'
CYTC-Rev	5'-TCCAGGGGCCTGACCTGTC-3'
FASN-For	5'-CCTGAGGCCCAACACGCAG-3'
FASN-Rev	5'-GCTTCTGCACGGCCTCAGG-3'
G6PD-For	5'-CCAAGAACATTCACGAGTCCTG-3'
G6PD-Rev	5'-GGACAGCCGGTCAGAGCTC-3'
GLS1-For	5'-CCTCAACTGGCCAAATTCAGTC-3'
GLS1-Rev	5'-CTGAAGACAGAAGGGAACTTTG-3'
GLS2-For	5'-GCTTTCCTAAGGGGGTGGAC-3'
GLS2-Rev	5'-GTGGCTGCCATGACACTGC-3'
GLUT1-For	5'-CAGTTTGGCTACAACACTGGAG-3'
GLUT1-Rev	5'-GCAGGATGCTCTCCCCATAG-3'
GOT1-For	5'-CACGAGTATCTGCCAATCCTG-3'

GOT1-Rev	5'-CCTACCCGCTTCTCCTTGAG-3'
HKII-For	5'-GTGGCACCCAGCTGTTTGAC-3'
HKII-Rev	5'-CGAGAAGGTAAAACCCAGTGG-3'
IDH1-For	5'-CGACCAAGTCACCAAGGATG-3'
IDH1-Rev	5'-GAACTCCTCAACCCTCTTCTC-3'
ITCH-For	5'-5TCTAGTAGCTGTGGTCGGGG-3'
ITCH-Rev	5'-CACAAGGCCACCGTGAAATG-3'
KLK3-For	5'-AGTGCGAGAAGCATTCCCAA-3'
KLK3-Rev	5'-CCCAGCAAGATCACGCTTTT-3'
LDHA-For	5'-GAAGGGAGAGATGATGGATCTC-3'
LDHA-Rev	5'-CTTATCTTCCAAGCCACGTAGG-3'
LKB1-For	5'-ATGGAGTACTGCGTGTGTGG-3'
LKB1-Rev	5'-GGTACTCCAGGCCGTCAATC-3'
MYC-For	5'-TTCGGGTAGTGGAAAACCAG-3'
MYC-Rev	5'-CAGCAGCTCGAATTTCTTCC-3'
NDUFA1-For	5'-GAGATTCTCCCCGGACTCTC-3'
NDUFA1-Rev	5'-CCCTTTTTTCCTTGCCCCCG-3'
OGDH-For	5'-GGTAGAAGCACAGCCCAACG-3'
OGDH-Rev	5'-CTGTGCTACATGGTGCCCTC-3'
P21-For	5'-GACACCACTGGAGGGTGACT-3'
P21-Rev	5'-CAGGTCCACATGGTCTTCCT-3'

PDHA1-For	5'-CCCCACAGACCATCTCATCAC-3'
PDHA1-Rev	5'-CCTTTTCGTCCTGTAAGCTCTG-3'
PDHK1-For	5'-GGATCGATTCTACATGAGTCGC-3'
PDHK1-Rev	5'-GTTTTCGATGAGATGGACTTCC-3'
PGC1A-For	5'-GACAGATGGAGACGTGACCAC-3'
PGC1A-Rev	5'-CTTAAGTAGAGACGGCTCTTCTG-3'
PKM2-For	5'-CAGAGGCTGCCATCTACCAC-3'
PKM2-Rev	5'-GAGGACGATTATGGCCCCAC-3'
PUMA-For	5'-GACGACCTCAACGCACAGTA-3'
PUMA-Rev	5'-CACCTAATTGGGCTCCATCT-3'
SDHC-For	5'-GGACAACCACTCCAGACTGG-3'
SDHC-Rev	5'-GGACAACCACTCCAGACTGG-3'
SREBP1-For	5'-CATTGAGCTCCTCTCTTGAAGC-3'
SREBP1-Rev	5'-GGGTACATCTTCAATGGAGTGG-3'
TFAM-For	5'-TGTCTGACTCTGAAAAGGAAGTGA-3'
TFAM-Rev	5'-ACATGAATCAAGCCTTGCCC-3'
TIGAR-For	5'-AAGTGGTGTGGGGGAGGTAG-3'
TIGAR-Rev	5'-CGGACAACAGTCAGAGCGAA-3'
TSC2-For	5'-CGTAGGCTACCCCGAGCA-3'
TSC2-Rev	5'-CAGACAGATTTCTCGTCCGC-3'
TXNIP-For	5'-CGCCTCCTGCTTGAAACTAAC-3'

TXNIP-Rev	5'-AATATACGCCGCTGGTTACACT-3'
VCL-For	5'-CAGTCAGACCCTTACTCAGTG-3'
VCL-Rev	5'-CAGCCTCATCGAAGGTAAGGA-3'
VDR-For	5'-TGGAGACTTTGACCGGAACG-3'
VDR-Rev	5'-GGGCAGGTGAATAGTGCCTT-3'
VEGFA-For	5'-GGAGACCTGGTTGTGTGTGTG-3'
VEGFA-Rev	5'-GCACGTGGATCCTGCCCTG-3'

4.1.9. siRNA

Table 10: List of siRNAs used in RNA interference experiments. *siRNAs listed below have been synthesized by Riboxx (Riboxx GmbH, Radebeul, Germany).*

TARGET	SENSE (5'-3')	ANTISENSE (5'-3')
AMPKα1	GGGGGCCACAAUCAAAGAUAU GGGGGAUUGGAACAUGAUUUA GGGGGAGAGCUAUUUGAUUAUA	AUAUCUUUGAUUGUGGCCCCC UAAAUCAUGUUCCAAUCCCCC UAUAAUCAAAUAGCUCUCCCCC
AR	GGGGGCUACUCUUCAGCAUUAUU GGGGGACUCAGCUGCCCCAUCCA GGGGGACGCUUCUACCAGCUCAC	AAUAAUGCUGAAGAGUAGCCCCC UGGAUGGGGCAGCUGAGUCCCCC GUGAGCUGGUAGAAGCGUCCCCC

4.2. Methods

4.2.1. Cell culture

All cell lines listed in **Table 7** were maintained in DMEM GlutaMAX™ supplemented with 10% (v/v) FCS and 1% (v/v) penicillin/streptomycin, with the exception of suspension cell lines, namely HL-60, Jurkat, and U937, which were maintained in RPMI GlutaMAX™ medium also supplemented with FCS and penicillin/streptomycin, at 10% and 1% (v/v), respectively. Culture flasks were kept in a standard cell culture incubator, set at 37°C with 5% CO_2 and appropriate humidity. Cellular proliferation was monitored microscopically, and cell lines were passaged upon reaching 70-80% confluency. Adherent cell lines were sub-cultured by aspirating the consumed medium, washing once with D-PBS, and incubating with TrypLE™ Express inside the incubator for 3-5 mins. Detached cells were then harvested in standard DMEM and transferred to a 15 mL falcon tube, spun down for 3 mins at 300 g in a centrifuge. Medium on top of the cellular pellet was aspirated, and fresh medium was used to re-suspend the pellet. Medium containing a known cell number, depending on the culture flask used, was then transferred back to the flask containing fresh medium. Suspension cells were passaged by harvesting them from the culture flask and transferring them to a 15 mL falcon tube, after which the same protocol used for the adherent cells was applied. Adherent cells were seeded in designated culture plates one day prior to treatment, and treatments were performed in fresh medium, whereas suspension cells were seeded and treated on the same day. Concentrations of drugs used as well as the treatment periods are indicated in both the corresponding methods subsection and/or the results section.

4.2.2. RNA extraction, cDNA synthesis, and RT-qPCR

For RNA extraction, different cell lines were seeded at varying densities in culture plates, depending on cells' proliferation rate and the duration of treatment. At the end of the treatment period, consumed medium was aspirated from adherent cells, and cells were washed once with D-PBS. For suspension cells, cells were harvested and transferred to 2.0 mL Eppendorf tubes, which were subsequently centrifuged at 300 g for 5 mins. Consumed medium was then

aspirated and the cellular pellet washed once with D-PBS, after which the tubes were centrifuged once again under the same conditions. 150 µL of QIAzol lysis reagent were added to each well (adherent cells) or Eppendorf tube (suspension cells), and incubated at room temperature for 5 mins. In the case of adherent cells, lysates were then transferred to 1.5 mL Eppendorf tubes for further steps. 30 µL of chloroform were then added to each tube, which were vortexed for 15 secs, and placed on ice for 15 mins. Tubes were then centrifuged at 13,000 g for 15 mins at a temperature of 4°C. The upper aqueous phase of the resulting biphasic solution was transferred to a fresh 1.5 mL Eppendorf tube, and RNA was precipitated using 75 µL isopropanol per tube. Tubes were then incubated at room temperature for 10 mins, after which they were centrifuged under the same conditions (13,000 g; 15 mins; 4°C). The solution was then discarded, and the RNA pellet was washed twice with 150 µL of 70% (v/v) ethanol in water. After a final centrifugation step (7,500 g; 5 mins; 4°C) and the discarding of ethanol, 30 µL of RNase free water were used to dissolve the RNA pellet. The concentration and purity of the resulting RNA samples were assessed by the NanoDrop 2000 UV-Vis Spectrophotometer.

cDNA was synthesized from 500 ng of RNA of each sample, using the ProtoScript® II first strand cDNA synthesis kit. RT-qPCR was performed using synthesized cDNA (1.0 µL), primers listed in **Table 9** (1.0 µL), reaction mix LightCycler® 480 SYBR Green I Master (2.5 µL), and nuclease-free water (0.5 µL), in a total reaction volume of 5 µL. The thermal cycler conditions comprised an initial denaturation step at 95°C for 5 mins, followed by 45 cycles of denaturation (95°C; 10 secs), annealing (60°C; 10 secs), and elongation (72°C; 20 secs). Melting curve analysis was performed at the end of every PCR run, and wells yielding false positive signals were excluded from further analyses. The ΔΔCt method was used to calculate the relative mRNA expression of genes in response to treatment, with vinculin used as the housekeeping gene.

4.2.3. RNA interference

LNCaP and MCF-7 cells were transiently transfected with the designated siRNAs, listed in **Table 10**, as well as a NC, by adding 50 pmol of siRNA/well in a 24-well plate, containing 100 µL/well of Opti-MEM Reduced Serum Medium. 1.5 µL/well Lipofectamine® 3000 were added, and the plate was left to incubate for 20 mins. Following this, 60,000 cells suspended in 500 µL of DMEM without antibiotics were added to each well, and the contents of the wells were

gently mixed by re-suspending using a micropipette. Knock-down efficiency was then confirmed by western blotting.

4.2.4. On-line monitoring of cellular metabolism

The Bionas 2500 biosensor chip system was used to assess the influence of $1,25(OH)_2D_3$ treatment on energy metabolism of prostate and breast cancer cells. This system enables on-line measurements of acidification and oxygen consumption rates, which reflect glycolytic and respiratory rates, respectively, as well as impedance, which acts as an indicator of cellular viability and adhesion. This system has been previously used to investigate the influence of various drugs on energy metabolism of different cancer cell lines [156, 157]. Experimentally, cells were seeded on sensor chips (SC1000) at a density of 200,000 cells/chip in 450 µL of full medium/chip. Six sensor chips were then transferred to the Bionas system on the following day and the experiment was commenced. The composition of the RM used is described in **Table 5**, with the main feature being the presence of a weak buffering system (1 mM HEPES), to enable rapid detection of minor fluctuations in the medium's acidification in response to cellular lactate production, as well as being less nutrient- and growth factor-rich compared to the cell culture medium used in the other experiments, to prevent excessive cellular growth and proliferation on chip. RM was introduced to the system in 8 min cycles, with 4 mins of pumping (at a rate of 56 µL/min) and 4 mins of stagnation, allowing for measurements. Untreated RM was introduced to the cells in this manner for an initial 6 h, to enable stabilization of the measurements, and to allow the cells to acclimate to the new environment. Treated medium contained 0.1% (v/v) of either $1,25(OH)_2D_3$ (reaching a final concentration of 100 nM) or DMSO, and was introduced to the system at the same described rate, for a total period of 72 h. Finally, a recovery period was included in which cells were subjected again to untreated RM for approximately 20 h.

To analyze changes in metabolic parameters of HL-60 cells, HydroDish® and OxoDish® 24-well plates were used, which measure medium pH (reflecting lactate production/glycolysis) and amount of dissolved oxygen in the medium (reflecting respiration), respectively. Cells were seeded at a density of 20,000 cells/well in 1.0 mL of RPMI GlutaMAX™ medium, and plates were subsequently placed on SDRs present in a standard cell culture incubator. The experiment was subsequently commenced, with measurements taken once every 3 mins. Cells remained

untreated for an initial 20 min period, to enable signal stabilization, after which measurements were halted, and the plates were taken out of the incubator for treatment. $1,25(OH)_2D_3$ and DMSO treatments were performed as described above, and additional controls were included, namely the glycolysis inhibitor 2-deoxyglucose (10 mM) and the mitochondrial complex I inhibitor metformin (2 mM), for pH and oxygen consumption measurements, respectively. Moreover, wells containing medium without cells were also included as a NC. After treatment, the plates were returned to the incubator and placed on SDRs, and the measurements were continued.

4.2.5. SRB assay

SRB assay was performed to investigate the effect of various treatments on cellular proliferation. Cells were seeded in 96-well plates at a density of 5,000 cells in 200 µL medium/well. The plates were treated the following day, and at the end of the treatment period, 100 µL/well of ice-cold trichloroacetic acid were added. Plates were then incubated at 4ºC for 1 h, after which contents were discarded, and the plates washed with water three times, and placed in a hybridization oven set at 65ºC for 30 mins. 100 µL/well of SRB solution (0.057 % (w/v) SRB in 1 % (v/v) acetic acid in water) were then added, and the plates were incubated for 30 mins at room temperature. SRB solution was then discarded, and the wells washed three times with 200 µL/well 1 % acetic acid, and the solution discarded after each time. The plates were then dried in a hybridization oven (65ºC; 30 mins), after which the dye was solubilized using 10 mM Tris buffer pH 10.5 (200 µL/well). To ensure complete solubility of the dye, the plates were placed in a thermomixer for 5 mins (25 ºC; 300 rpm), and the absorbance of wells was measured at 535 nm in a plate reader. Changes in cellular proliferation in response to treatments were calculated by normalizing the absorbance of drug-treated wells to that of DMSO-treated wells.

4.2.6. Enzymatic assays: GOx and G6PD activity measurements

Levels of glucose in the medium were determined using the GOx assay. 50,000 cells in 0.5 mL medium/well were added to 48-well plates and treated with $1,25(OH)_2D_3$ (100 nM) for different time points. At the end of the treatment period, 10 µL of the supernatant were collected, and

glucose standards of varying concentrations (0.1-1.0 g/L glucose in water) were prepared. Both samples and standards were diluted 10 times, and 5 µL of each sample and standard were mixed with 240 µL of the GOx enzyme mix (described in **Table 5**) in 96-well plates. Plates were then incubated at room temperature for 1 h, after which the absorbance of the samples was measured at 450 nm using a plate reader. The calibration curve constructed from the absorbance obtained from the different standards was used to calculate the concentration of glucose in the medium of cells treated with either DMSO or $1,25(OH)_2D_3$. SRB assay was performed for normalization of the results.

For the analysis of G6PD activity, MCF-7 cells were seeded in petri-dishes (100 x 20 mm) at a density of 1,000,000 cells/dish in 10 mL of medium/dish, and treated the following day with either DMSO or $1,25(OH)_2D_3$ (100 nM) for a period of 72h. Cells were subsequently harvested, washed once with D-PBS, centrifuged for 3 mins at 300 g, the D-PBS aspirated, and the cellular pellet placed on ice. 500 µL of lysis buffer for crude extracts (described in **Table 5**) were used to re-suspend the pellet, and 200 mg of acid-washed glass beads (diameter 425-600 µm) were added to the suspension. Cells were subsequently lysed using a bead mill (1-2 min; 30 Hz), and then placed immediately on ice. The supernatant was then collected by centrifuging the samples (5 mins; maximum speed; 4°C), and Bradford assay was performed to determine protein concentration. Briefly, 200 µL/well of Bradford reagent were added to 96-well plates. 2 µL of each sample were added to each well, with each sample pipetted in 3 technical replicates. Additionally, 2 µL/well lysis buffer were also added to wells containing Bradford reagent, to serve as the blank in the spectrophotometric measurement. BSA standards (100-1500 µg/mL) were also prepared and similarly added to wells containing Bradford reagent, to provide data points for a calibration curve. After 10 mins of incubation on a Thermomixer (300 rpm) at 25°C, the absorbance of the samples was measured at 595 nm using a plate reader.

500 ng of total protein per sample were added to a solution containing the G6PD reaction mixture described in **Table 5**, together with 0.5 mM G6P and 1 mM NADP+, reaching a total volume of 100 µL. The absorbance of the samples was kinetically monitored at 345 nm using a plate reader. The reduction of NADP+ to NADPH by G6PD results in an increase in absorbance, and the rate of increase correlates with the enzyme's activity.

4.2.7. FACS analysis of intracellular ROS, mitochondrial mass/membrane potential, and glucose uptake

For FACS experiments, cells were seeded in 6-well plates at a density of 200,000 cells/well in 2.0 mL of medium. Suspension cells were treated on the same day, while adherent cells were treated the following day in fresh medium. Cells were treated with DMSO or $1,25(OH)_2D_3$ (100 nM) for the designated treatment period, after which the experiment was started. 250,000 cells were harvested from each well, spun down (3 min; 300 g), and the medium discarded, for the analysis of either intracellular ROS, mitochondrial mass or membrane potential. For intracellular ROS determination, 500 µL of DMEM without phenol red, containing DHE at a final concentration of 15 µM, were used to resuspend the cellular pellet, and then incubated for 15 mins in the dark with mild shaking. The samples were then spun down in a centrifuge (3 min; 300 g) and the medium containing DHE was carefully discarded. The cellular pellet was then re-suspended in 500 µL of DMEM without phenol red and FACS analysis was performed using the FL-2 channel.

For mitochondrial mass and membrane potential measurements, the initially harvested cellular pellet (approximately 250,000 cells) was washed once with D-PBS, and spun down (3 min; 300 g). Cells were then re-suspended in 500 µL DMEM without phenol red containing either 7.5 nM MitoTracker Green or 2 µM JC-1, for the analysis of mitochondrial mass and membrane potential, respectively. The medium used to dissolve MitoTracker Green also lacked FCS. Cells were incubated with the dyes for 30 mins, after which cells were spun down in a centrifuge (3 mins; 300 g), and the medium discarded. The cellular pellet was finally re-suspended in 500 µL DMEM without phenol red and FACS analysis was performed. FL-1 and FL-2 channels were used for the detection of JC-1 monomers and J-aggregates, respectively, and the FL-1 channel was used to assess mitochondrial mass in cells. The FL-2:FL-1 ratio positively correlated with mitochondrial membrane potential.

The glucose uptake experiment was performed by replacing the culture medium of cells at the end of the treatment period with medium containing 50 µM 2-NBDG. For adherent cells, the procedure involved aspirating the old culture medium and immediately replacing it with fresh medium containing the fluorescently-labelled glucose analog. Suspension cells on the other hand were harvested, spun down (3 min; 300 g), and then re-suspended in the new 2-NBDG-containing medium. Culture plates were subsequently placed back in a standard incubator for

2 h, after which cells were harvested, spun down (3 min; 300 g), and re-suspended in 500 µL of DMEM without phenol red. Intracellular levels of 2-NBDG were then assessed by FACS, using the FL-1 channel.

4.2.8. Western blotting

Cells were seeded in 6-well plates at a final density of 500,000 cells/well in 2 mL medium/well, and treated with the various molecules at the concentrations and for the time periods indicated in the text. At the end of the treatment period, the old medium was gently aspirated, and cells were washed once with D-PBS (2 mL/well). After aspirating the D-PBS, 90 µL of lysis buffer for SDS-PAGE described in **Table 5** were added to each well, and the culture plates were placed on ice for approximately 5 mins. Cellular lysates were then transferred to fresh 1.5 mL Eppendorf tubes, and spun down in a centrifuge set at 4°C for 15 mins at maximum speed. The supernatants were then transferred to fresh 1.5 mL Eppendorf tubes, and the protein concentration of samples was determined by Bradford assay.

For western blot sample preparation, volumes of cell lysates corresponding to equal amounts of proteins (approximately 50 µg) were mixed with 5x gel loading buffer, the composition of which is described in **Table 5**, and the volumes of the samples were normalized using 6M urea buffer. Samples were then denatured by placing them in a thermomixer set at 65°C for 10 mins. Equal sample volumes were then loaded on SDS-PAGE gels (composition described in **Table 5**), and gel electrophoresis was run (100 V; 2 h).

Proteins were then transferred by semi-dry blotting. Filter papers and PVDF membranes were cut in the exact dimensions of the gel. 3 filter papers were soaked in anode buffer (composition in **Table 5**) and sequentially placed on the anode plate of the transfer machine, with careful removal of trapped air bubbles with the addition of each layer. A PVDF membrane, first activated by brief incubation in methanol, was immersed in anode buffer and then placed on the filter paper stacked layers. The gel, first immersed in cathode buffer (composition in **Table 5**), was then carefully placed on top of the membrane. 3 additional layers of filter papers, soaked in cathode buffer, were placed on top of the gel, one after the other, carefully eliminating trapped air bubbles between the layers to ensure efficient transfer. A current of 2.5 mA/cm^2 was subsequently applied for 30 mins. At the end of the transfer, the PVDF membrane was carefully

removed from the transfer sandwich and washed once with 1x Tris-buffered saline (TBS)/Tween for 5 mins on an orbital shaker. The membrane was then incubated with Ponceau S solution for 10 mins on an orbital shaker, after which mild washing with TBS/Tween was applied, and the transfer efficiency documented by imaging. The membrane was then washed several times with TBS/Tween, until the Ponceau S stain was completely removed, and then the membrane was incubated with blocking solution, composed of 5% (w/v) non-fat dry milk in TBS/Tween, for at least 1-2 h at room temperature on an orbital shaker. Afterwards, the membrane was washed once with TBS/Tween before overnight incubation at 4°C with the primary antibody, which was diluted in a solution of 5% (w/v) BSA in TBS/Tween (dilutions employed were those recommended by the supplier). The membrane was then washed once with TBS/Tween on an orbital shaker, and then incubated for 1 h with anti-mouse or –rabbit HRP-linked secondary antibody, dissolved in a ratio of 1:5000 in 5% (w/v) non-fat dry milk in TBS/Tween. The membrane was then washed 3 times with TBS/Tween, 5 mins each time on an orbital shaker. Target bands were visualized by the LAS3000 Imaging System, using a commercially available enhanced chemiluminescence solution.

4.2.9. GC/MS-based metabolite quantification

GC/MS experiments were kindly performed by Dr. Michael Büttner (Metabolomics Core Technology Platform, Center for Organismal Studies, Heidelberg University). A clear description of the followed protocol is available in reference [90]. LNCaP, MCF-7, and MDA-MB-231 cells were seed in cell culture petri-dishes (145x20 mm) at an initial density of 2,000,000 cells/dish, in 15 mL of full medium. The following day, the medium was replaced with DMSO- or $1,25(OH)_2D_3$ (100 nM)-treated medium, and the petri-dishes were then placed in a standard incubator for 72 h. At the end of the treatment period, the medium was aspirated, the dishes placed on ice, and cells were washed with 10 mL ice-cold 0.9% (w/v) NaCl in water. The saline was then carefully aspirated, and 1.2 mL of saline was added to each dish, and used to harvest cells by scraping. Cells were transferred to fresh 1.5 mL Eppendorf tubes, re-suspended several times, and a 50 µL aliquot of each sample was set aside for total cell number determination. Tubes were then spun down in a centrifuge (300 g; 5 mins), and the supernatant carefully discarded. The samples were then shock-frozen by placing the tubes in liquid nitrogen, and were subsequently stored in a -80ºC until analysis.

4.2.10. Statistical analyses

Microsoft Excel and GraphPad Prism were used for statistical analyses. A two-tailed Student's t-test was used to compare between treated and untreated cells, with p-values less than or equal to 0.05 identified as statistically significant. *, **, and *** are used to depict p-values less than or equal to 0.05, 0.01, and 0.001, respectively. Error bars represent the SD, unless otherwise stated in the figure legend.

5. REFERENCES

1. Wolf G. The discovery of vitamin D: the contribution of Adolf Windaus. *J Nutr.* 2004; 134:1299-302.
2. Norman AW. From vitamin D to hormone D: fundamentals of the vitamin D endocrine system essential for good health. *Am J Clin Nutr.* 2008; 88:491S-499S.
3. Holick MF. Vitamin D deficiency. *N Engl J Med.* 2007; 357:266-81.
4. Hossein-nezhad A, Holick MF. Vitamin D for health: a global perspective. *Mayo Clin Proc.* 2013; 88:720-55.
5. Cheng JB, Levine MA, Bell NH, Mangelsdorf DJ, Russell DW. Genetic evidence that the human CYP2R1 enzyme is a key vitamin D 25-hydroxylase. *Proc Natl Acad Sci U S A.* 2004; 101:7711-5.
6. Zerwekh JE. Blood biomarkers of vitamin D status. *Am J Clin Nutr.* 2008; 87:1087S-91S.
7. Deeb KK, Trump DL, Johnson CS. Vitamin D signalling pathways in cancer: potential for anticancer therapeutics. *Nat Rev Cancer.* 2007; 7:684-700.
8. Haussler MR, Jurutka PW, Mizwicki M, Norman AW. Vitamin D receptor (VDR)-mediated actions of 1alpha,25(OH)(2)vitamin D(3): genomic and non-genomic mechanisms. *Best Pract Res Clin Endocrinol Metab.* 2011; 25:543-59.
9. Feldman D, Krishnan AV, Swami S, Giovannucci E, Feldman BJ. The role of vitamin D in reducing cancer risk and progression. *Nat Rev Cancer.* 2014; 14:342-57.
10. Garland CF, Garland FC. Do sunlight and vitamin D reduce the likelihood of colon cancer? *Int J Epidemiol.* 1980; 9:227-31.
11. Moukayed M, Grant WB. The roles of UVB and vitamin D in reducing risk of cancer incidence and mortality: A review of the epidemiology, clinical trials, and mechanisms. *Rev Endocr Metab Disord.* 2017; 18:167-182.
12. Bolland MJ, Grey A, Gamble GD, Reid IR. Calcium and vitamin D supplements and health outcomes: a reanalysis of the Women's Health Initiative (WHI) limited-access data set. *Am J Clin Nutr.* 2011; 94:1144-9.
13. Wang TJ, Zhang F, Richards JB, Kestenbaum B, van Meurs JB, Berry D, Kiel DP, Streeten EA, Ohlsson C, Koller DL, Peltonen L, Cooper JD, O'Reilly PF, Houston DK, Glazer NL, Vandenput L, Peacock M, Shi J, Rivadeneira F, McCarthy MI, Anneli P, de Boer IH, Mangino M, Kato B, Smyth DJ, Booth SL, Jacques PF, Burke GL, Goodarzi

M, Cheung CL, Wolf M, Rice K, Goltzman D, Hidiroglou N, Ladouceur M, Wareham NJ, Hocking LJ, Hart D, Arden NK, Cooper C, Malik S, Fraser WD, Hartikainen AL, Zhai G, Macdonald HM, Forouhi NG, Loos RJ, Reid DM, Hakim A, Dennison E, Liu Y, Power C, Stevens HE, Jaana L, Vasan RS, Soranzo N, Bojunga J, Psaty BM, Lorentzon M, Foroud T, Harris TB, Hofman A, Jansson JO, Cauley JA, Uitterlinden AG, Gibson Q, Jarvelin MR, Karasik D, Siscovick DS, Econs MJ, Kritchevsky SB, Florez JC, Todd JA, Dupuis J, Hypponen E, Spector TD. Common genetic determinants of vitamin D insufficiency: a genome-wide association study. *Lancet.* 2010; 376:180-8.

14. Powe CE, Evans MK, Wenger J, Zonderman AB, Berg AH, Nalls M, Tamez H, Zhang D, Bhan I, Karumanchi SA, Powe NR, Thadhani R. Vitamin D-binding protein and vitamin D status of black Americans and white Americans. *N Engl J Med.* 2013; 369:1991-2000.
15. Wang S, Huo D, Kupfer S, Alleyne D, Ogundiran TO, Ojengbede O, Zheng W, Nathanson KL, Nemesure B, Ambs S, Olopade OI, Zheng Y. Genetic variation in the vitamin D related pathway and breast cancer risk in women of African ancestry in the root consortium. *Int J Cancer.* 2018; 142:36-43.
16. Huss L, Butt ST, Almgren P, Borgquist S, Brandt J, Forsti A, Melander O, Manjer J. SNPs related to vitamin D and breast cancer risk: a case-control study. *Breast Cancer Res.* 2018; 20:1.
17. Anderson LN, Cotterchio M, Knight JA, Borgida A, Gallinger S, Cleary SP. Genetic variants in vitamin d pathway genes and risk of pancreas cancer; results from a population-based case-control study in ontario, Canada. *PLoS One.* 2013; 8:e66768.
18. Ly LH, Zhao XY, Holloway L, Feldman D. Liarozole acts synergistically with 1alpha,25-dihydroxyvitamin D3 to inhibit growth of DU 145 human prostate cancer cells by blocking 24-hydroxylase activity. *Endocrinology.* 1999; 140:2071-6.
19. Swami S, Krishnan AV, Peehl DM, Feldman D. Genistein potentiates the growth inhibitory effects of 1,25-dihydroxyvitamin D3 in DU145 human prostate cancer cells: role of the direct inhibition of CYP24 enzyme activity. *Mol Cell Endocrinol.* 2005; 241:49-61.
20. Cross HS, Bareis P, Hofer H, Bischof MG, Bajna E, Kriwanek S, Bonner E, Peterlik M. 25-Hydroxyvitamin D(3)-1alpha-hydroxylase and vitamin D receptor gene expression in human colonic mucosa is elevated during early cancerogenesis. *Steroids.* 2001; 66:287-92.

21. Hendrickson WK, Flavin R, Kasperzyk JL, Fiorentino M, Fang F, Lis R, Fiore C, Penney KL, Ma J, Kantoff PW, Stampfer MJ, Loda M, Mucci LA, Giovannucci E. Vitamin D receptor protein expression in tumor tissue and prostate cancer progression. *J Clin Oncol.* 2011; 29:2378-85.

22. Berger U, McClelland RA, Wilson P, Greene GL, Haussler MR, Pike JW, Colston K, Easton D, Coombes RC. Immunocytochemical determination of estrogen receptor, progesterone receptor, and 1,25-dihydroxyvitamin D3 receptor in breast cancer and relationship to prognosis. *Cancer Res.* 1991; 51:239-44.

23. Evans SR, Nolla J, Hanfelt J, Shabahang M, Nauta RJ, Shchepotin IB. Vitamin D receptor expression as a predictive marker of biological behavior in human colorectal cancer. *Clin Cancer Res.* 1998; 4:1591-5.

24. Colston K, Colston MJ, Feldman D. 1,25-dihydroxyvitamin D3 and malignant melanoma: the presence of receptors and inhibition of cell growth in culture. *Endocrinology.* 1981; 108:1083-6.

25. Abe E, Miyaura C, Sakagami H, Takeda M, Konno K, Yamazaki T, Yoshiki S, Suda T. Differentiation of mouse myeloid leukemia cells induced by 1 alpha,25-dihydroxyvitamin D3. *Proc Natl Acad Sci U S A.* 1981; 78:4990-4.

26. Saramaki A, Banwell CM, Campbell MJ, Carlberg C. Regulation of the human p21(waf1/cip1) gene promoter via multiple binding sites for p53 and the vitamin D3 receptor. *Nucleic Acids Res.* 2006; 34:543-54.

27. Toropainen S, Vaisanen S, Heikkinen S, Carlberg C. The down-regulation of the human MYC gene by the nuclear hormone 1alpha,25-dihydroxyvitamin D3 is associated with cycling of corepressors and histone deacetylases. *J Mol Biol.* 2010; 400:284-94.

28. Hsieh TY, Ng CY, Mallouh C, Tazaki H, Wu JM. Regulation of growth, PSA/PAP and androgen receptor expression by 1 alpha,25-dihydroxyvitamin D3 in the androgen-dependent LNCaP cells. *Biochem Biophys Res Commun.* 1996; 223:141-6.

29. Zhao XY, Ly LH, Peehl DM, Feldman D. Induction of androgen receptor by 1alpha,25-dihydroxyvitamin D3 and 9-cis retinoic acid in LNCaP human prostate cancer cells. *Endocrinology.* 1999; 140:1205-12.

30. Shafi AA, Yen AE, Weigel NL. Androgen receptors in hormone-dependent and castration-resistant prostate cancer. *Pharmacol Ther.* 2013; 140:223-38.

31. Zhao XY, Ly LH, Peehl DM, Feldman D. 1alpha,25-dihydroxyvitamin D3 actions in LNCaP human prostate cancer cells are androgen-dependent. *Endocrinology.* 1997; 138:3290-8.

32. Murthy S, Agoulnik IU, Weigel NL. Androgen receptor signaling and vitamin D receptor action in prostate cancer cells. *Prostate.* 2005; 64:362-72.

33. Palmer HG, Larriba MJ, Garcia JM, Ordonez-Moran P, Pena C, Peiro S, Puig I, Rodriguez R, de la Fuente R, Bernad A, Pollan M, Bonilla F, Gamallo C, de Herreros AG, Munoz A. The transcription factor SNAIL represses vitamin D receptor expression and responsiveness in human colon cancer. *Nat Med.* 2004; 10:917-9.

34. Larriba MJ, Munoz A. SNAIL vs vitamin D receptor expression in colon cancer: therapeutics implications. *Br J Cancer.* 2005; 92:985-9.

35. Leyssens C, Verlinden L, Verstuyf A. The future of vitamin D analogs. *Front Physiol.* 2014; 5:122.

36. Carlberg C. Molecular basis of the selective activity of vitamin D analogues. *J Cell Biochem.* 2003; 88:274-81.

37. Nayeri S, Danielsson C, Kahlen JP, Schrader M, Mathiasen IS, Binderup L, Carlberg C. The anti-proliferative effect of vitamin D3 analogues is not mediated by inhibition of the AP-1 pathway, but may be related to promoter selectivity. *Oncogene.* 1995; 11:1853-8.

38. Hansen CM, Maenpaa PH. EB 1089, a novel vitamin D analog with strong antiproliferative and differentiation-inducing effects on target cells. *Biochem Pharmacol.* 1997; 54:1173-9.

39. Carlberg C, Quack M, Herdick M, Bury Y, Polly P, Toell A. Central role of VDR conformations for understanding selective actions of vitamin D(3) analogues. *Steroids.* 2001; 66:213-21.

40. Corrie PG. Cytotoxic chemotherapy: clinical aspects. *Medicine.* 2008; 36:24-28.

41. Sherman MH, Yu RT, Engle DD, Ding N, Atkins AR, Tiriac H, Collisson EA, Connor F, Van Dyke T, Kozlov S, Martin P, Tseng TW, Dawson DW, Donahue TR, Masamune A, Shimosegawa T, Apte MV, Wilson JS, Ng B, Lau SL, Gunton JE, Wahl GM, Hunter T, Drebin JA, O'Dwyer PJ, Liddle C, Tuveson DA, Downes M, Evans RM. Vitamin D receptor-mediated stromal reprogramming suppresses pancreatitis and enhances pancreatic cancer therapy. *Cell.* 2014; 159:80-93.

42. El-Shemi AG, Refaat B, Kensara OA, Mohamed AM, Idris S, Ahmad J. Paricalcitol Enhances the Chemopreventive Efficacy of 5-Fluorouracil on an Intermediate-Term Model of Azoxymethane-Induced Colorectal Tumors in Rats. *Cancer Prev Res (Phila).* 2016; 9:491-501.

43. Ma Y, Yu WD, Hershberger PA, Flynn G, Kong RX, Trump DL, Johnson CS. 1alpha,25-Dihydroxyvitamin D3 potentiates cisplatin antitumor activity by p73 induction in a squamous cell carcinoma model. *Mol Cancer Ther.* 2008; 7:3047-55.

44. Nishioka C, Ikezoe T, Yang J, Yokoyama A. Sunitinib, an orally available receptor tyrosine kinase inhibitor, induces monocytic differentiation of acute myelogenous leukemia cells that is enhanced by 1,25-dihydroxyvitamin D(3). *Leukemia.* 2009; 23:2171-3.

45. Vander Heiden MG, Cantley LC, Thompson CB. Understanding the Warburg effect: the metabolic requirements of cell proliferation. *Science.* 2009; 324:1029-33.

46. Costello LC, Franklin RB. The clinical relevance of the metabolism of prostate cancer; zinc and tumor suppression: connecting the dots. *Mol Cancer.* 2006; 5:17.

47. Zadra G, Photopoulos C, Loda M. The fat side of prostate cancer. *Biochim Biophys Acta.* 2013; 1831:1518-32.

48. Lloyd SM, Arnold J, Sreekumar A. Metabolomic profiling of hormone-dependent cancers: a bird's eye view. *Trends Endocrinol Metab.* 2015; 26:477-85.

49. Possemato R, Marks KM, Shaul YD, Pacold ME, Kim D, Birsoy K, Sethumadhavan S, Woo HK, Jang HG, Jha AK, Chen WW, Barrett FG, Stransky N, Tsun ZY, Cowley GS, Barretina J, Kalaany NY, Hsu PP, Ottina K, Chan AM, Yuan B, Garraway LA, Root DE, Mino-Kenudson M, Brachtel EF, Driggers EM, Sabatini DM. Functional genomics reveal that the serine synthesis pathway is essential in breast cancer. *Nature.* 2011; 476:346-50.

50. Vander Heiden MG. Targeting cancer metabolism: a therapeutic window opens. *Nat Rev Drug Discov.* 2011; 10:671-84.

51. Levine AJ, Puzio-Kuter AM. The control of the metabolic switch in cancers by oncogenes and tumor suppressor genes. *Science.* 2010; 330:1340-4.

52. Fridman JS, Lowe SW. Control of apoptosis by p53. *Oncogene.* 2003; 22:9030-40.

53. Muller PA, Vousden KH. Mutant p53 in cancer: new functions and therapeutic opportunities. *Cancer Cell.* 2014; 25:304-17.

54. Berkers CR, Maddocks OD, Cheung EC, Mor I, Vousden KH. Metabolic regulation by p53 family members. *Cell Metab.* 2013; 18:617-33.

55. Fruman DA, Chiu H, Hopkins BD, Bagrodia S, Cantley LC, Abraham RT. The PI3K Pathway in Human Disease. *Cell.* 2017; 170:605-635.

56. Ortega-Molina A, Serrano M. PTEN in cancer, metabolism, and aging. *Trends Endocrinol Metab.* 2013; 24:184-9.

57. Robey RB, Hay N. Is Akt the "Warburg kinase"?-Akt-energy metabolism interactions and oncogenesis. *Semin Cancer Biol.* 2009; 19:25-31.

58. Laplante M, Sabatini DM. mTOR signaling at a glance. *J Cell Sci.* 2009; 122:3589-94.

59. Gordan JD, Thompson CB, Simon MC. HIF and c-Myc: sibling rivals for control of cancer cell metabolism and proliferation. *Cancer Cell.* 2007; 12:108-13.

60. Hardie DG, Ross FA, Hawley SA. AMP-activated protein kinase: a target for drugs both ancient and modern. *Chem Biol.* 2012; 19:1222-36.

61. Alessi DR, Sakamoto K, Bayascas JR. LKB1-dependent signaling pathways. *Annu Rev Biochem.* 2006; 75:137-63.

62. Liang J, Mills GB. AMPK: a contextual oncogene or tumor suppressor? *Cancer Res.* 2013; 73:2929-35.

63. Qiu F, Huang J, Sui M. Targeting arginine metabolism pathway to treat arginine-dependent cancers. *Cancer Lett.* 2015; 364:1-7.

64. Lukey MJ, Katt WP, Cerione RA. Targeting amino acid metabolism for cancer therapy. *Drug Discov Today.* 2017; 22:796-804.

65. Mullarky E, Lucki NC, Beheshti Zavareh R, Anglin JL, Gomes AP, Nicolay BN, Wong JC, Christen S, Takahashi H, Singh PK, Blenis J, Warren JD, Fendt SM, Asara JM, DeNicola GM, Lyssiotis CA, Lairson LL, Cantley LC. Identification of a small molecule inhibitor of 3-phosphoglycerate dehydrogenase to target serine biosynthesis in cancers. *Proc Natl Acad Sci U S A.* 2016; 113:1778-83.

66. Gross MI, Demo SD, Dennison JB, Chen L, Chernov-Rogan T, Goyal B, Janes JR, Laidig GJ, Lewis ER, Li J, Mackinnon AL, Parlati F, Rodriguez ML, Shwonek PJ, Sjogren EB, Stanton TF, Wang T, Yang J, Zhao F, Bennett MK. Antitumor activity of the glutaminase inhibitor CB-839 in triple-negative breast cancer. *Mol Cancer Ther.* 2014; 13:890-901.

67. Ye D, Xiong Y, Guan KL. The mechanisms of IDH mutations in tumorigenesis. *Cell Res.* 2012; 22:1102-4.

68. Garber K. Cancer anabolic metabolism inhibitors move into clinic. *Nat Biotechnol.* 2016; 34:794-5.

69. Yen K, Travins J, Wang F, David MD, Artin E, Straley K, Padyana A, Gross S, DeLaBarre B, Tobin E, Chen Y, Nagaraja R, Choe S, Jin L, Konteatis Z, Cianchetta G, Saunders JO, Salituro FG, Quivoron C, Opolon P, Bawa O, Saada V, Paci A, Broutin S, Bernard OA, de Botton S, Marteyn BS, Pilichowska M, Xu Y, Fang C, Jiang F, Wei W, Jin S, Silverman L, Liu W, Yang H, Dang L, Dorsch M, Penard-Lacronique V, Biller

SA, Su SM. AG-221, a First-in-Class Therapy Targeting Acute Myeloid Leukemia Harboring Oncogenic IDH2 Mutations. *Cancer Discov.* 2017; 7:478-493.

70. Morales DR, Morris AD. Metformin in cancer treatment and prevention. *Annu Rev Med.* 2015; 66:17-29.
71. Flavin R, Peluso S, Nguyen PL, Loda M. Fatty acid synthase as a potential therapeutic target in cancer. *Future Oncol.* 2010; 6:551-62.
72. Pike LS, Smift AL, Croteau NJ, Ferrick DA, Wu M. Inhibition of fatty acid oxidation by etomoxir impairs NADPH production and increases reactive oxygen species resulting in ATP depletion and cell death in human glioblastoma cells. *Biochim Biophys Acta.* 2011; 1807:726-34.
73. Camarda R, Zhou AY, Kohnz RA, Balakrishnan S, Mahieu C, Anderton B, Eyob H, Kajimura S, Tward A, Krings G, Nomura DK, Goga A. Inhibition of fatty acid oxidation as a therapy for MYC-overexpressing triple-negative breast cancer. *Nat Med.* 2016; 22:427-32.
74. Carracedo A, Cantley LC, Pandolfi PP. Cancer metabolism: fatty acid oxidation in the limelight. *Nat Rev Cancer.* 2013; 13:227-32.
75. Samudio I, Harmancey R, Fiegl M, Kantarjian H, Konopleva M, Korchin B, Kaluarachchi K, Bornmann W, Duvvuri S, Taegtmeyer H, Andreeff M. Pharmacologic inhibition of fatty acid oxidation sensitizes human leukemia cells to apoptosis induction. *J Clin Invest.* 2010; 120:142-56.
76. Zheng W, Tayyari F, Gowda GA, Raftery D, McLamore ES, Shi J, Porterfield DM, Donkin SS, Bequette B, Teegarden D. 1,25-dihydroxyvitamin D regulation of glucose metabolism in Harvey-ras transformed MCF10A human breast epithelial cells. *J Steroid Biochem Mol Biol.* 2013; 138:81-9.
77. Ferreira GB, Vanherwegen AS, Eelen G, Gutierrez AC, Van Lommel L, Marchal K, Verlinden L, Verstuyf A, Nogueira T, Georgiadou M, Schuit F, Eizirik DL, Gysemans C, Carmeliet P, Overbergh L, Mathieu C. Vitamin D3 Induces Tolerance in Human Dendritic Cells by Activation of Intracellular Metabolic Pathways. *Cell Rep.* 2015;
78. Hoyer-Hansen M, Bastholm L, Szyniarowski P, Campanella M, Szabadkai G, Farkas T, Bianchi K, Fehrenbacher N, Elling F, Rizzuto R, Mathiasen IS, Jaattela M. Control of macroautophagy by calcium, calmodulin-dependent kinase kinase-beta, and Bcl-2. *Mol Cell.* 2007; 25:193-205.
79. Wang J, Lian H, Zhao Y, Kauss MA, Spindel S. Vitamin D3 induces autophagy of human myeloid leukemia cells. *J Biol Chem.* 2008; 283:25596-605.

80. Wang RC, Levine B. Calcipotriol induces autophagy in HeLa cells and keratinocytes. *J Invest Dermatol.* 2011; 131:990-3.

81. Yuk JM, Shin DM, Lee HM, Yang CS, Jin HS, Kim KK, Lee ZW, Lee SH, Kim JM, Jo EK. Vitamin D3 induces autophagy in human monocytes/macrophages via cathelicidin. *Cell Host Microbe.* 2009; 6:231-43.

82. Tavera-Mendoza LE, Westerling T, Libby E, Marusyk A, Cato L, Cassani R, Cameron LA, Ficarro SB, Marto JA, Klawitter J, Brown M. Vitamin D receptor regulates autophagy in the normal mammary gland and in luminal breast cancer cells. *Proc Natl Acad Sci U S A.* 2017; 114:E2186-E2194.

83. Rabinowitz JD, White E. Autophagy and metabolism. *Science.* 2010; 330:1344-8.

84. Ben-Shoshan M, Amir S, Dang DT, Dang LH, Weisman Y, Mabjeesh NJ. 1alpha,25-dihydroxyvitamin D3 (Calcitriol) inhibits hypoxia-inducible factor-1/vascular endothelial growth factor pathway in human cancer cells. *Mol Cancer Ther.* 2007; 6:1433-9.

85. Reichrath J, Reichrath S, Heyne K, Vogt T, Roemer K. Tumor suppression in skin and other tissues via cross-talk between vitamin D- and p53-signaling. *Front Physiol.* 2014; 5:166.

86. Stambolsky P, Tabach Y, Fontemaggi G, Weisz L, Maor-Aloni R, Siegfried Z, Shiff I, Kogan I, Shay M, Kalo E, Blandino G, Simon I, Oren M, Rotter V. Modulation of the vitamin D3 response by cancer-associated mutant p53. *Cancer Cell.* 2010; 17:273-85.

87. Bao BY, Ting HJ, Hsu JW, Lee YF. Protective role of 1 alpha, 25-dihydroxyvitamin D3 against oxidative stress in nonmalignant human prostate epithelial cells. *Int J Cancer.* 2008; 122:2699-706.

88. Chen KS, DeLuca HF. Isolation and characterization of a novel cDNA from HL-60 cells treated with 1,25-dihydroxyvitamin D-3. *Biochim Biophys Acta.* 1994; 1219:26-32.

89. Abu El Maaty MA, Wolfl S. Vitamin D as a Novel Regulator of Tumor Metabolism: Insights on Potential Mechanisms and Implications for Anti-Cancer Therapy. *Int J Mol Sci.* 2017; 18:

90. Abu El Maaty MA, Alborzinia H, Khan SJ, Buttner M, Wolfl S. 1,25(OH)2D3 Disrupts glucose metabolism in prostate cancer cells leading to a truncation of the tca cycle and inhibition of txnip expression. *Biochim Biophys Acta.* 2017;

91. Mycielska ME, Patel A, Rizaner N, Mazurek MP, Keun H, Patel A, Ganapathy V, Djamgoz MB. Citrate transport and metabolism in mammalian cells: prostate epithelial cells and prostate cancer. *Bioessays.* 2009; 31:10-20.

92. Adekola K, Rosen ST, Shanmugam M. Glucose transporters in cancer metabolism. *Curr Opin Oncol.* 2012; 24:650-4.

93. Stoltzman CA, Peterson CW, Breen KT, Muoio DM, Billin AN, Ayer DE. Glucose sensing by MondoA:Mlx complexes: a role for hexokinases and direct regulation of thioredoxin-interacting protein expression. *Proc Natl Acad Sci U S A.* 2008; 105:6912-7.

94. Wu N, Zheng B, Shaywitz A, Dagon Y, Tower C, Bellinger G, Shen CH, Wen J, Asara J, McGraw TE, Kahn BB, Cantley LC. AMPK-dependent degradation of TXNIP upon energy stress leads to enhanced glucose uptake via GLUT1. *Mol Cell.* 2013; 49:1167-75.

95. Ludwig DL, Kotanides H, Le T, Chavkin D, Bohlen P, Witte L. Cloning, genetic characterization, and chromosomal mapping of the mouse VDUP1 gene. *Gene.* 2001; 269:103-12.

96. Tokumitsu H, Inuzuka H, Ishikawa Y, Ikeda M, Saji I, Kobayashi R. STO-609, a specific inhibitor of the Ca(2+)/calmodulin-dependent protein kinase kinase. *J Biol Chem.* 2002; 277:15813-8.

97. Polek TC, Stewart LV, Ryu EJ, Cohen MB, Allegretto EA, Weigel NL. p53 Is required for 1,25-dihydroxyvitamin D3-induced G0 arrest but is not required for G1 accumulation or apoptosis of LNCaP prostate cancer cells. *Endocrinology.* 2003; 144:50-60.

98. Wilde BR, Ayer DE. Interactions between Myc and MondoA transcription factors in metabolism and tumourigenesis. *Br J Cancer.* 2015; 113:1529-33.

99. Shen L, O'Shea JM, Kaadige MR, Cunha S, Wilde BR, Cohen AL, Welm AL, Ayer DE. Metabolic reprogramming in triple-negative breast cancer through Myc suppression of TXNIP. *Proc Natl Acad Sci U S A.* 2015; 112:5425-30.

100. Carroll PA, Diolaiti D, McFerrin L, Gu H, Djukovic D, Du J, Cheng PF, Anderson S, Ulrich M, Hurley JB, Raftery D, Ayer DE, Eisenman RN. Deregulated Myc requires MondoA/Mlx for metabolic reprogramming and tumorigenesis. *Cancer Cell.* 2015; 27:271-85.

101. Yin X, Giap C, Lazo JS, Prochownik EV. Low molecular weight inhibitors of Myc-Max interaction and function. *Oncogene.* 2003; 22:6151-9.

102. Massie CE, Lynch A, Ramos-Montoya A, Boren J, Stark R, Fazli L, Warren A, Scott H, Madhu B, Sharma N, Bon H, Zecchini V, Smith DM, Denicola GM, Mathews N, Osborne M, Hadfield J, Macarthur S, Adryan B, Lyons SK, Brindle KM, Griffiths J,

Gleave ME, Rennie PS, Neal DE, Mills IG. The androgen receptor fuels prostate cancer by regulating central metabolism and biosynthesis. *EMBO J.* 2011; 30:2719-33.

103. Zhao XY, Peehl DM, Navone NM, Feldman D. 1alpha,25-dihydroxyvitamin D3 inhibits prostate cancer cell growth by androgen-dependent and androgen-independent mechanisms. *Endocrinology.* 2000; 141:2548-56.
104. Yang M, Vousden KH. Serine and one-carbon metabolism in cancer. *Nat Rev Cancer.* 2016; 16:650-62.
105. Hoyer-Hansen M, Bastholm L, Mathiasen IS, Elling F, Jaattela M. Vitamin D analog EB1089 triggers dramatic lysosomal changes and Beclin 1-mediated autophagic cell death. *Cell Death Differ.* 2005; 12:1297-309.
106. Stanton RC. Glucose-6-phosphate dehydrogenase, NADPH, and cell survival. *IUBMB Life.* 2012; 64:362-9.
107. Patra KC, Hay N. The pentose phosphate pathway and cancer. *Trends Biochem Sci.* 2014; 39:347-54.
108. Zhou J, Chng WJ. Roles of thioredoxin binding protein (TXNIP) in oxidative stress, apoptosis and cancer. *Mitochondrion.* 2013; 13:163-9.
109. Zhou J, Yu Q, Chng WJ. TXNIP (VDUP-1, TBP-2): a major redox regulator commonly suppressed in cancer by epigenetic mechanisms. *Int J Biochem Cell Biol.* 2011; 43:1668-73.
110. Alvarez-Diaz S, Larriba MJ, Lopez-Otin C, Munoz A. Vitamin D: Proteases, protease inhibitors and cancer. *Cell Cycle.* 2010; 9:32-7.
111. Zhang P, Wang C, Gao K, Wang D, Mao J, An J, Xu C, Wu D, Yu H, Liu JO, Yu L. The ubiquitin ligase itch regulates apoptosis by targeting thioredoxin-interacting protein for ubiquitin-dependent degradation. *J Biol Chem.* 2010; 285:8869-79.
112. Schwartz AG, Pashko LL. Dehydroepiandrosterone, glucose-6-phosphate dehydrogenase, and longevity. *Ageing Res Rev.* 2004; 3:171-87.
113. Yang Y, Su D, Zhao L, Zhang D, Xu J, Wan J, Fan S, Chen M. Different effects of LDH-A inhibition by oxamate in non-small cell lung cancer cells. *Oncotarget.* 2014; 5:11886-96.
114. Swami S, Krishnan AV, Feldman D. 1alpha,25-Dihydroxyvitamin D3 down-regulates estrogen receptor abundance and suppresses estrogen actions in MCF-7 human breast cancer cells. *Clin Cancer Res.* 2000; 6:3371-9.

115. Simboli-Campbell M, Narvaez CJ, Tenniswood M, Welsh J. 1,25-Dihydroxyvitamin D3 induces morphological and biochemical markers of apoptosis in MCF-7 breast cancer cells. *J Steroid Biochem Mol Biol.* 1996; 58:367-76.

116. Zhou X, Zheng W, Nagana Gowda GA, Raftery D, Donkin SS, Bequette B, Teegarden D. 1,25-Dihydroxyvitamin D inhibits glutamine metabolism in Harvey-ras transformed MCF10A human breast epithelial cell. *J Steroid Biochem Mol Biol.* 2016; 163:147-56.

117. Shalev A. Minireview: Thioredoxin-interacting protein: regulation and function in the pancreatic beta-cell. *Mol Endocrinol.* 2014; 28:1211-20.

118. Butler LM, Zhou X, Xu WS, Scher HI, Rifkind RA, Marks PA, Richon VM. The histone deacetylase inhibitor SAHA arrests cancer cell growth, up-regulates thioredoxin-binding protein-2, and down-regulates thioredoxin. *Proc Natl Acad Sci U S A.* 2002; 99:11700-5.

119. Abu El Maaty MA, Almouhanna F, Wolfl S. Expression of TXNIP in Cancer Cells and Regulation by 1,25(OH)(2)D(3): Is It Really the Vitamin D(3) Upregulated Protein? *Int J Mol Sci.* 2018; 19:

120. Afzal I, Cunningham P, Naftalin RJ. Interactions of ATP, oestradiol, genistein and the anti-oestrogens, faslodex (ICI 182780) and tamoxifen, with the human erythrocyte glucose transporter, GLUT1. *Biochem J.* 2002; 365:707-19.

121. Ferrer-Mayorga G, Gomez-Lopez G, Barbachano A, Fernandez-Barral A, Pena C, Pisano DG, Cantero R, Rojo F, Munoz A, Larriba MJ. Vitamin D receptor expression and associated gene signature in tumour stromal fibroblasts predict clinical outcome in colorectal cancer. *Gut.* 2016;

122. Lyssiotis CA, Kimmelman AC. Metabolic Interactions in the Tumor Microenvironment. *Trends Cell Biol.* 2017; 27:863-875.

123. Wilmanski T, Buhman K, Donkin SS, Burgess JR, Teegarden D. 1alpha,25-dihydroxyvitamin D inhibits de novo fatty acid synthesis and lipid accumulation in metastatic breast cancer cells through down-regulation of pyruvate carboxylase. *J Nutr Biochem.* 2017; 40:194-200.

124. Monteith GR, Prevarskaya N, Roberts-Thomson SJ. The calcium-cancer signalling nexus. *Nat Rev Cancer.* 2017; 17:367-380.

125. Lehen'kyi V, Flourakis M, Skryma R, Prevarskaya N. TRPV6 channel controls prostate cancer cell proliferation via Ca(2+)/NFAT-dependent pathways. *Oncogene.* 2007; 26:7380-5.

126. Lehen'kyi V, Raphael M, Oulidi A, Flourakis M, Khalimonchyk S, Kondratskyi A, Gordienko DV, Mauroy B, Bonnal JL, Skryma R, Prevarskaya N. TRPV6 determines the effect of vitamin D3 on prostate cancer cell growth. *PLoS One.* 2011; 6:e16856.

127. Park HU, Suy S, Danner M, Dailey V, Zhang Y, Li H, Hyduke DR, Collins BT, Gagnon G, Kallakury B, Kumar D, Brown ML, Fornace A, Dritschilo A, Collins SP. AMP-activated protein kinase promotes human prostate cancer cell growth and survival. *Mol Cancer Ther.* 2009; 8:733-41.

128. Karner CM, Long F. Glucose metabolism in bone. *Bone.* 2017;

129. Kim JM, Jeong D, Kang HK, Jung SY, Kang SS, Min BM. Osteoclast precursors display dynamic metabolic shifts toward accelerated glucose metabolism at an early stage of RANKL-stimulated osteoclast differentiation. *Cell Physiol Biochem.* 2007; 20:935-46.

130. Jin Z, Wei W, Yang M, Du Y, Wan Y. Mitochondrial complex I activity suppresses inflammation and enhances bone resorption by shifting macrophage-osteoclast polarization. *Cell Metab.* 2014; 20:483-98.

131. Esen E, Lee SY, Wice BM, Long F. PTH Promotes Bone Anabolism by Stimulating Aerobic Glycolysis via IGF Signaling. *J Bone Miner Res.* 2015; 30:1959-68.

132. Bikle DD. Vitamin D and bone. *Curr Osteoporos Rep.* 2012; 10:151-9.

133. Wang WL, Chatterjee N, Chittur SV, Welsh J, Tenniswood MP. Effects of 1alpha,25 dihydroxyvitamin D3 and testosterone on miRNA and mRNA expression in LNCaP cells. *Mol Cancer.* 2011; 10:58.

134. Reczek CR, Chandel NS. The Two Faces of Reactive Oxygen Species in Cancer. *Annu Rev Cancer Biol.* 2017; 1:79-98.

135. Khandrika L, Kumar B, Koul S, Maroni P, Koul HK. Oxidative stress in prostate cancer. *Cancer Lett.* 2009; 282:125-36.

136. Shigemura K, Sung SY, Kubo H, Arnold RS, Fujisawa M, Gotoh A, Zhau HE, Chung LW. Reactive oxygen species mediate androgen receptor- and serum starvation-elicited downstream signaling of ADAM9 expression in human prostate cancer cells. *Prostate.* 2007; 67:722-31.

137. Mehraein-Ghomi F, Lee E, Church DR, Thompson TA, Basu HS, Wilding G. JunD mediates androgen-induced oxidative stress in androgen dependent LNCaP human prostate cancer cells. *Prostate.* 2008; 68:924-34.

138. Pathak S, Singh R, Verschoyle RD, Greaves P, Farmer PB, Steward WP, Mellon JK, Gescher AJ, Sharma RA. Androgen manipulation alters oxidative DNA adduct levels

in androgen-sensitive prostate cancer cells grown in vitro and in vivo. *Cancer Lett.* 2008; 261:74-83.

139. Miyake H, Hara I, Kamidono S, Eto H. Oxidative DNA damage in patients with prostate cancer and its response to treatment. *J Urol.* 2004; 171:1533-6.

140. Okoh V, Deoraj A, Roy D. Estrogen-induced reactive oxygen species-mediated signalings contribute to breast cancer. *Biochim Biophys Acta.* 2011; 1815:115-33.

141. Song H, Cho D, Jeon JH, Han SH, Hur DY, Kim YS, Choi I. Vitamin D(3) up-regulating protein 1 (VDUP1) antisense DNA regulates tumorigenicity and melanogenesis of murine melanoma cells via regulating the expression of fas ligand and reactive oxygen species. *Immunol Lett.* 2003; 86:235-47.

142. Gao P, Zhang H, Dinavahi R, Li F, Xiang Y, Raman V, Bhujwalla ZM, Felsher DW, Cheng L, Pevsner J, Lee LA, Semenza GL, Dang CV. HIF-dependent antitumorigenic effect of antioxidants in vivo. *Cancer Cell.* 2007; 12:230-8.

143. Klein EA, Thompson IM, Jr., Tangen CM, Crowley JJ, Lucia MS, Goodman PJ, Minasian LM, Ford LG, Parnes HL, Gaziano JM, Karp DD, Lieber MM, Walther PJ, Klotz L, Parsons JK, Chin JL, Darke AK, Lippman SM, Goodman GE, Meyskens FL, Jr., Baker LH. Vitamin E and the risk of prostate cancer: the Selenium and Vitamin E Cancer Prevention Trial (SELECT). *JAMA.* 2011; 306:1549-56.

144. Parikh H, Carlsson E, Chutkow WA, Johansson LE, Storgaard H, Poulsen P, Saxena R, Ladd C, Schulze PC, Mazzini MJ, Jensen CB, Krook A, Bjornholm M, Tornqvist H, Zierath JR, Ridderstrale M, Altshuler D, Lee RT, Vaag A, Groop LC, Mootha VK. TXNIP regulates peripheral glucose metabolism in humans. *PLoS Med.* 2007; 4:e158.

145. Minn AH, Hafele C, Shalev A. Thioredoxin-interacting protein is stimulated by glucose through a carbohydrate response element and induces beta-cell apoptosis. *Endocrinology.* 2005; 146:2397-405.

146. Shaked M, Ketzinel-Gilad M, Ariav Y, Cerasi E, Kaiser N, Leibowitz G. Insulin counteracts glucotoxic effects by suppressing thioredoxin-interacting protein production in INS-1E beta cells and in Psammomys obesus pancreatic islets. *Diabetologia.* 2009; 52:636-44.

147. Xu G, Chen J, Jing G, Shalev A. Thioredoxin-interacting protein regulates insulin transcription through microRNA-204. *Nat Med.* 2013; 19:1141-6.

148. Xu G, Chen J, Jing G, Shalev A. Preventing beta-cell loss and diabetes with calcium channel blockers. *Diabetes.* 2012; 61:848-56.

149. Giovannucci E, Harlan DM, Archer MC, Bergenstal RM, Gapstur SM, Habel LA, Pollak M, Regensteiner JG, Yee D. Diabetes and cancer: a consensus report. *Diabetes Care.* 2010; 33:1674-85.

150. Giangreco AA, Nonn L. The sum of many small changes: microRNAs are specifically and potentially globally altered by vitamin D3 metabolites. *J Steroid Biochem Mol Biol.* 2013; 136:86-93.

151. Saxena G, Chen J, Shalev A. Intracellular shuttling and mitochondrial function of thioredoxin-interacting protein. *J Biol Chem.* 2010; 285:3997-4005.

152. Peehl DM, Shinghal R, Nonn L, Seto E, Krishnan AV, Brooks JD, Feldman D. Molecular activity of 1,25-dihydroxyvitamin D3 in primary cultures of human prostatic epithelial cells revealed by cDNA microarray analysis. *J Steroid Biochem Mol Biol.* 2004; 92:131-41.

153. Lin R, Nagai Y, Sladek R, Bastien Y, Ho J, Petrecca K, Sotiropoulou G, Diamandis EP, Hudson TJ, White JH. Expression profiling in squamous carcinoma cells reveals pleiotropic effects of vitamin D3 analog EB1089 signaling on cell proliferation, differentiation, and immune system regulation. *Mol Endocrinol.* 2002; 16:1243-56.

154. Maiuri MC, Galluzzi L, Morselli E, Kepp O, Malik SA, Kroemer G. Autophagy regulation by p53. *Curr Opin Cell Biol.* 2010; 22:181-5.

155. Jones RG, Plas DR, Kubek S, Buzzai M, Mu J, Xu Y, Birnbaum MJ, Thompson CB. AMP-activated protein kinase induces a p53-dependent metabolic checkpoint. *Mol Cell.* 2005; 18:283-93.

156. Alborzinia H, Can S, Holenya P, Scholl C, Lederer E, Kitanovic I, Wolfl S. Real-time monitoring of cisplatin-induced cell death. *PLoS One.* 2011; 6:e19714.

157. Cheng X, Kim JY, Ghafoory S, Duvaci T, Rafiee R, Theobald J, Alborzinia H, Holenya P, Fredebohm J, Merz KH, Mehrabi A, Hafezi M, Saffari A, Eisenbrand G, Hoheisel JD, Wolfl S. Methylisoindigo preferentially kills cancer stem cells by interfering cell metabolism via inhibition of LKB1 and activation of AMPK in PDACs. *Mol Oncol.* 2016; 10:806-24.